ECO-76: C-2-1

THE APPLICATION OF REMOTE SENSING TO THE DEVELOPMENT AND FORMULATION OF HYDROLOGIC PLANNING MODELS

Peter A. Castruccio, Harry L. Loats, Jr.

Thomas R. Fowler

FINAL REPORT - NAS8-30539

ECOSYSTEMS INTERNATIONAL, INC.

Post Office Box 225

Gambrills, Maryland 21054

JANUARY 11, 1976

ECO-76: C-2-1

THE APPLICATION OF REMOTE SENSING TO THE DEVELOPMENT AND FORMULATION OF HYDROLOGIC PLANNING MODELS

Peter A. Castruccio, Harry L. Loats, Jr.

Thomas R. Fowler

FINAL REPORT - NAS8-30539

ECOSYSTEMS INTERNATIONAL, INC.

Post Office Box 225

Gambrills, Maryland 21054

JANUARY 11, 1976

TABLE OF CONTENTS

FIGURES

TABLES

ACKNOWLEDGEMENT

ECOsystems International, Inc., wishes to acknowledge the assistance of the following groups and individuals in acquisition of data valuable to this study:

Heggie N. Holtan, Agricultural Research Service

James B. Burford, Agricultural Research Service

Nazir Baig, Maryland- National Capital Park and Planning Commission

Alex Wolf, Maryland Department of State Planning

PREFACE

The launch of LANDSAT has for the first time provided the water resource manager and practical hydrologist with broad prospects for efficient acquisition of essentially real-time data. These are usable for hydrologic land use assessment, surface cover classification, physiographic analysis, surface water inventory, and for the extraction of information pertinent to soil properties. This information has value not only by and in itself, but also to construct the watershed transfer function for hydrologic planning models aimed at estimating peak outflow from rainfall inputs.

The reduction of satellite data to practical, operational information requires a clear, easily applicable methodology for converting these data into quantitative hydrologic parameters.

The fundamental objective of this effort is the development of such a methodology and its transfer to hydrologic users. It was realized that such technology transfer could be made far more effective by the parallel development and eventual demonstration of the results of a model, specifically structured to take full advantage of the capability of LANDSAT -- for example, its frequent recurrence and consequent ability to determine seasonal variations in the watershed's conditions. The category of Planning Models was chosen for development and demonstration because of its great practical importance in the design of waterworks, because of the wide diffusion of such models down to capillary levels within the hierarchy of water resources users, and because their implementation is relatively simpler than real-time management

models, thus making optimum use of the resources available for this effort.

Consequently, the effort was structured along two major routes: the development of a hydrologic planning model specifically based upon remotely sensed inputs, including its test and verification from existing records; and the application of LANDSAT data to supplying the model's quantitative parameters and coefficients. Included was the investigation of the use of LANDSAT data as information inputs to all categories of hydrologic models requiring quantitative surface parameters for their effective functioning.

The effort thus far has consisted of two phases. The first focused on the definition of the "drivers" - those hydrologic processes to which peak runoff is most sensitive - and upon the synthesis of a simple yet effective model for the estimation of long-recurrence outflows. The results of the first phase effort were presented in the Final Report, "The Application of Remote Sensing to the Development and Formulation of Hydrologic Planning Models," dated January, 1975.[1] The second phase has extended this work to include the development of a routing model for use in sensitivity analyses, and a quantitative investigation of the accuracy and completeness of the hydrologic information which can be extracted from remotely-sensed imagery.

This document reports the findings and conclusions of the Phase-two effort: it includes a summary of the results of the earlier work.

CHAPTER I

REVIEW OF THE FIRST PHASE EFFORT

Of critical concern to water resources planners and engineers is the ability to forecast peak flow events. The capacity to estimate the magnitude and duration of large-recurrence outflows has a significant impact upon the accuracy of sizing and designing waterworks, and thus on their cost.

The tool available to the planner for these purposes is the hydrologic model. Although the inputs of different models vary, all require significant quantities of physiographic and hydrologic information; these data are typically expensive to obtain and are often only partially available. Remote sensing offers a new source of information which formerly had to be acquired by less efficient means or ignored altogether.

The first phase of this effort conducted from February to December 1974 addressed four pertinent topics:

1) Identification of the "drivers" of peak flow events, i.e., the hydrologic phenomena (infiltration, antecedent soil moisture, etc.) to which the watershed's outflow is most sensitive.

2) The development of a model compatible to the maximum degree with remotely-sensed hydrologic inputs.

3) Verification of the model for actual watersheds.

4) Preliminary identification of the efficiency of remote sensing in determining the parameters of the model.

1.1) Investigation of Driver Phenomena

The purpose of this investigation was to achieve a valid statistical comparison of the rates and magnitudes of the hydrologic processes contributing to the runoff from long-recurrence events. This was accomplished over a significant sample of watersheds, with wide variation of climatology, terrain, and physiography. The comparison allowed the determination of which are important and which can be neglected without significant loss of accuracy.

Rain falling on a watershed is subject to several processes which abstract water and govern the flow. Those which produce the most significant changes to flow rates and volumes "drive" the basin outflow. Table 1 describes the hydrologic processes; Table 2 presents the "drivers" of each. Figure 1 synopsizes their relative contributions to the peak event. It shows that several processes can be omitted in the formulation of a peak rate model because of their limited impact. For example, the rates corresponding to interflow, percolation, and evapotranspiration are very slow in comparison with other processes such as rainfall, infiltration and overland flow. Also, interception and depression storage become saturated early in large rainfall events.

Therefore, except for very special circumstances, peak flow can be adequately modelled by considering only precipitation, infiltration and surface flow - both overland and in the channels.

TABLE 1

SUMMARY DESCRIPTIONS OF HYDROLOGIC PROCESSES

HYDROLOGIC PROCESS	DESCRIPTION
Interception	Moisture caught and stored on plant leaves and stems or other impermeable objects; eventually evaporated back into the atmosphere.
Infiltration	Downward movement of water from the surface into the soil.
A) Interflow	Lateral subsurface water movement toward stream channels.
B) Percolation	Downward movement of water through soil to groundwater (area where pores of soil or rock are filled with water).
C) Base Runoff	Water from interflow and percolation which moves underground to the channel.
Evapotranspiration	
A) Evaporation	Upward movement of water in gaseous state from the surface.
B) Transpiration	Movement of water through plants to the atmosphere.
Precipitation Excess	
A) Depression Storage	Retention of excess rainfall in surface depressions.
B) Surface Flow	Uninfiltrated water which flows over land surface to stream channels.
C) Channel Flow	Flow of water in natural channels.
Total Runoff	Sum of runoff from underground processes (base runoff) and overland flow (direct runoff).

TABLE 2

POTENTIALLY IMPORTANT DRIVERS AS RELATED TO HYDROLOGIC PROCESSES

HYDROLOGIC PROCESS	PRINCIPAL DRIVERS	SECONDARY DRIVERS
Overland Flow	Slope Roughness of Soil & Cover Drainage Density & Pattern	— —
Infiltration	Soil Permeability Antecedent Soil Moisture Soil Moisture Capacity	Vegetative Cover Slope Water Turbidity Temperature
A) Interflow	Soil Permeability Subsurface Moisture Gradient Flow Length, Slope	— —
B) Percolation	Soil Permeability Subsurface Moisture Gradient Soil Depth	— —
Evapotranspiration		
A) Evaporation	Temperature Antecedent Soil Moisture Soil Permeability	Water Turbidity Wind
B) Transpiration	Temperature Solar Radiation Vegetative Cover Antecedent Soil Moisture	Wind
Depression Storage & Detention	Depression Density Cover Retention	Slope
Interception	Duration of Rainfall Intensity of Rainfall Cover Composition, Age, Density	Evaporation Rate

FIGURE I RATES OF HYDROLOGIC PROCESSES

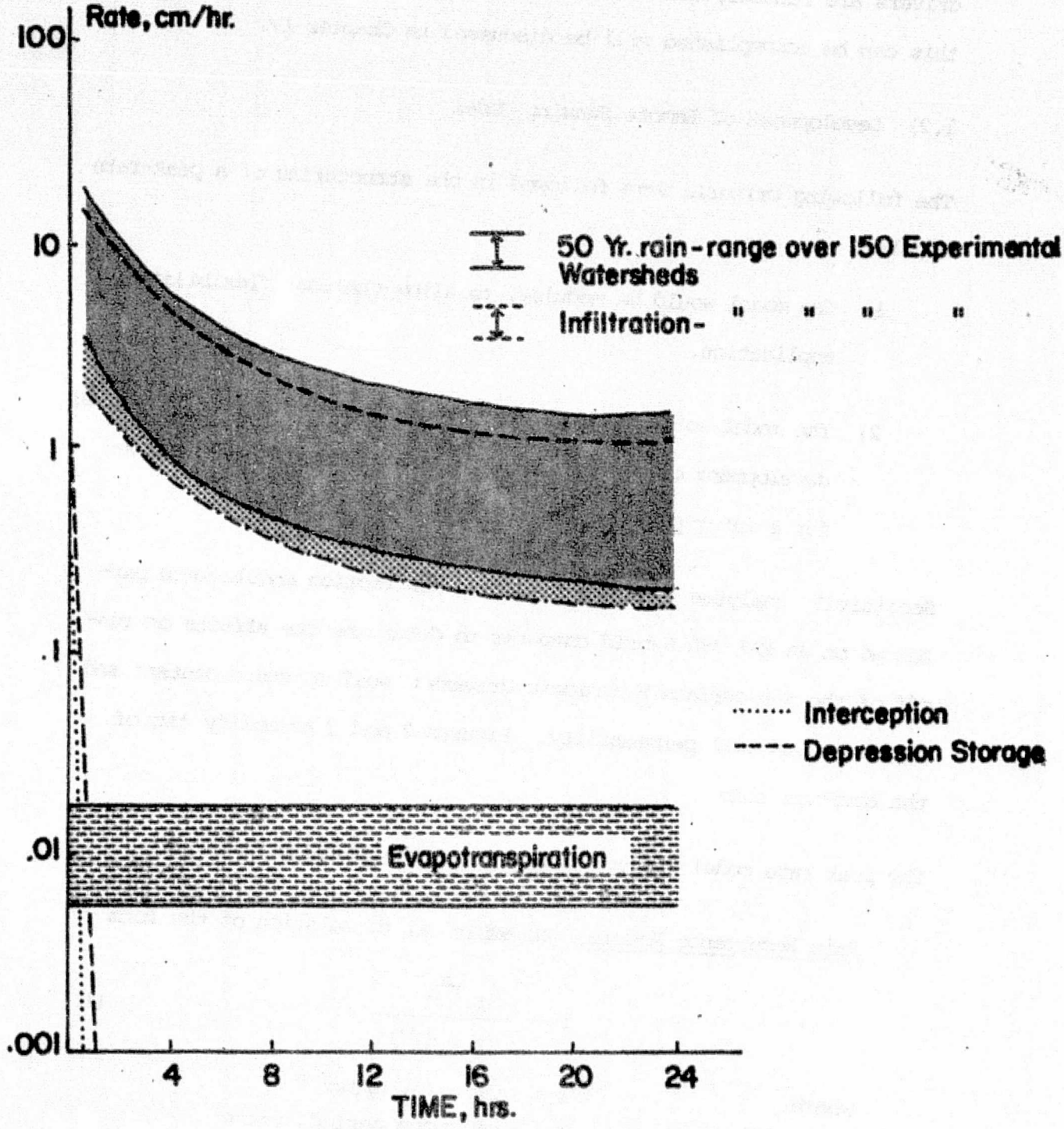

The set of the principal drivers of planning models can thus be defined as shown in Table 3 which also indicates that several of the drivers are remotely measurable or inferrable. The means by which this can be accomplished will be discussed in Chapter IV.

1.2) Development of Remote Sensing Model

The following criteria were followed in the structuring of a peak-rate model:

1) The model would be modular, to allow the user flexibility of application.

2) The model would provide the long-recurrence peak outflow rate; development of a model to yield the hydrograph was reserved for a later phase of the effort.

Sensitivity analyses of the sub-surface abstraction module were performed on an EAI 380 Hybrid computer to determine the effects on run-off of the sub-surface hydrologic drivers: soil moisture content and capacity, and soil permeability. Figures 2 and 3 exemplify two of the computer runs.

The peak rate model was constructed from the following modules:

Rain Recurrence Module: an empirical formulation of the form

$$i = \frac{\alpha_1 T^{\alpha_2}}{(t + d)^{\alpha_3}} \qquad (1)$$

where: i = rain rate, m/sec.
T = recurrence period, years

TABLE 3

PLANNING MODEL COMPONENTS

PROCESSES	DRIVERS	REMOTE SENSING POTENTIAL
Overland Flow	Slope	*
	Surface Friction	*
	Drainage Density & Pattern	*
Infiltration	Soil Permeabilities	
	Soil Moisture Capacity	
	Antecedent Soil Moisture	*
Rainfall	Regional & Seasonal	
	Recurrence Statistics	

FIGURE 2 INFLUENCE OF SOIL DEPTH UPON RUNOFF

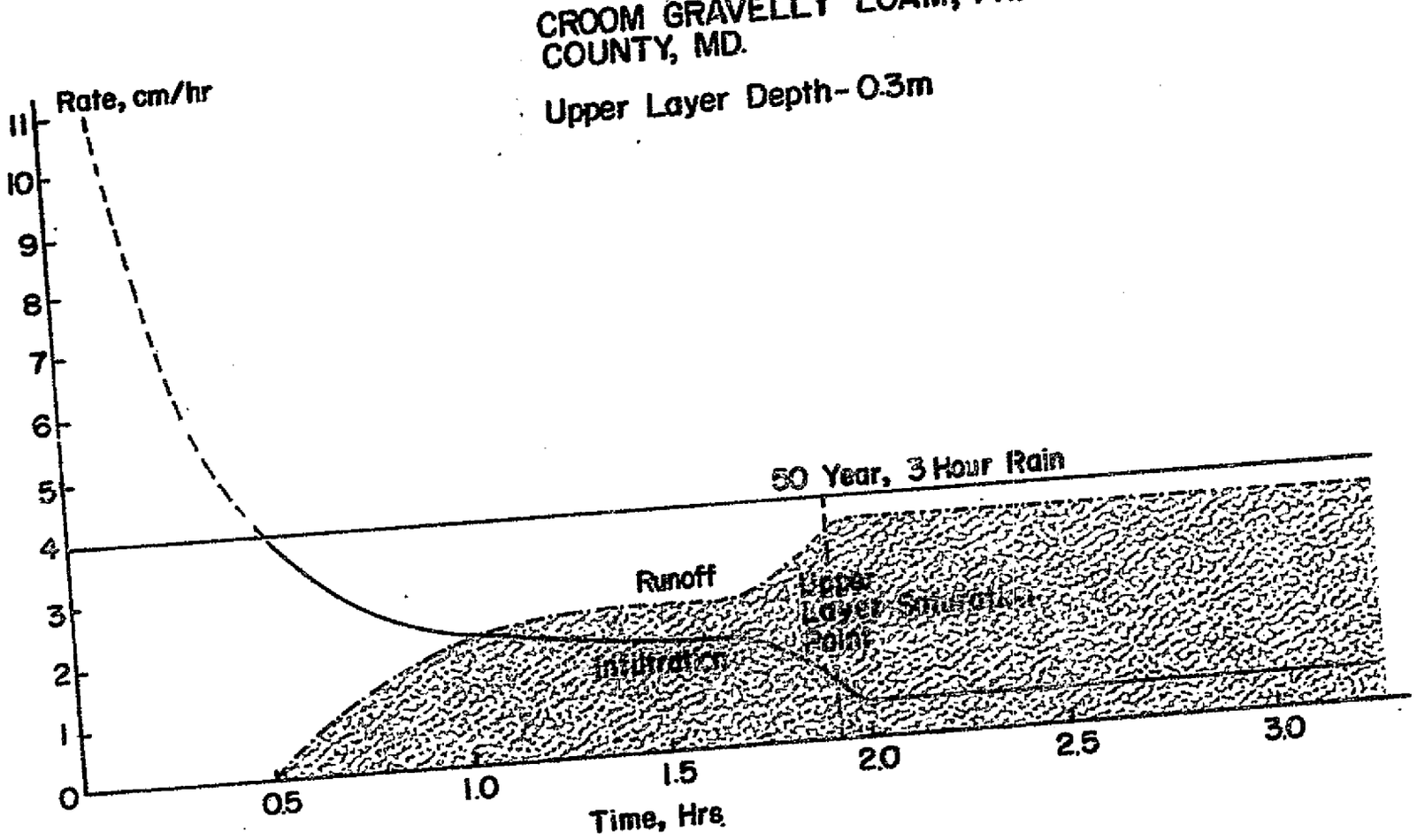

EFFECT OF ANTECEDENT SOIL MOISTURE CONTENT ON INFILTRATION AND RUNOFF

CROOM GRAVELLY LOAM, PRINCE GEORGE'S COUNTY, MD.

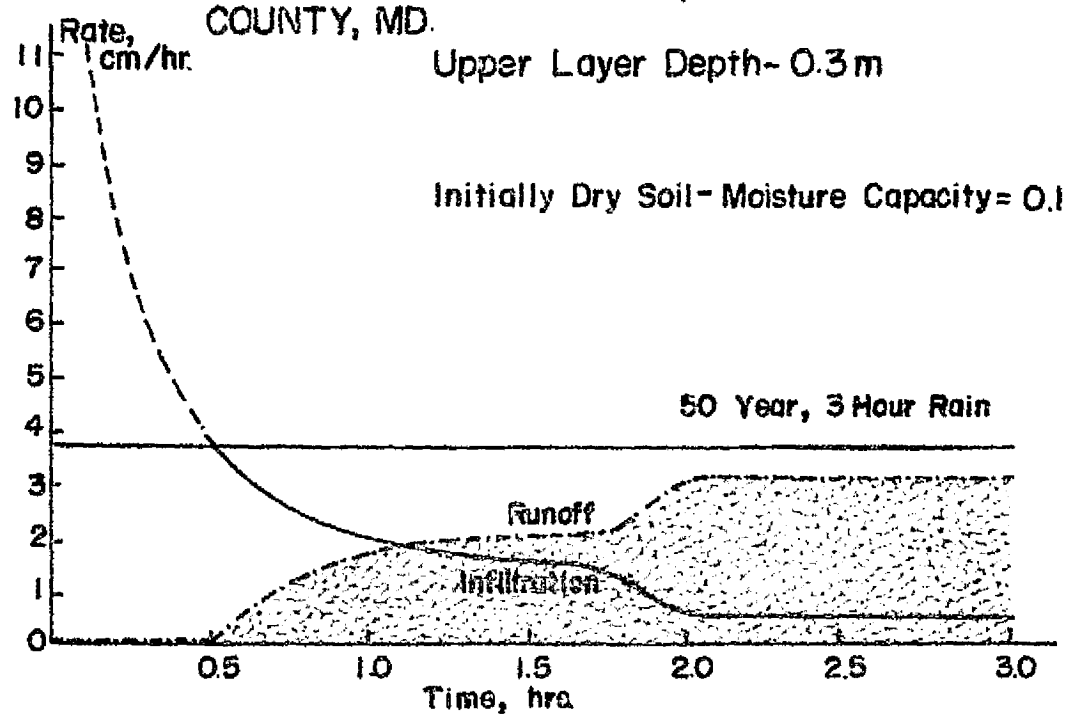

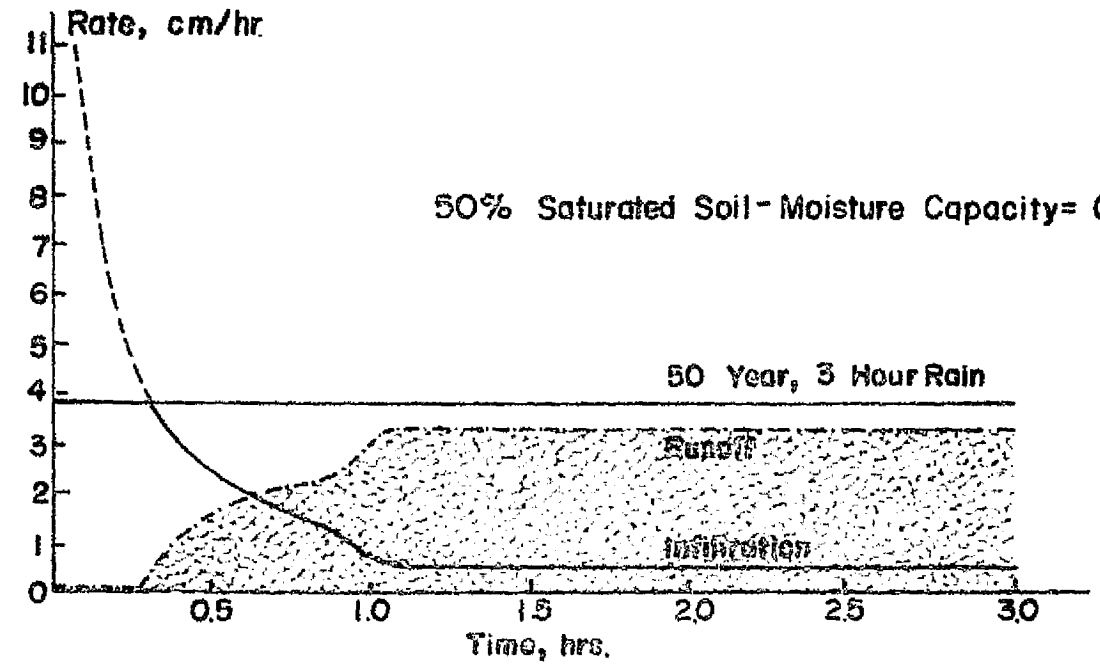

FIGURE 3

t = rain duration, hrs.

α_1, α_2, α_3, d = constants, functions of location

This was used to calculate the expected magnitude of large recurrence rainfalls.

Rainfall Spatial Correction Module: the introduction of a factor to convert point rainfall to its areal equivalent for large basins. As watershed area increases, effective rainfall must be diminished. An empirical relation, as shown in Figure 4, was used for this purpose.

Sub-surface Abstractions (Infiltration) Module: the Holtan infiltration equation:

$$\dot{I} = GI \cdot \bar{a} \cdot (S_a - I)^{1.4} + \dot{I}_f \qquad (2)$$

where:
- $\dot{I}$ = infiltration rate
- GI = maturity of cover index
- $\bar{a}$ = average vegetative cover factor
- S_a = average available soil moisture capacity
- I = cumulative infiltration
- $\dot{I}_f$ = saturated infiltration rate

Holtan's equation was selected for use because 1) it explicitly includes surface observables (the $\bar{a}$ and GI factors) which are potentially remotely sensible, 2) it is currently being applied over a diverse range of cover and soil types so empirical verification exists and 3) its results do not differ appreciably from those of other widely-used formulations.

FIGURE 4 WEATHER SERVICE
RAINFALL AREA-DEPTH CURVE

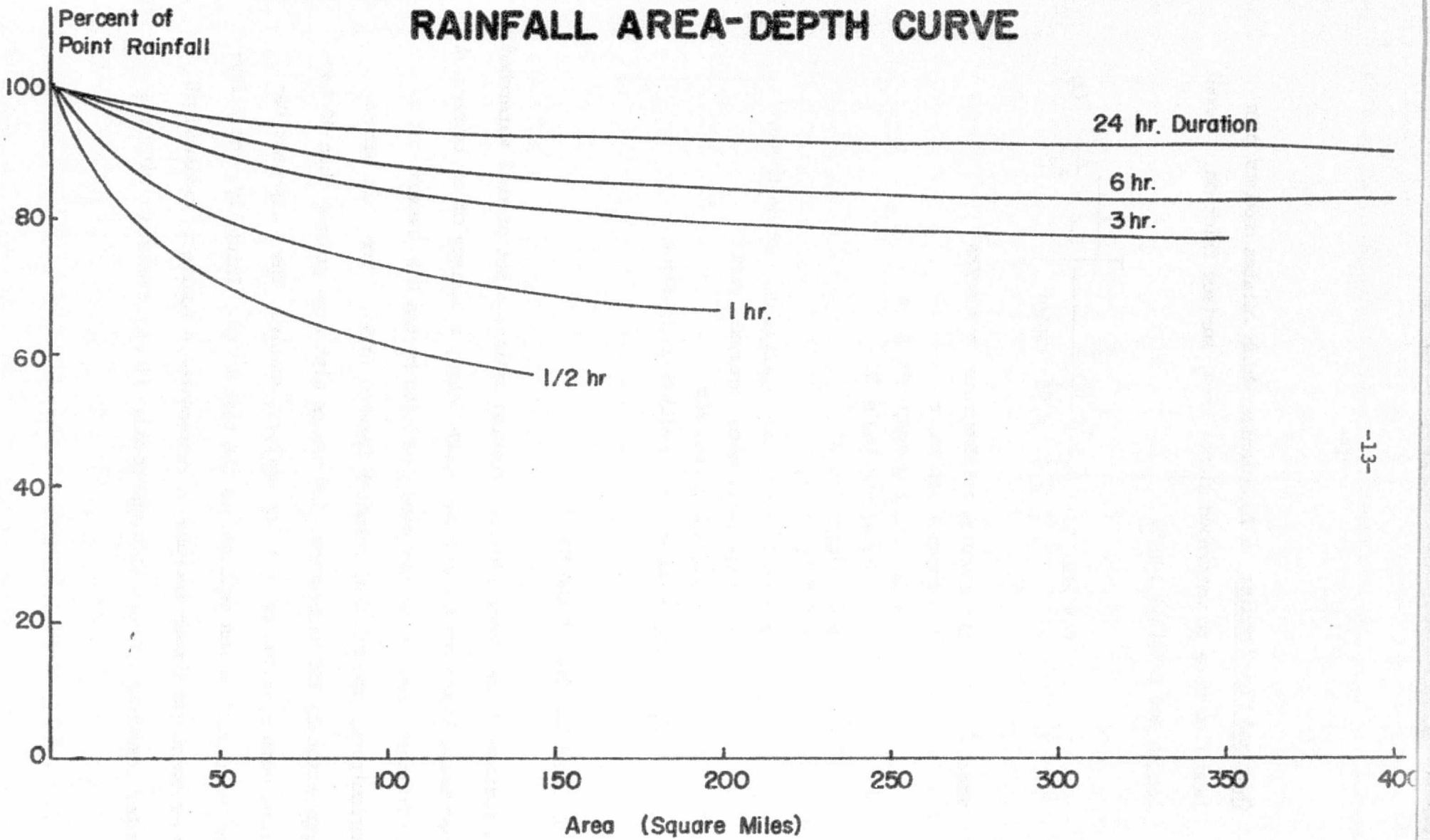

Overland Flow Module: a formulation which relates maximum overland flow rate to watershed slope, area, surface friction, channel length and rainfall input.

$$Q = 2L\bar{l}\ \xi \left[\frac{\phi\ (\bar{l})\ (\bar{n})^{\frac{3}{5}}}{\xi^{\frac{2}{5}}\ s^{\frac{3}{10}}\ (3600)} \right]^{\frac{1}{0.4 - \frac{1}{\alpha_3}}} \qquad (3)$$

where:

Q = maximum outflow rate, $m^3/sec/km^2$

L = channel length, m

$\bar{l}$ = length of average strip, m

$\bar{n}$ = average Manning's "n"

ϕ = routing factor

$\xi = K\ \alpha_1\ T^{\alpha_2}$

K = infiltration and spatial correction factor

T = rain recurrence interval, years

s = average slope, m/m

α_1, α_2, α_3 = constants, function of location

1.3) Verification of the Model

Validation of the model required testing against a set of real watersheds possessing long-term records and representing a variety of environmental conditions. Such a set has been developed by the U.S. Department of Agriculture, Agricultural Research Service (ARS). From this set of approximately 250 watersheds, 158 basins with area greater than 40 hectares were selected to form the analytic sample. The fifty-year recurrence outflow was selected as the test event. Initially, the fifty-year event was chosen because it represented a realistic estimate of water resources project life and because it was consistent with the

length of available records. The selection was made subject to further verification which has been completed and is described in Section 3.3. Initial verification of the model was made on a s et of nine basins selected for geographic and hydrologic diversity. A typical description of such a test basin appears in Figure 5. The parameters necessary for application of the model were calculated from the ARS data. A summary of the parameters for the test subset of nine basins is provided in Table 4.

The computed flow rate and the rate statistically derived from the measurement records were compared. Computation of peak flow was also made using other models in common usage - the Rational Formula, the S.C.S. model, and Cook's equation - for the same watershed sample. The results are presented in Table 5 and Figure 6. The peak-rate model yielded estimates within $\pm$ 15% of those derived from runoff records for seven of the nine test watersheds.

The results for two watersheds - Reynolds, Idaho, and Chickasha, Oklahoma, exceeded the ±15% accuracy bound. It appeared that these large errors might be attributable to the "complexity" of the two basins, both of which are composed of numerous sub-basins of diverse characteristics, hence requiring more complex routing than incorporated in the model. The development of the routing module will be described in Chapter III.

1.4) Identification of the Role of Remote Sensing in Hydrologic Modelling

A visual analysis was performed of one watershed at Chickasha, Oklahoma, from black and white, Band 5, LANDSAT imagery taken on October 20, 1973.

FIGURE 5

RIESEL (WACO) TEXAS ECO-7

Area 4.5 Km^2

Slope .021 m/m

Length of Channel 6.6 Km^2

Drainage Density 1/680 m/m^2

$$i = \frac{.054\ T^{.17}}{(t+.1)^{.78}}$$

Cover

60% Pasture
6% Small grain
3% Corn
7% Cotton
9% Row grains
2% Gravel & paved roads
13% Other, mostly weeds

Soils

66% Wilson clay loam
24% Burleson Heiden clay
4% Frio clay loam
3% Crockett loam
2% Burleson clay
1% Houston Black clay

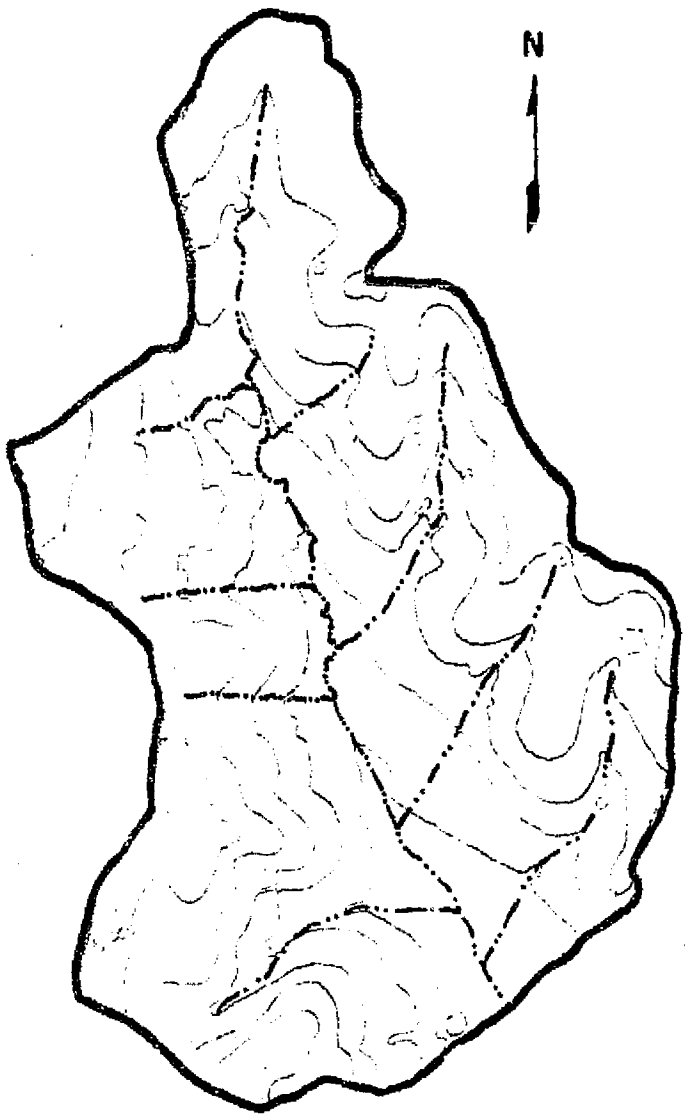

TABLE 4

PEAK RATE MODEL PARAMETERS

ECO NO.	LOCATION	ξ_{60}	MAIN CHANNEL LENGTH L,m	OVERLAND FLOW LENGTH l, m.	Φ	$\bar{n}$	$\bar{s}$	Q_{60} m3/sec/km2	K
1	DANVILLE, VT.	4.8×10^{-6}	9314	805	2.0	.079	.12	.91	.28
2	COSHOCTON,O.	1.4×10^{-5}	515	163	1.73	.048	.172	25.5	.71
3	BLACKSBURG, VA.	1.4×10^{-5}	5000	167	12.1	.039	.123	1.01	.62
4	OXFORD, MISS.	1.4×10^{-5}	12,000	858	2.61	.060	.114	10.8	.61
5	FENNIMORE, WISC.	1.4×10^{-5}	1545	165	3.26	.034	.080	12.5	.70
6	CHICKASHA, OKLA.	2.0×10^{-5}	34719	500	34.4	.038	.058	.08	.68
7	WACO TEX.	2.2×10^{-5}	3285	263	3.1	.035	.021	11.5	.76
8	SAFFORD, ARIZ.	1.2×10^{-6}	3549	133	6.8	.020	.020	5.3	.73
9	REYNOLDS, IDAHO	2.8×10^{-7}	21451	169	32.2	.038	.176	.001	.60

TABLE 5 COMPARISON OF RESULTS FOR THE FIFTY YEAR PEAK FLOW EVENT

	Q_{50} - $m^3/sec/km^2$				
	Records	ECO	Rational	SCS	Cook
1. Danville Vt.	0.95	0.91	4.8	2.14	5.49
2. Coshocton, Ohio	10.6	25.5	17.6	4.4	12.6
3. Blacksburg. Va	1.33	1.01	12.7	7.5	11.1
4. Oxford Miss.	11.9	10.8	7.3	3.1	8.4
5. Fennimore Wisc.	11.8	12.5	18.8	3.5	13.1
6. Chickasha, Okla	0.88	0.08	3.3	2.9	6.44
7. Waco, Texas	13.6	11.5	15.4	22.8	5.7
8. Safford, Ariz.	6.25	5.3	14.4	15.2	5.0
9. Reynolds, Idaho	0.67	0.001	1.7	13.7	3.9

FIGURE 6 COMPARISON OF ACTUAL VRS PREDICTED 50-YEAR RECURRENCE FLOW

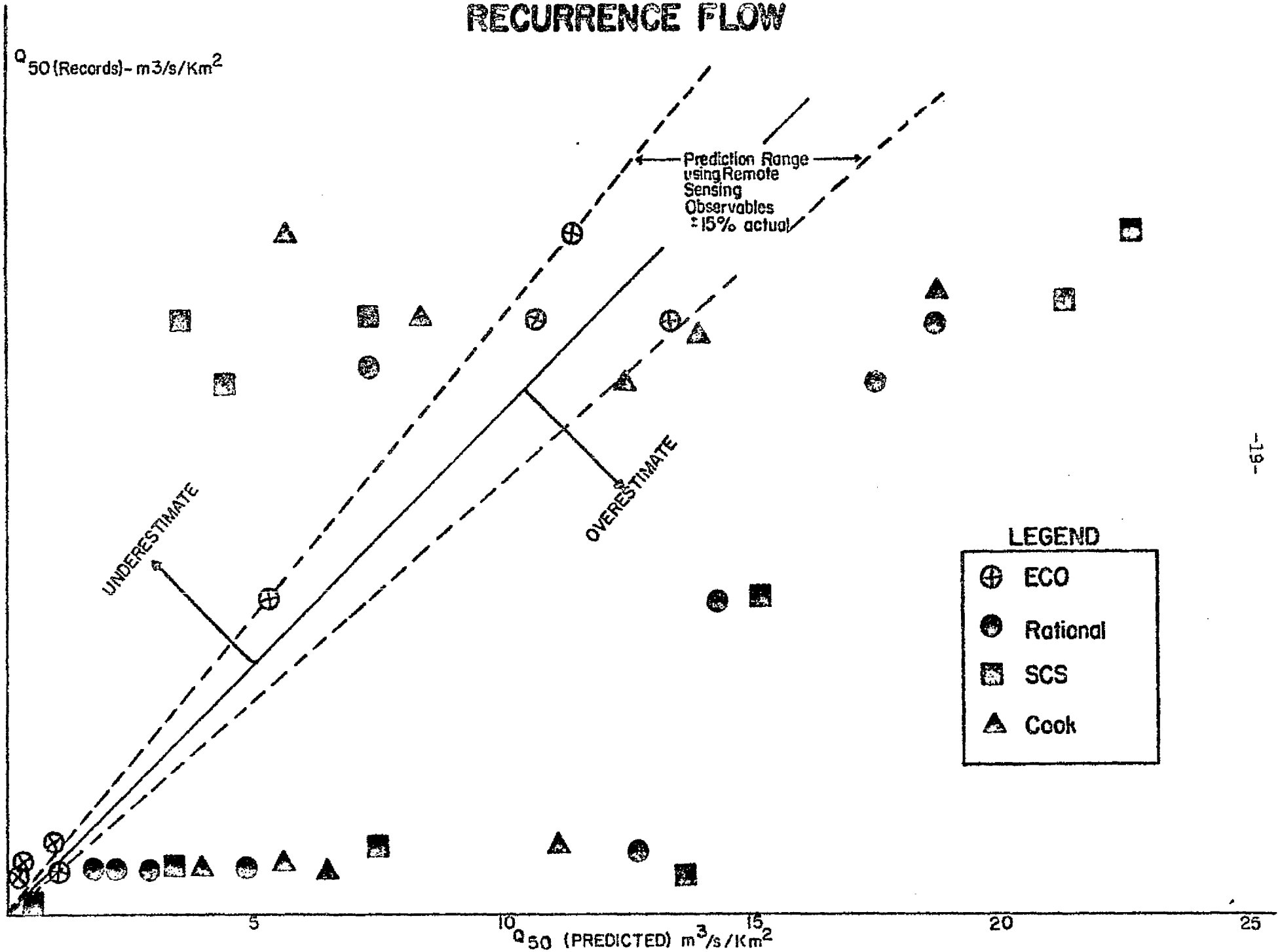

The findings of this analysis are summarized in the following:

1) Substantial hydrologic information can be measured from low resolution, single-band, black and white imagery from LANDSAT. The parameters identified and measured were: surface water bodies, Land Use Type 2 and 3 surface cover classes, channel length, and watershed area.

2) Of particular value are seasonal LANDSAT observations. For example, the October imagery showed the watershed when vegetation density was low; this made the higher-order streams visible. More channels could be measured from the image than appeared on the U.S.G.S. topographic map at the same scale. LANDSAT imagery clearly shows that effective drainage density varies cyclically throughout the year.

3) It became apparent that published records do not reflect current surface cover conditions, since the watershed's land use typically alters with time. For example, the October 1973 LANDSAT imagery demonstrated that surface cover had changed from that described in the latest published data (1967).

4) Discrepancies in published data on the extent of surface water were easily measurable. For example, some impoundments had been added to the watershed under analysis since the U.S.G.S. map was last updated. The effect of the impoundments in increasing the surface water area of the watershed was clearly visible.

1.5) Conclusions from the First Phase Effort

1. An improved model for the prediction of peak flow events was structured, specifically designed to take maximum advantage of the data and information stream available from remote sensing.

2. The model was exercised to predict the peak runoff from nine experimental Agricultural Research Service watersheds, selected from among a set of 158 instrumented and well-described watersheds.

3. The predictions of the new model in its simplified version were tested against:

   a. The predictions from three of the most employed contemporary planning models -- i.e., the Rational Formula method, Cook's method, and the Soil Conservation method; and,

   b. The statistical recurrence analysis of the stream-gage records of the nine test watersheds.

4. The results indicate that, within the range of applicability of its simplified version, the model appears to be an improvement over conventional hydrologic planning models.

5. The feasibility of extracting the model inputs and parameters from remotely sensed information was identified by visual analysis of LANDSAT imagery.

CHAPTER II

APPROACH TO THE PHASE 2 EFFORT

The Phase 2 effort concentrated in two areas:

1) The improvement and extended verification of the planning model, including routing.

2) The analysis of LANDSAT imagery to determine practical procedures for the extraction of quantitative hydrologic information usable in Planning Models.

The first area included four tasks. In the first task, the application of the peak-rate model to the test watersheds was extended to include a larger, statistically significant sample. Estimation errors of the large-recurrence flow event with respect to runoff records were determined; the results were compared with estimates derived from other commonly employed models.

The remaining three tasks aimed at the improvement of the model's accuracy by further analysis of the following important factors:

In the second task, the time-profile of the critical rainfall and runoff statistics from the 158 ARS watershed sample were analyzed to ascertain regional and seasonal characteristics of peak flows and to determine what is the "planning rain," i.e., the rainfall which defines the critical outflow.

The third task addressed the sensitivity of overland flow to changes of physical basin parameters. This was assessed through computer runs of a strip model.

The fourth task addressed the inclusion of "complex" watersheds. A routing model based on remotely-sensed inputs was synthesized.

The second area consisted of three tasks:

In the first, techniques for extraction of hydrologic data were analyzed.

In the second task, an investigation was undertaken to determine the information content of each MSS band and multi-band combinations. LANDSAT imagery from two test watersheds was interpreted and compared to topographic map ground truth to ascertain which hydrologic features could be identified.

The third task addressed an in-depth quantitative analysis of a single basin from LANDSAT data. A Maryland watershed was selected for this analysis because of the availability of recent, seasonal ground truth, and also because of the watershed's rapid development, which adds the possibility of assessing the effects of land use changes on hydrologic properties.

The relationships of these tasks to each other and to the overall objectives are depicted in Figure 7.

FIGURE 7 FLOW CHART OF CURRENT EFFORT

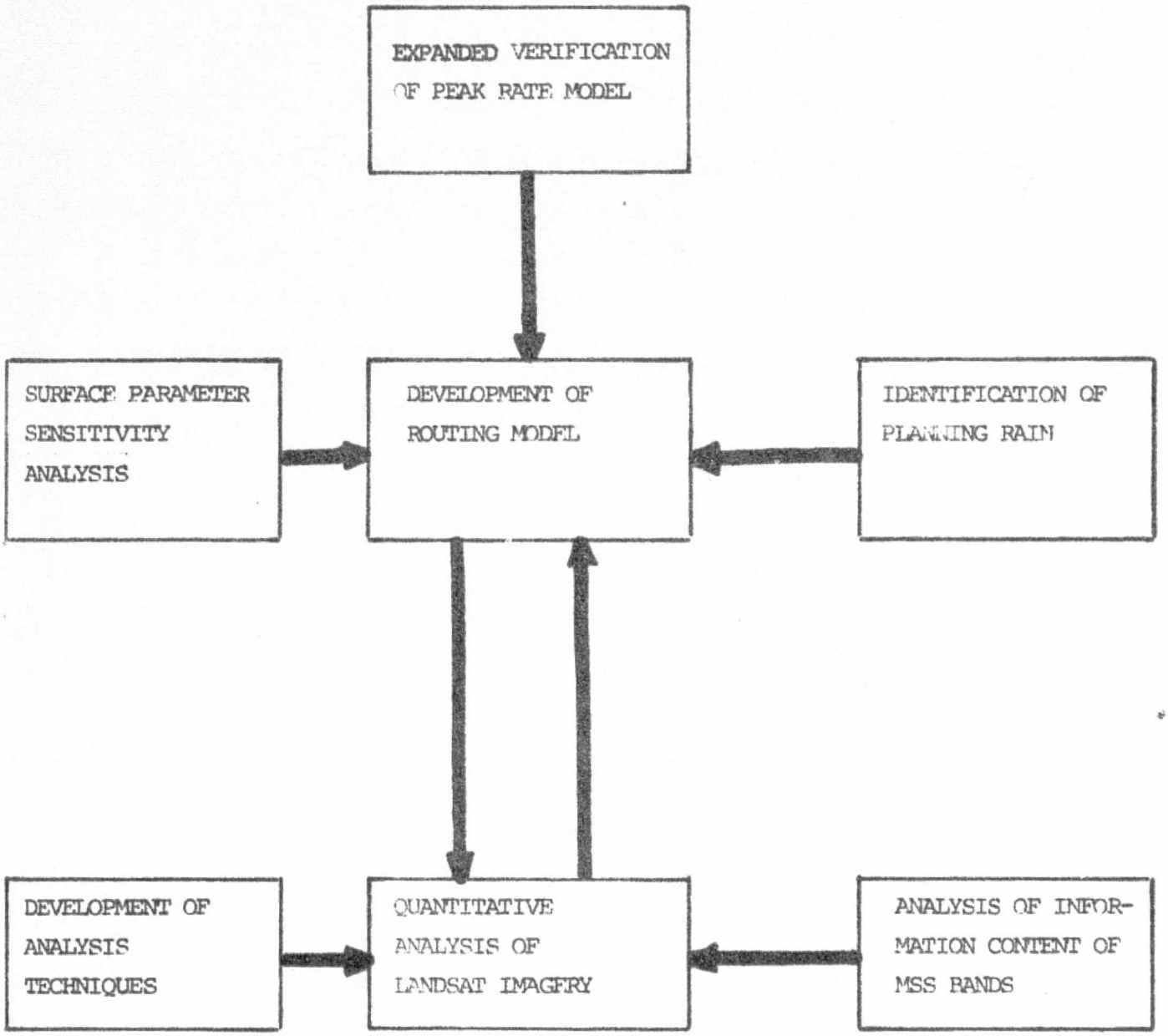

CHAPTER III

EXPANDED VERIFICATION OF PEAK-RATE MODEL AND DEVELOPMENT OF ROUTING MODEL

3.1) Expanded Verification of Peak-Rate Model

Seven of the nine watersheds selected for verification in the Phase 1 effort and which yielded the best results were essentially "simple "- composed of a main channel without contributing sub-areas. An additional twenty-four basins satisfying these criteria were selected in this effort. These watersheds, however, were chosen to include a wider range of physiographic, geographic, and hydrologic characteristics. They ranged in area from 40 to about 2000 hectares.

The parameters required by the model were computed for each watershed as follows:

1) Main channel length was measured with a map wheel from U.S.G.S. topographic maps.

2) The average infiltration rate was computed by determining the weighted average of the types of soil. The U.S. Soil Conservation Service classifies soils in the United States with respect to infiltration rates in four classes, designated A, B, C, and D, respectively. Class A denotes soils with high infiltration rates even when thoroughly wetted. They consist chiefly of deep, well-to-excessively drained sands or gravels. Class B denotes soils with moderate infiltration rates when thoroughly wetted. These are chiefly moderately deep to deep, and moderately well to well-drained soils with moderately fine to moderately coarse textures. Class C includes

soils having low infiltration rates when thoroughly wetted. They consist chiefly of soils containing a layer which impedes downward movement of water, or soils with moderately fine to fine texture. Class D represents soils with very low infiltration rates when thoroughly wetted. These soils consist chiefly of clay soils, soils with a permanent high water table, soils with a clay layer at or near the surface layer and shallow soils over nearly impervious material.

An average watershed soil class was determined by computing a weighted average of the above data. It was calculated by assigning values of 1, 2, 3, and 4 to classes A, B, C, and D, respectively. For example, for Coshocton #194, 86% of the soils are type C, while 14% are type B. The average class was, then:

$$(0.86)\cdot(3) + (0.14)\cdot(2) = 2.86$$

Therefore, mean soil class for Coshocton is approximately C, so the characteristics of this class were used in the model.

Average soil class was translated to average saturated, or final, infiltration rate by using the values for each soil type given by H. Holtan, et. al., for the USDAHL-70 watershed model (2). These values are presented in Table 6. The character of the soil vis-a-vis layers of soil which constitute an impediment to flow are used to determine the choice of the value within the range. A low value for impeding layer of clay; a mid value for loam; and a high value for sand.

FINAL INFILTRATION RATE FOR SOIL CLASSES

Table 6

Soil Class	Final Infiltration Rate Range (cm/hr)
A	1.14 - .76
B	0.76 - .38
C	0.38 - .12
D	0.12 - .00

AVAILABLE STORAGE CAPACITY BY SOIL TYPE

Table 7

Soil Type	Available Storage Capacity m/m
Sand	0.29
Sandy Loam	0.29
Loam	0.25
Clay Loam	0.22
Silty Clay	0.20
Clay	0.18

After average final infiltration rate was calculated, available water storage per unit depth was computed. Values of available storage capacity were assigned on the basis of soil type, according to Table 7. A weighted average was taken to determine the available storage capacity (S_a). An average vegetative factor ($\bar{a}$) was computed for the watershed. First, the distribution of cover was determined from the data base (for example, 11% cultivated, 58% grassland, etc..). Then each type of cover was assigned a value according to Table 8. A weighted average was computed according to percentage of each type of vegetative cover in the watershed. The input set for the Holtan equation was then complete.

3) The average infiltration $\dot{I}$ over time was then calculated by the Holtan equation:

$$\dot{I} = GI \cdot \bar{a} \cdot (S_a - I)^{1.4} + \dot{I}_f$$

4) The approximate time of concentration was computed by applying the empirical equation developed by Kerby (3). The time of concentration is the time required for rainfall from the most remote point of basin to reach the outlet. It therefore defines the minimum rainfall duration for the basin to reach peak outflow. The Kerby formula was used to give an initial estimate of the duration of the peak rain, subject to iterative validation as described in Section 3.3. It is of the form:

Table 8
VEGETATIVE COVER FACTORS (a) FOR HOLTAN'S EQUATION

COVER	GOOD CONDITION	POOR CONDITION
Fallow	0.30	0.10
Row Crops	0.20	0.10
Small Grains	0.30	0.20
Hay (legumes)	0.40	0.20
Hay (sod)	0.60	0.40
Pasture (bunch grass)	0.40	0.20
Temporary Pasture (sod)	0.60	0.40
Permanent Pasture (sod)	1.0	0.80
Woods and Forests	1.0	0.80

$$t_c = \frac{2Ln}{3\sqrt{s}}$$

Where: t_c = time of concentration

L = distance from the most remote point in the basin to the channel, in a direction parallel to the slope

s = slope

n = retardance coefficient, according to Table 9.

5) An average surface friction factor, Manning's "n", was calculated for each watershed. Values shown in Table 10 were weighted according to the percent of the basin in each cover class.

6) Gumbel's Extreme Value technique was applied to the flow records of the expanded sample to compute the fifty-year recurrence flow, to be compared ultimately with predictions of the same event by the model. The formula is as follows:

$$Q_{50} = \mu + \beta s$$

Where: Q_{50} = fifty-year recurrence outflow rate

μ = mean of flow records

s = standard deviation of flow records

β = constant, function of the number of years of record

Table 11 shows values for μ, β and s for different recurrence intervals.

7) Average basin slope was computed by a weighted average of the slopes, using the data from A.R.S. records.

Table 9

RETARDANCE COEFFICIENT - KERBY'S EQUATION

Type of Surface	Value of n
Smooth impervious surface	0.02
" bare packed soil	0.10
Poor grass, cultivated row crops or moderately rough bare surface	0.20
Pasture or average grass	0.40
Deciduous timberland	0.60
Conifer timberland, deciduous timberland with deep forest litter or dense grass	0.80

Table 10

MANNING'S ROUGHNESS COEFFICIENT FOR OVERLAND FLOW FOR VARIOUS SURFACE TYPES

Watershed Surface	Manning's "N"
Smooth Asphalt	0.013
Concrete (Trowel Finish)	0.013
Rough Asphalt	0.016
Concrete (Unfinished)	0.017
Smooth Earth (Bare)	0.018
Firm Gravel	0.020
Cemented Rubble Masonry	0.025
Pasture (Short Grass)	0.030
Pasture (High Grass)	0.035
Cultivated Area (Row Crops)	0.035
Cultivated Area (Field Crops)	0.040
Scattered Brush, Heavy Weeds	0.045
Light Brush and Trees (Winter)	0.050
Light Brush and Trees (Summer)	0.060
Dense Brush (Winter)	0.070
Dense Brush (Summer)	0.100
Heavy Timber	0.100
Idle Land	0.030
Grass Land	0.032

VALUES OF β FOR DIFFERENT SAMPLE SIZE & RECURRENCE

Sample size, years of record	Recurrence interval, years					
	10	20	25	50	75	100
15	1.703	2.410	2.632	3.321	3.721	4.005
20	1.625	2.302	2.517	3.179	3.563	3.836
25	1.575	2.235	2.444	3.088	3.463	3.729
30	1.541	2.188	2.393	3.026	3.393	3.653
40	1.495	2.126	2.326	2.943	3.301	3.554
50	1.466	2.086	2.283	2.889	3.241	3.491
60	1.446	2.059	2.253	2.852	3.200	3.446
70	1.430	2.038	2.230	2.824	3.169	3.413
75	1.423	2.029	2.220	2.812	3.155	3.400
100	1.401	1.998	2.187	2.770	3.109	3.349

8) The ϕ factor indicated earlier was computed from the formula:

$$\phi = 1 + \frac{k_1 k_2}{k_3^{\frac{2}{3}} k_4^{\frac{1}{2}}}$$

Where, k_1, k_2, k_3, k_4 are ratios of the overland to channel parameters of surface friction factor, flow length, flow depth and slope, respectively.

This factor is essentially the routing component of the peak rate model in that it accounts for channel flow in time of concentration calculations. A detailed derivation can be found in Reference 1.

9) Infiltration abstractions were included in the form of the K factor which reduces actual precipitation to precipitation excess. The K term was calculated by comparing the rain rate occurring over the time of concentration with the average infiltration rate for the same period. For example, the rate (P) for the 50-year recurrence, t_c - duration rain in the Blacksburg watershed is 0.109 meters/hour. The infiltration equation, using the constants for this watershed, derived as explained previously is:

$$\dot{I}_{cm/hr} = 0.72\ (4.97 - I)^{1.4} + 0.38$$

For t_c = .52 hours (from the Kirpich formula), the infiltration rate will fall from 7.1 cm/hr to 3.4 cm/hr, with an

average value equal to approximately 4.2 cm/hr.

The K factor, therefore, for this case equals:

$$1 - \frac{\dot{I}}{\dot{P}} = 1 - \frac{0.042 \text{ m/hr}}{0.109 \text{ m/hr}} = 0.62$$

In other words, for this particular rain event, and for the Blacksburg watershed, approximately 62% of the rainfall becomes runoff.

10) All model input requirements are summarized for the watershed sample in Table 12. It is clear that a great diversity of hydrologic and physiographic conditions is represented.

11) To enable comparison of results with the SCS model outlined in Reference 4, an average SCS curve number was computed. Curve number values were taken from Table 13 according to average soil group. The determining factor in choosing a curve number is vegetative cover. A weighted average yielded a final curve number.

Using the parameters developed above, the peak rate model was run for each of the 31 simple watersheds. The S.C.S. formula, Cooks model and the Rational formula were also run for the same sample. The results are shown in Table 14: and, for the peak rate model alone, in Figure 8. Mean errors for the peak rate model were 56% compared with 62.5%, 99.2%, and 80.3%, for the S.C.S., Cook, and Rational models, respectively.

TABLE 12

MODEL INPUT REQUIREMENTS FOR EXTENDED WATERSHED SAMPLE

BASIN	n	L (m)	ℓ (m)	s	ξ ($\times 10^{-5}$)	α_1 ($\times 10^{-5}$)	α_2	α_3	k	ϕ
Coshocton #5	.048	700	241	.155	1.410	1.08	.15	.83	.772	1.546
Coshocton #10	.049	869	80	.162	1.315	1.08	.15	.83	.677	2.646
Coshocton #92	.046	2367	209	.166	1.09	1.08	.15	.83	.561	3.275
Coshocton #94	.048	3940	232	.159	.987	1.08	.15	.83	.507	5.016
Coshocton #95	.050	5297	227	.169	.915	1.08	.15	.83	.470	7.077
Coshocton #97	.051	8291	222	.172	.959	1.08	.15	.83	.494	11.96
Coshocton #194	.048	515	163	.172	1.4	1.08	.15	.83	.713	1.4
Coshocton #196	.051	902	119	.172	1.189	1.08	.15	.83	.612	1.97
Coshocton #994	.023	17020	242	.172	1.321	1.08	.15	.83	.680	72.0
Iowa City #40	.042	6360	149	.103	1.053	1.178	.151	.79	.495	19.4
Fennimore #41	.033	1580	165	.08	1.420	1.139	.14	.78	.721	3.42
Fennimore #42	.035	837	162	.05	1.524	1.139	.14	.78	.774	2.002
Hastings #56	.035	2415	78.8	.059	1.535	1.214	.172	.836	.703	12.56
Hastings #57	.037	1610	89.3	.061	1.751	1.214	.172	.836	.736	5.7
Hastings #58	.0353	1503	75.4	.057	1.359	1.214	.172	.836	.571	4.91
Hastings #59	.034	14220	92.1	.053	1.111	1.214	.172	.836	.467	96.21
Stillwater #81	.032	1690	107	.073	1.916	1.404	.17	.792	.702	6.26
Waco #83	.035	2400	218	.020	2.383	1.5	.17	.78	.817	3.287

TABLE 12 (cont.)

BASIN	n	L	ℓ	s	ξ ($\times 10^{-5}$)	α_1 ($\times 10^{-5}$)	α_2	α_3	K	ϕ
Waco #84	.034	3590	231	.021	2.116	1.5	.17	.78	.725	1.373
Waco #85	.034	9480	192	.021	2.011	1.5	.17	.78	.689	2.501
Waco #88	.034	692	110	.025	2.585	1.5	.17	.78	.886	1.924
Waco #89	.034	902	203	.024	2.634	1.5	.17	.78	.903	1.797
Waco #90	.036	644	175	.026	2.395	1.5	.17	.78	.8895	1.692
Albuquerque #98	.02	1450	169	.183	1.071	.66	.166	.793	.848	5.947
Albuquerque #100	.022	966	116	.085	.970	.66	.166	.793	.768	3.232
Safford #115 (W-1)	.022	3860	108	.02	1.45	.75	.19	.8	.922	8.478
Safford #117 (W-4)	.02	5800	113	.120	1.179	.75	.19	.8	.748	30.05
Safford #118 (W-7)	.02	5470	89.1	.11	1.37	1.06	.75	.19	.860	26.49
Danville #1	.079	9314	805	.120	.48	9.17	.16	.77	.28	2.04
Oxford #37	.060	13109	858	.114	1.5	1.36	.14	.75	.61	2.61
Chickasha #73	.038	34719	500	.058	2.03	1.53	.17	.82	.683	34.4
Fennimore #	.034	1545	165	.08	1.38	1.14	.14	.78	.695	3.26
Reynolds #14	.036	21451	189	.176	.28	2.2	.25	.71	.048	37.23

Table 13
SCS CURVE NUMBERS

Land Use or Cover	Treatment or practice	Hydrologic Condition	Hydrologic Soil group			
			A	B	C	D
Row crops	Straight row	Poor	72	81	88	91
	Straight row	Good	67	78	85	89
	Contoured	Poor	70	79	84	88
	Contoured	Good	65	75	82	86
Small grain	Straight row	Poor	65	76	84	88
	Contoured	Good	61	73	81	84
Legumes or rotation	Contoured	Good	55	69	78	83
Native pasture or range		Fair	49	69	79	84
		Good	39	61	74	80
Woods		Fair	36	60	73	79
		Good	25	55	70	77

TABLE 14

SUMMARY OF MODEL RESULTS

WATERSHED	RECORDS, Q_{50} $m^3/sec./km^2$	PEAK RATE MODEL % ERROR (Q_{50})	S.C.S. % ERROR (Q_{50})	COOK % ERROR (Q_{50})	RATIONAL % ERROR (Q_{50})
Coshocton #5	7.62	109 (15.9)	-50 (3.82)	39 (10.6%)	143 (18.5)
Coshocton #10	12.3	62 (19.9)	-55 (5.55)	27 (15.6)	19 (14.6)
Coshocton #92	5.12	7 (5.48)	35 (6.89)	112 (10.83)	80 (9.20)
Coshocton #94	6.05	-53 (2.82)	-10 (5.44)	82 (11.04)	27 (7.71)
Coshocton #95	4.63	-72 (1.29)	35 (6.27)	164 (12.24)	31 (6.07)
Coshocton #97	4.82	-87 (.62)	-22 (3.74)	74 (8.37)	-11 (4.29)
Coshocton #194	10.6	141 (25.5	-58 (4.4)	19 (12.6)	66 (17.6)
Coshocton #196	19.3	-41 (11.3)	-78 (4.34)	-41 (11.39)	-41 (11.40)
Coshocton #994	2.69	-96 (.11)	13 (3.04)	212 (8.39)	-16 (2.26)
Iowa City	5.93	-89 (.68)	-29 (4.20)	139 (14.2)	-27 (4.32)
Fennimore #W-1	11.8	10 (12.5)	-66 (4.06)	-1 (11.1)	10 (13.0)
Fennimore #W-4	12.98	63 (21.2)	76 (22.9)	2 (12.7)	20 (15.6)
Hastings #W-3	16.4	-86 (2.24)	-53 (7.71)	38 (22.6)	-40 (9.87)
Hastings #W-5	10.5	-45 (5.75)	21 (12.7)	3 (10.2)	5 (11.0)
Hastings #W-8	4.54	-81 (.84)	43 (6.50)	99 (9.05)	7 (4.86)
Hastings #W-11	3.57	-98 (.088)	-1 (3.55)	142 (8.63)	-16 (2.99)
Stillwater #W-4	20.6	-29 (14.6)	-47 (10.9)	-50 (10.3)	-28 (14.8)
Waco #C	13.5	17 (15.8)	13 (15.2)	-87 (1.81)	3 (13.9)
Waco #D	13.6	15 (11.5)	68 (22.8)	-58 (5.7)	13 (15.4)

TABLE 14 (cont'd)

SUMMARY OF MODEL RESULTS

WATERSHED	RECORDS, Q_{50} $m^3/sec./km^2$	PEAK RATE MODEL % ERROR (Q_{50})	S.C.S. % ERROR (Q_{50})	COOK % ERROR (Q_{50})	RATIONAL % ERROR (Q_{50})
Waco #G	7.41	-94 (.408)	68 (7.35)	-1 (7.35)	-25 (5.54)
Waco #W-2	33.3	11 (37.05)	-26 (24.5)	-26 (24.7)	-19 (27.1)
Waco #Y	23.1	17 (27.06)	49 (34.4)	-42 (13.3)	-10 (20.8)
Waco #Y-2	29.2	53 (44.68)	00 (29.1)	-33 (19.5)	-19 (23.6)
Albuquerque #W-1	6.72	55 (10.4)	59 (10.7)	8 (7.23)	21 (8.16)
Albuquerque #W-3	7.61	50 (11.42)	-2 (7.46)	79 (13.6)	98 (15.1)
Safford #W-1	6.25	-15 (5.3)	143 (15.2)	-20 (5.00)	130 (14.4)
Safford #W-4	3.65	-52 (1.77)	95 (7.10)	141 (8.79)	142 (8.84)
Safford #W-V	5.56	93 (10.73)	62 (9.02)	109 (11.6)	119 (12.2)
Danville #W-1	.95	-4 (.91)	125 (2.14)	478 (5.49)	405 (4.8)
Blacksburg #W-1	1.33	-24 (1.01)	464 (7.5)	735 (11.1)	855 (12.7)
Oxford #W-10	11.9	-9 (10.8)	-74 (3.1)	-29 (8.4)	-39 (7.3)
		$\bar{x}$ = 54.1 σ = 36.5	$\bar{x}$ = 62.5 σ = 81.8	$\bar{x}$ = 99.2 σ =149.3	$\bar{x}$ = 80.3 σ = 163.2

FIGURE 8

5! YEAR RECURRENCE DIS(ARGE:. ECO PEAK RATE ODEL VS. RECORDS

31 WATERSHED SAMPLE

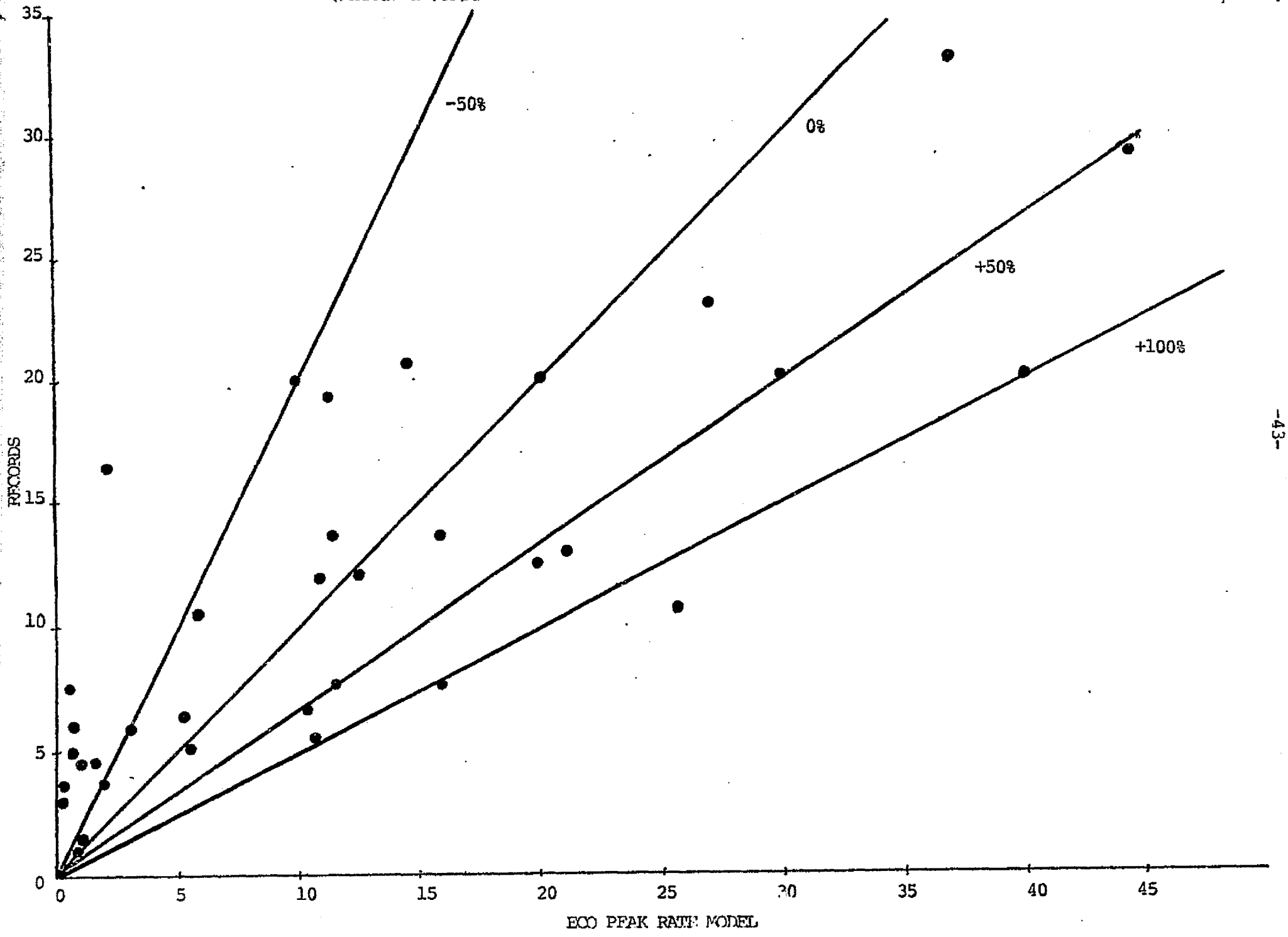

Two statistical tests were run to determine the significance of these results for the 31 watershed sample. The first tested whether the variance of the peak rate model was lower than the variances of the other three; the second tested the significance of the differences among the means. The results are summarized in Table 15.

In the first test, significant differences were established between the variance of the peak rate model and the other models.

In the second case, statistical differences between the means of the peak rate model could be shown for the Cook method, but not for the other two. The computations are presented in Appendix A.

These results indicate that the reduction in variability of forecast achieved by the peak rate model is statistically significant. The mean error of estimate was improved also, but within the limits of the sample size significance can be demonstrated for one of the three cases.

3.2) Investigations to Improve the Accuracy of the Peak-Rate Model

Development of the peak rate model made apparent several potential sources of forecast errors. To improve prediction accuracy, several questions were addressed:

1) What is the "planning rain," i.e. what rainfall input corresponds to the peak flow output and what are its temporal and areal distributions?

TABLE 15

STATISTICAL ANALYSIS OF MODEL FORECAST ERRORS

1) Cochran's Test for Equality of Variance

Test Hypothesis (H_o): $\sigma^2_{ECO} = \sigma^2_{SCS, Cook, Rational}$

Accept H_o if $G < .7652$ $(g_{0.05})$

	S^2	test statistic (G)	
ECO Peak Rate	1332.25	-	
SCS	6691.24	0.83	Reject Ho
Cook	22290.49	0.94	Reject Ho
Rational	26634.24	0.93	Reject Ho

∴ H_o rejected for all cases; ECO peak rate variance is significantly less at 95% confidence level

2) "T" Test for Equality of Means

Test hypothesis (H_o): $\mu_{ECO} = \mu_{SCS, Cook, Rational}$

Accept H_o if $T < 1.311$ $(t_{0.10})$

	$\bar{x}$	s	df	T	
ECO	54.1	36.5	-	-	
SCS	62.5	81.8	41	0.52	Accept H_o
Cook	99.2	149.3	34	1.63	Reject H_o
Rational	80.3	163.2	33	1.09	Accept H_o

∴ H_o rejected for Cook model at 90% confidence level

2) What seasonal and geographic factors are pertinent? Do rainfall and runoff exhibit propensities to occur during particular seasons in particular locations? What seasonally variant conditions should be included in the model?

3) What is the quantitative sensitivity of basin runoff to variations in surface parameters? How accurately does one need to measure slope, friction factors, etc. to obviate the introduction of unacceptable errors.

4) How should the appropriate basin sub-area be selected? Since values for each micro element of the basin are costly to measure in practice, how should the hydrologic parameters be combined into an average value yielding correct results?

The following four sections describe each question and present the corresponding analyses. The results from these analyses will be incorporated in the model in a subsequent phase of this effort.

3.2.1) Analysis of Rainfall Characteristics

The recurrence formula given in Chapter 1

$$i = \frac{\alpha_1 T^{\alpha_2}}{(t + d)^{\alpha_3}}$$

is implicitly based upon the assumption that the rainfall is of constant intensity throughout its period of occurrence. The reason is that most raingages measure rainfall mass rather than rate: it is thus practically convenient to divide the reading of the gage by the

duration. Equation (1) is therefore in essence an integral equation: its correct statement should be the following:

$$V = \int_0^t i\,dt$$

where:

V = rain mass, or volume, fallen within the time interval, t.

In actuality, the time behavior of i affects the runoff. It is therefore not surprising that, in general, no single type of rain event causes the peak basin outflow. A fifty-year recurrence runoff, for example, can be produced by one intense rainfall or by a series of lesser events. This fact, already indicated by various researchers, was verified for the watershed test sample by examining the relation between large-recurrence rainfalls and runoffs.

The recurrence interval of the runoff was calculated using the Weibull plotting position technique, giving a regression line fitted through the annual runoff peaks over the period of record. The peaks were ranked from largest to smallest and the probability of the occurrence was assigned according to:

$$P = \frac{m}{n + 1}$$

Where: P = occurrence probability
m = plotting rank (largest outflow = 1)
n = years of record

These points were plotted as shown in Figure 9. If the distribution is assumed to be normal, the regression line can be drawn by assigning the mean discharge to P = 0.5. The mean plus the standard deviation, assuming normality, will have a P = 0.165, and the mean flow minus the standard deviation will have P = 0.835. From this line, the recurrence interval of any discharge rate can be estimated.

The recurrence interval of the causative rainfall was computed from the empirical relation used in the rainfall module, Equation (1). The values of the coefficients in the equation were calculated from records for each location. The profiles of the rainfall rate were identified from analysis of detailed records of rainfall and runoff rates and masses at time intervals of a few minutes. In several watersheds, the largest runoff events were identified, the corresponding hydrographs charted, and the hyetographs of the generating rainfall or rainfalls overlayed thereon. Figures 10a, b, depict typical examples.

Comparisons between the profiles of related high-recurrence rainfalls and runoffs are also given in Figure 10. The conclusion is that no easily-discernible relation appears to exist between the runoff and the mass of rainfall of equal recurrence. Thus the selection of the "planning rain" is not as simple as might be expected. Since obviously some assumptions must be made, it is valuable to know how sensitive basin discharge is to the choice of rainfall profile for equal masses of rainfall.

FIGURE 9

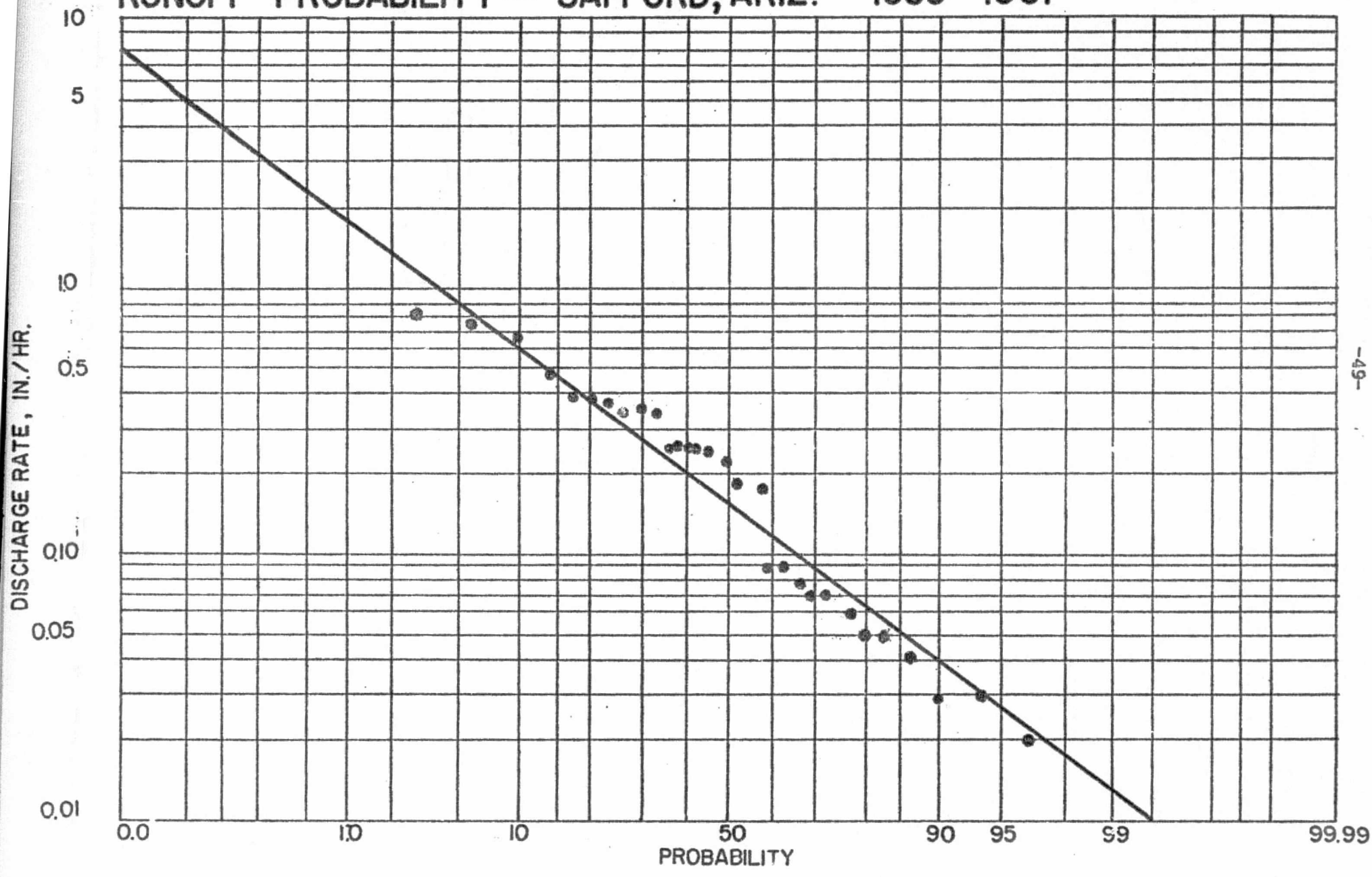
RUNOFF PROBABILITY — SAFFORD, ARIZ. 1939 - 1967
DISCHARGE RATE, IN./HR.
10
5
1.0
0.5
0.10
0.05
0.01
0.0
1.0
10
50
90
95
99
99.99
PROBABILITY

FIGURE 10A

PEAK RAINFALL AND RUNOFF - ALBUQUERQUE, N.M., #W-1
24 JUNE 1957

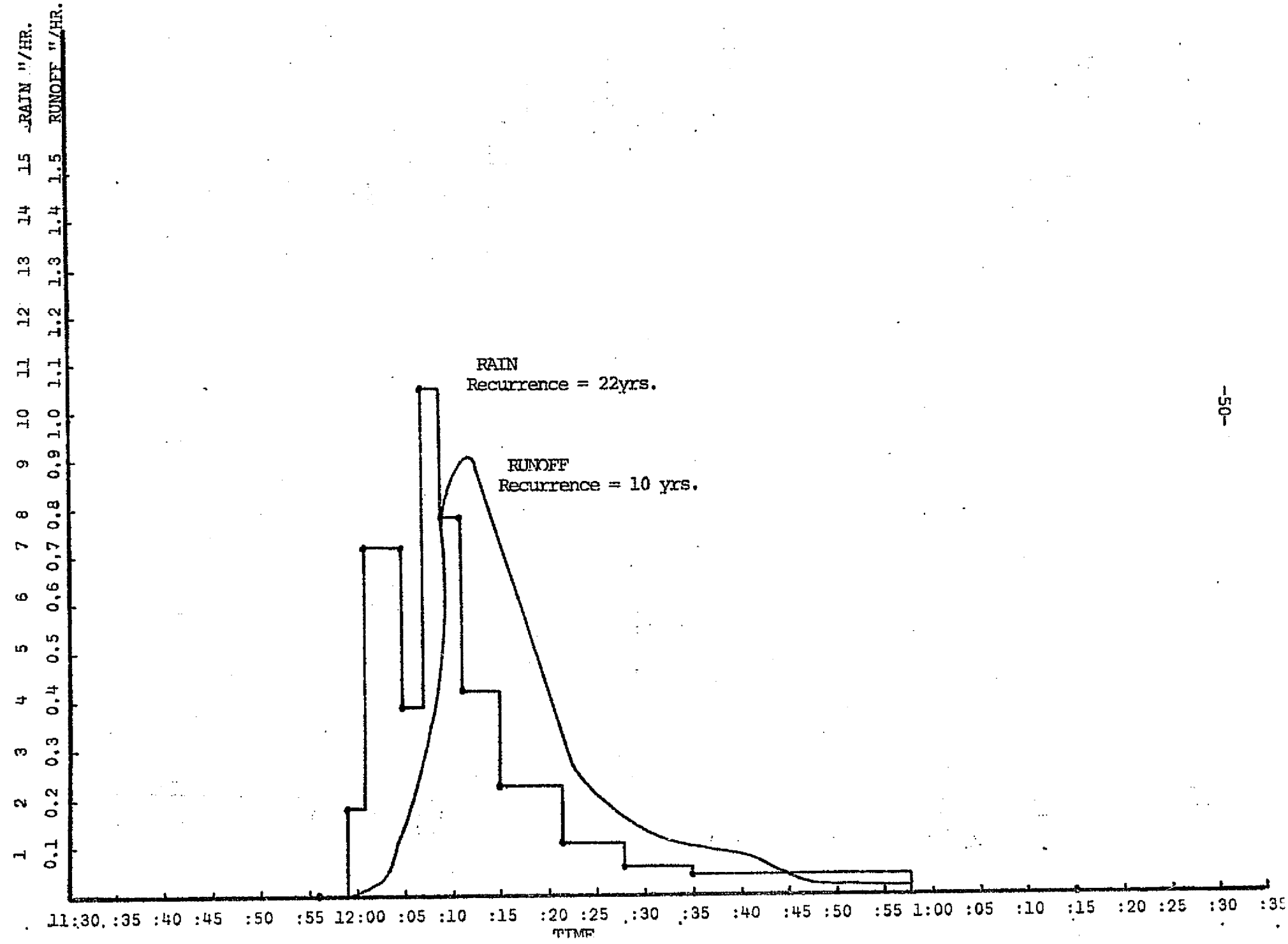

FIGURE .OB

PEAK RAINFALL AND RUNOFF COSHOCTON, O., #97
COSHOCTON #97 6-04-41

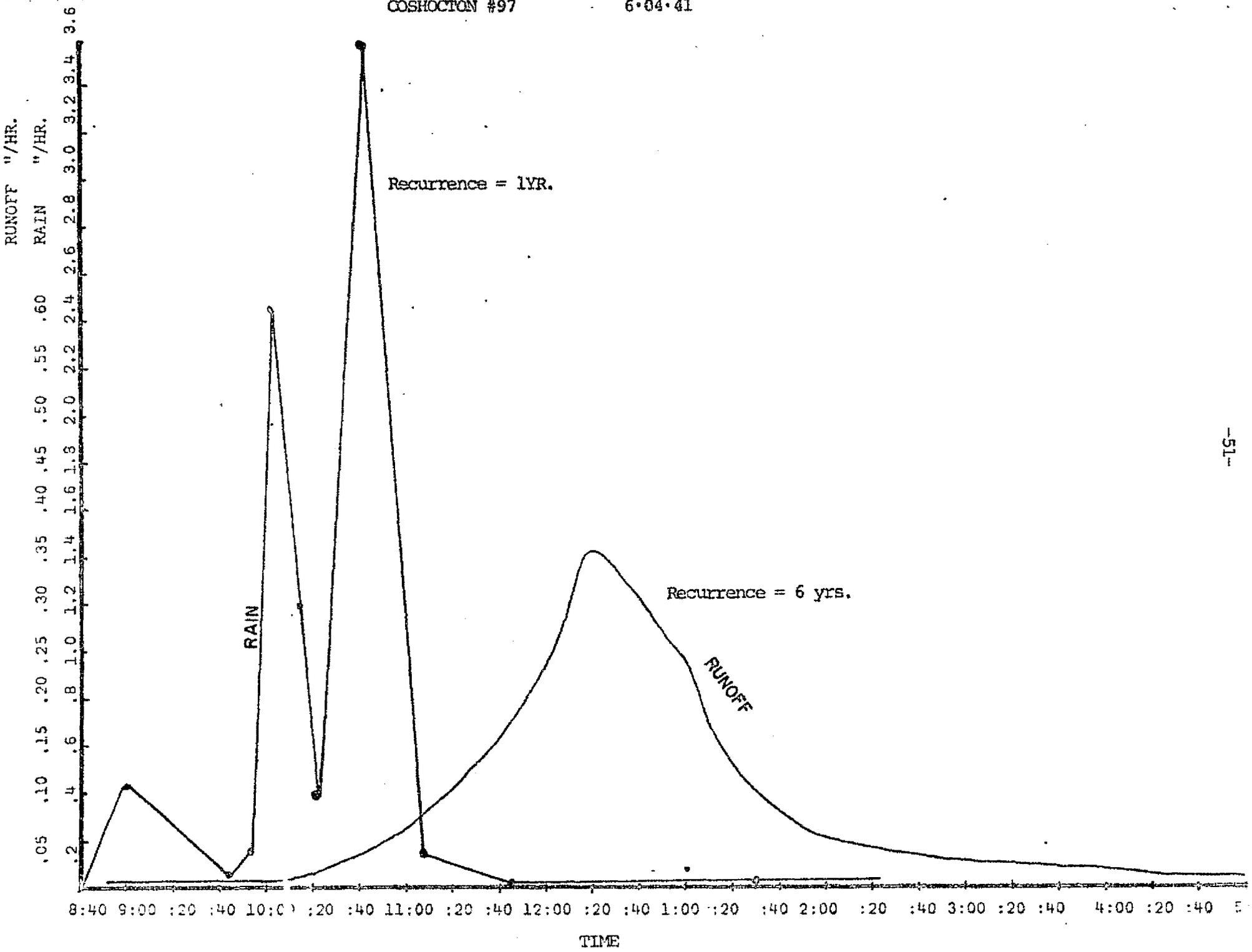

As a first step, a computer model developed by D.E. Overton was used to gage the effect of the temporal profile of the rain upon the runoff. The model simulates the runoff resultant from a given rainfall input for a unit width "strip" of any length. A detailed derivation of the model is contained in Reference 5. Two features are noted here:

1) The model accounts for several important surface variables of watersheds. It accepts rainfall inputs of varying magnitudes and temporal distributions over strips which can have variable slopes, dimensions, and surface covers.

2) The model was previously validated with accurate results from simulation of several hundred rainfall-runoff situations by the U.S. Army Corps of Engineers.

A series of computer simulations was made to assess the sensitivity of the runoff peak to the temporal profile of the rainfall and to the time of occurrence of the rainfall maximum, using parameters typical of those of the A.R.S. watershed sample. Several rainfalls of equal volume but with the different temporal profiles shown in Figure 11 were simulated. The resultant runoff hydrographs are shown in Figure 12. A significant difference in outflow is apparent between the constant rain and rains of triangular shape. With reference to Figure 10, the large recurrence rain profiles taken from the records tend to be triangularly shaped. It thus appears that the triangular profile should be used.

FIGURE II SENSITIVITY TO TIME OF RAINFALL PEAK - RAINFALL INPUTS

1 PLANE, N = .05, S = .05, L = 1000'

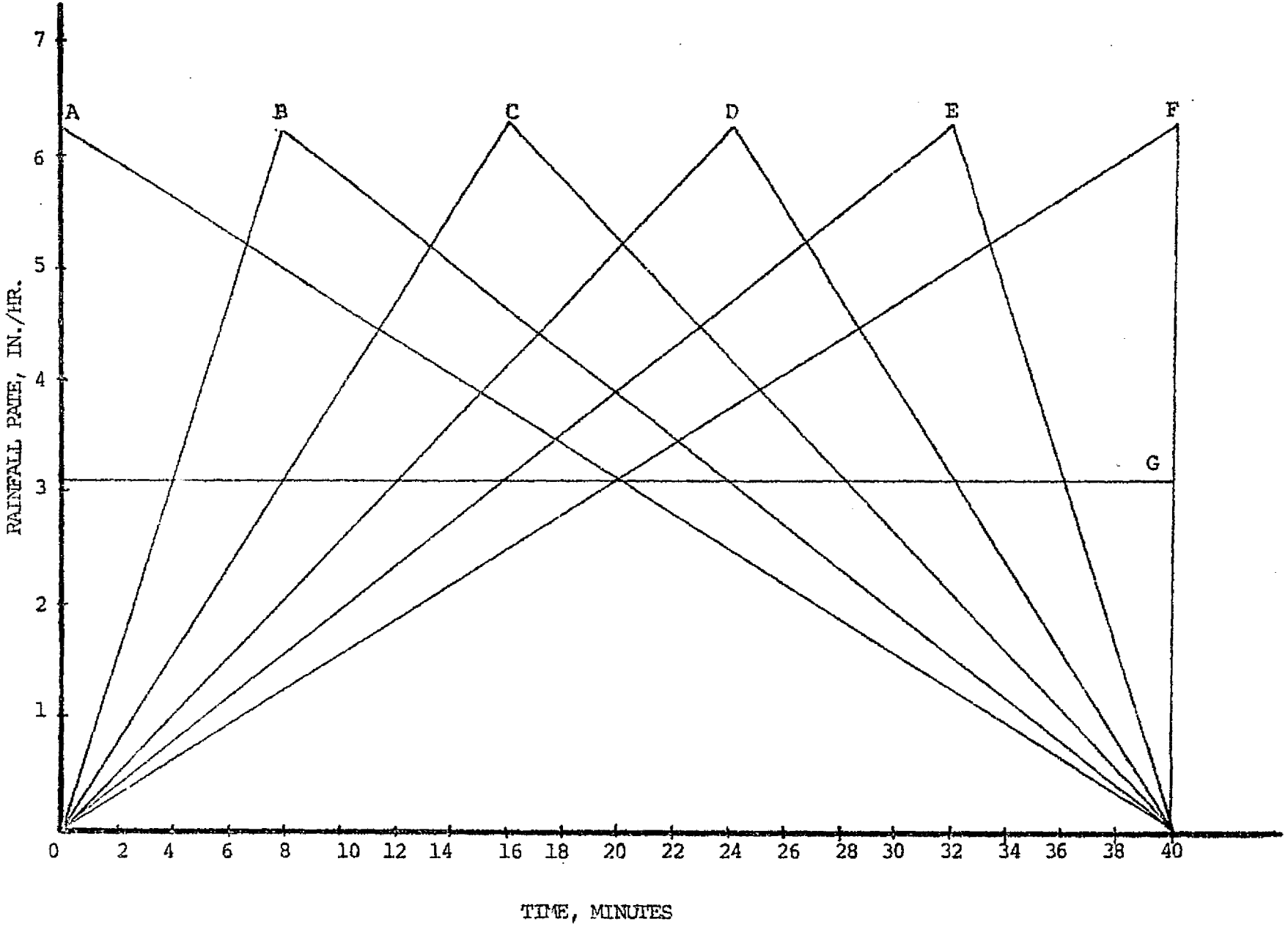

FIGURE 12

SENSITIVITY TO RAINFALL PEAK TIME, RUNOFF OUTPUT

1 PLANE S = .05 N=.05 L=1000'

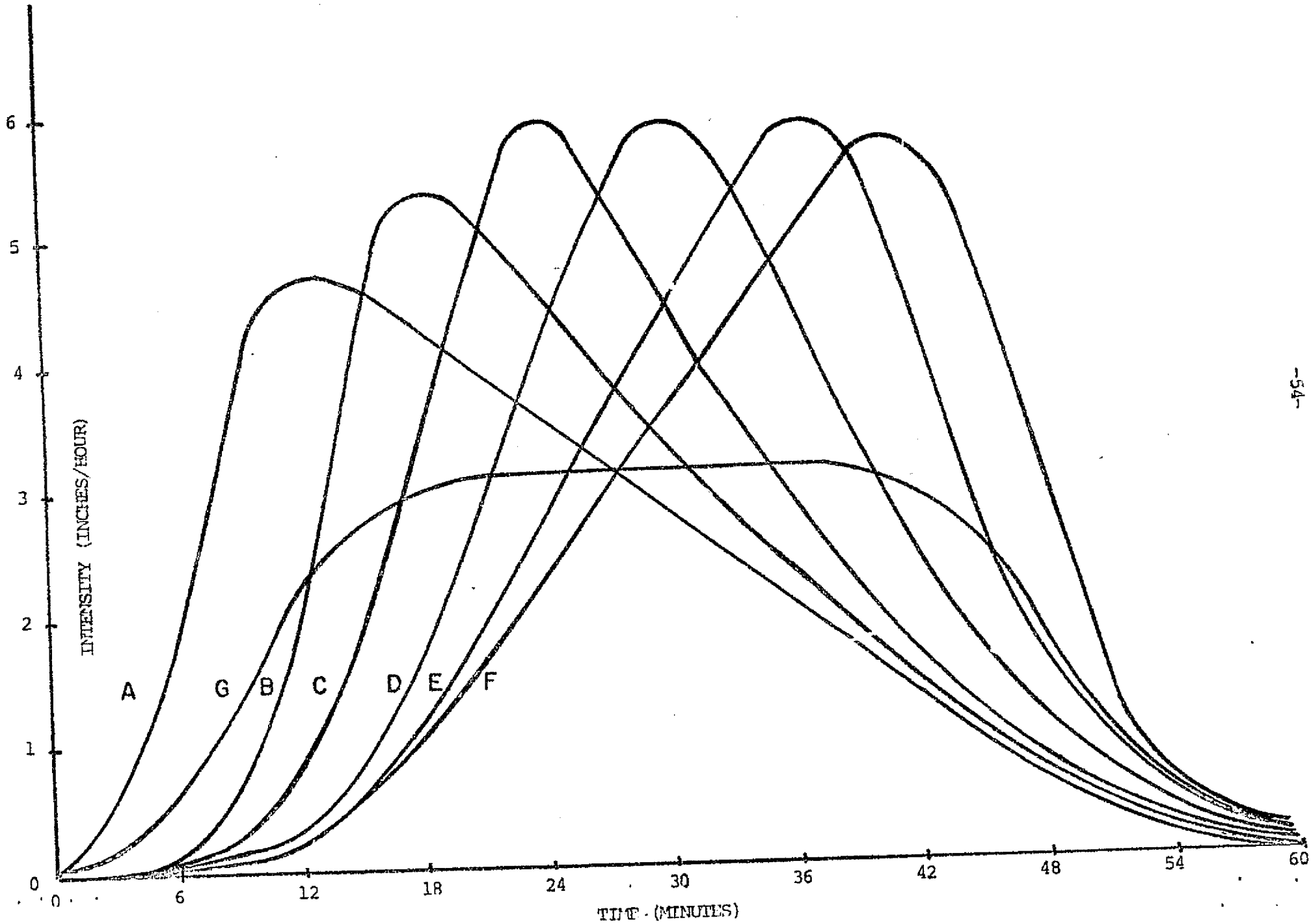

As regards the sensitivity to timing of the rainfall peak, Figure 12 shows that, among the triangular rainfalls, the discharge peak varies as the time of peak rain, rising to a maximum and then falling off. The highest discharge peak results from rainfalls C and D. Though special conditions, such as irregular basin shape, can alter the conclusion, it appears valid to assume that the planning rain should have its maximum occur near the midpoint of its duration.

The appropriate duration can be estimated as well. Figure 12 shows that the highest runoff rate which can be expected from a rainfall of the volume input will occur at about minute 31. This gives an empirical estimate of the strip watershed's time of concentration. Referring to Figure 13, it can be seen that the sensitivity of discharge rate to occurrence of the peak is least in the neighborhood of t_c. It may be concluded, then, that the rainfall must be at least of duration t_c to ensure that the watershed reaches its ultimate outflow rate.

For the strip watershed simulated, the Kerby formula for the time of concentration gave an estimate of t_c of 33 minutes, satisfactory for setting the planning rain duration.

Two characteristics of the planning rain are thus defined. Its temporal profile should be triangular and its duration should be equal to the time of concentration of the basin. It remains to determine its recurrence interval.

Figure 14 shows how this question can be addressed. It presents the rainfall rates plotted against their respective recurrence intervals

FIGURE 13 SENSITIVITY OF DISCHARGE RATE TO TIME OF DISCHARGE PEAK

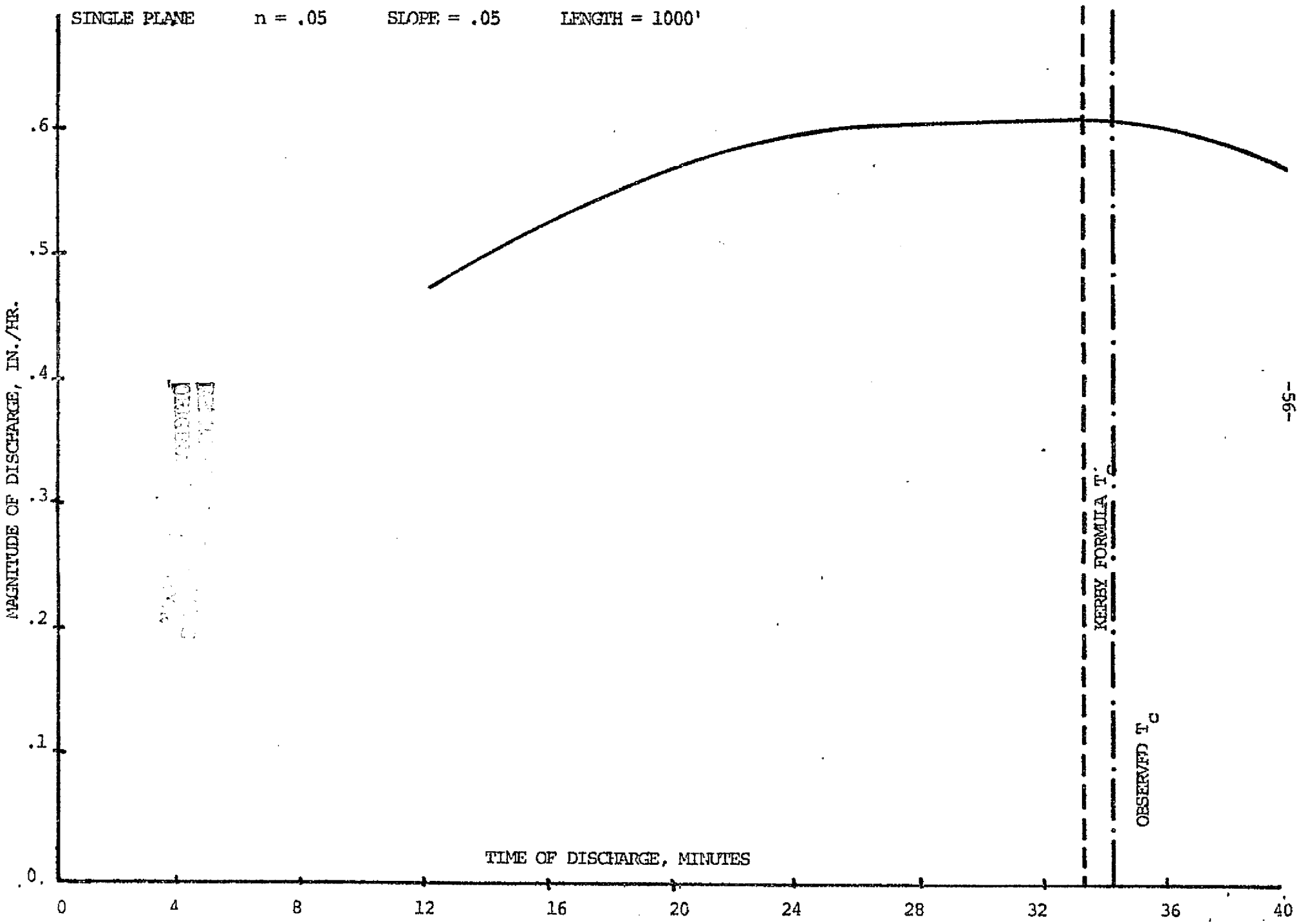

FIGURE 14 RECURRENCE INTERVAL VS. RAIN RATE

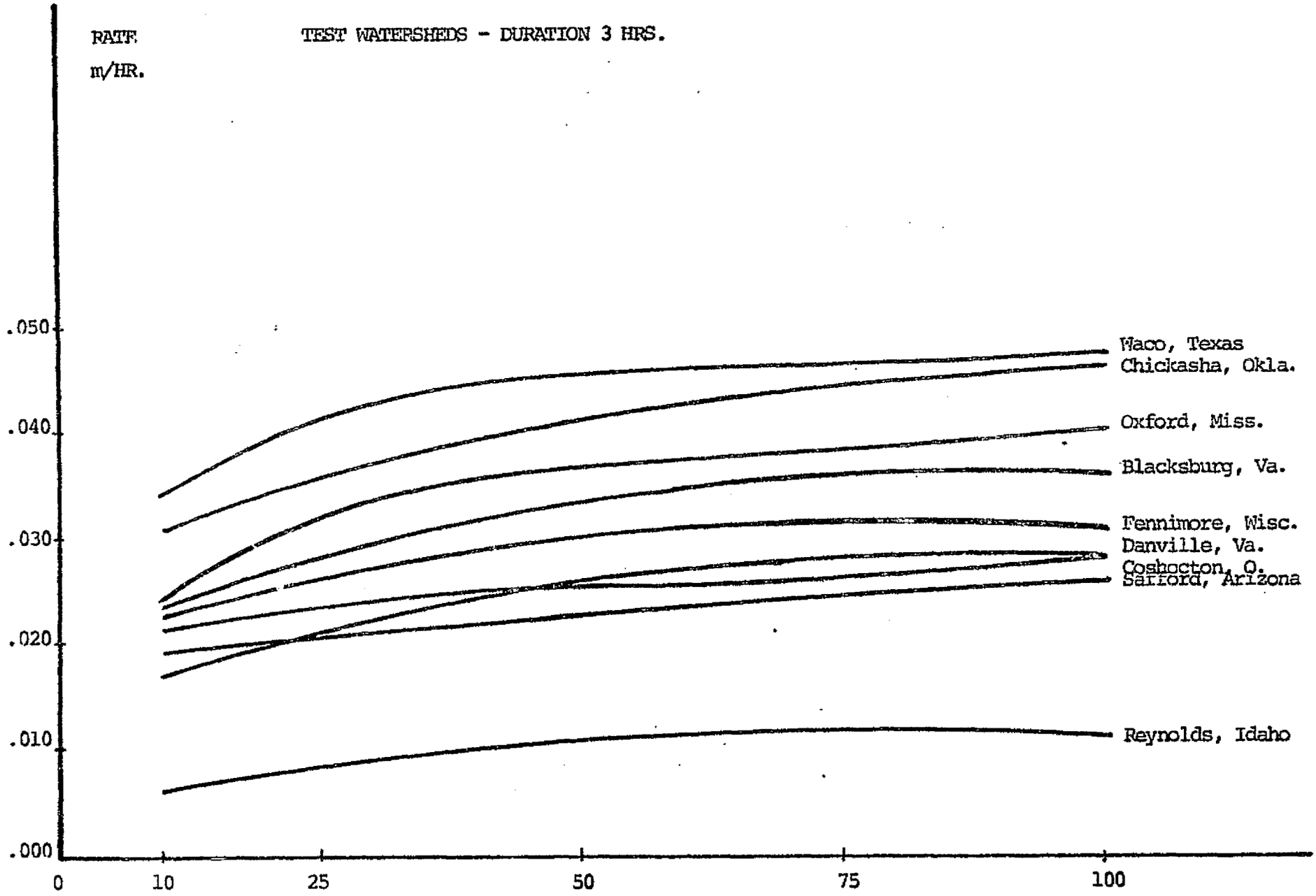

for the nine watershed sample. A marked similarity in the form of all the curves is apparent. For recurrence periods greater than approximately 50 years, the increase in rain rate is small. This suggests that, for recurrences greater than this value, the choice of rainfalls is fairly insensitive. The planning rain for development of the routing model was therefore selected as one of triangular shape, with duration equal to the time of concentration, and of recurrence interval of 50 years.

3.2.2) Analysis of Seasonal Factors Affecting Peak Flow Events

Watersheds are not static, but vary with time due to man-made alterations, and cyclically within each year because of the effect of seasonal changes. The response of watersheds to rainfall inputs, therefore, will also vary with time and season. Thus hydrologic planning models will be most accurate if they mirror the conditions extant in the basin during the season when the peaks are most likely to occur. It is therefore important to ascertain whether runoff peaks exhibit seasonal regularities and to identify the critical seasons for the watershed under study.

A geographically diverse sample of watersheds was selected for this analysis, comprising 15 ARS basins with records longer than 15 years. The annual peak discharge for each basin by year and month of occurrence was recorded, and a chart prepared showing the probability that an annual peak would happen in any given month. Figure 15 exemplifies the findings. The analysis permits the tentative conclusion that in the regions where peak events are dominated by surface para-

FIGURE 15

PEAK RATE OCCURENCE

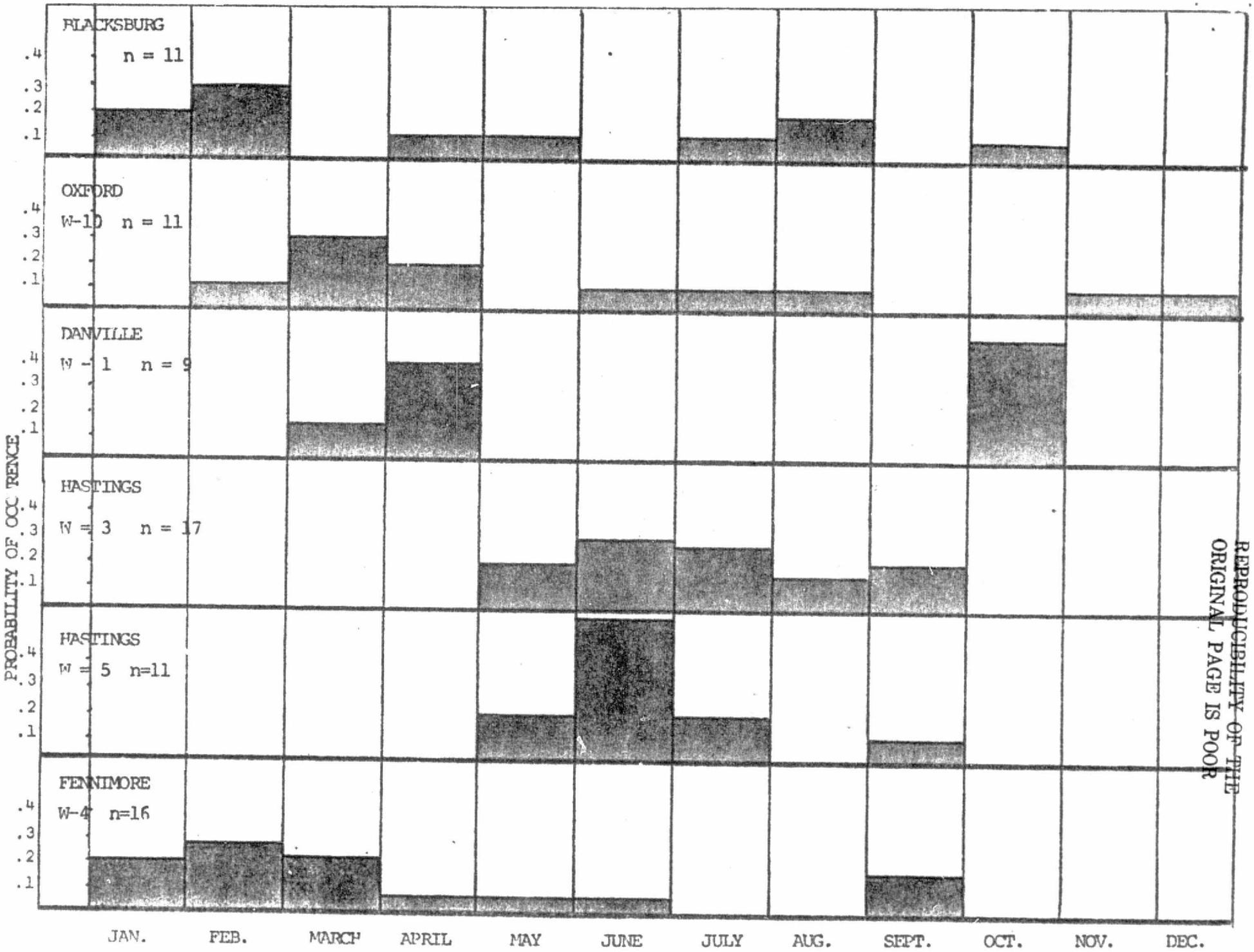

meters, (Danville, Blacksburg) the distribution is bimodal, i.e. flood peaks tend to occur in two distinct periods of the year, typically late spring and late summer. Watersheds in transition regions (Coshocton, Waco) exhibit a less marked seasonal tendency. The probability of occurrence of peak flows is more equally spread over a six to nine month interval. Those basins which are heavily sub-surface dominant (Safford, Albuquerque) show single-mode distributions. Nearly all their peak flows occur within a three month period in late summer.

For each sample basin the annual peak discharges were ranked from largest to smallest over the period of record. These data were graphed to show larger-recurrence flows at the top, and the more frequent events at the bottom. Figures 16, 17 and 18 show the modal effects described above. Other conclusions which can be drawn are as follows:

1) In the sub-surface dominant areas, flows occur during one season (July-September) regardless of recurrence intervals. The sample contained five such basins with a total of 126 annual peaks: 86% of these occurred in the interval above, with most of the remainder in June and October.

2) Figure 19 demonstrates an effect observed in several of the other watersheds. Though lower-recurrence flows occur in many different months, the highest 3 or 4 flow events are confined to about three consecutive months.

FIGURE 16 BIMODAL DISTRIBUTION (SURFACE DOMINANT)

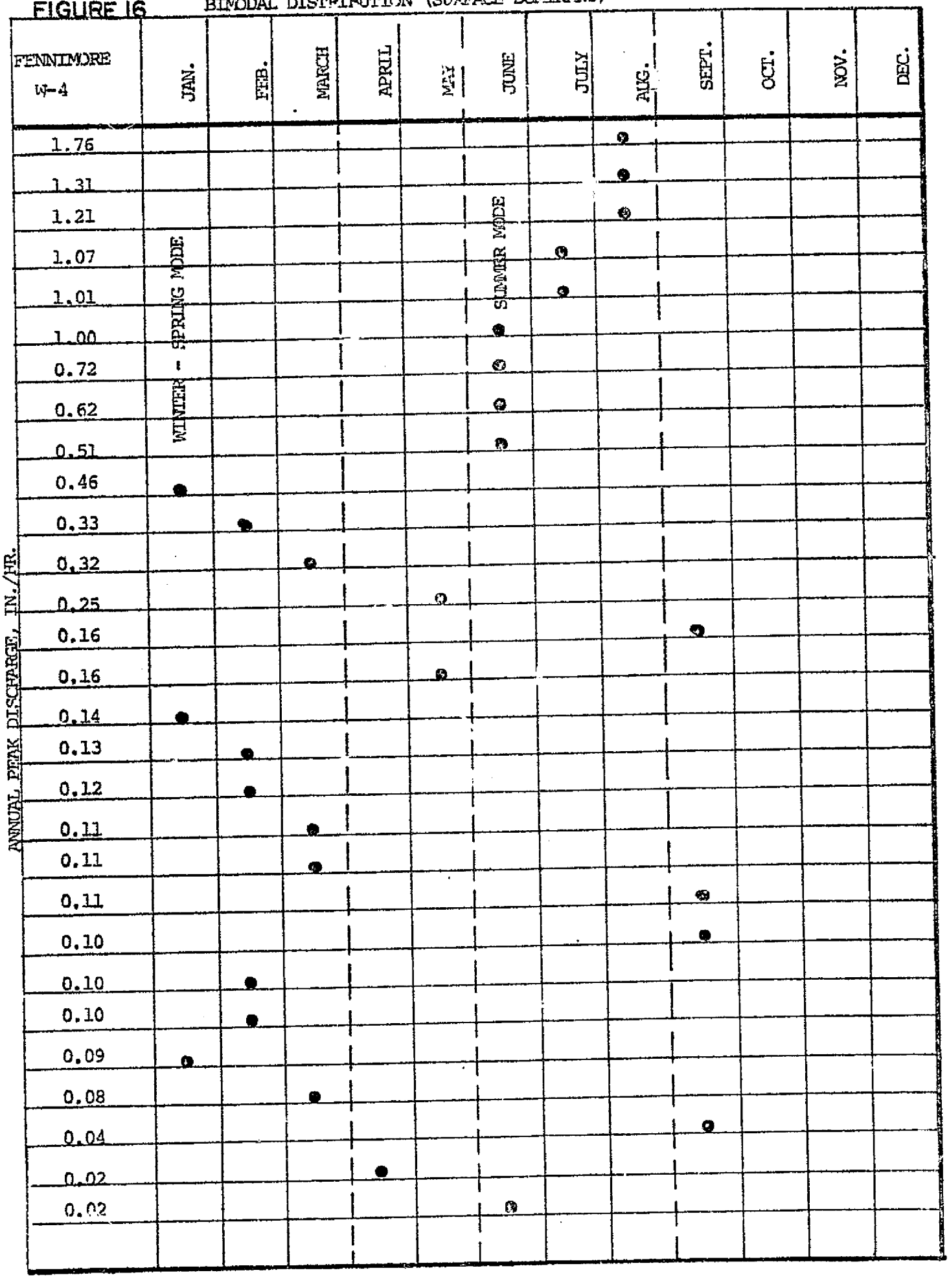

SINGLE MODE DISTRIBUTION (SUBSURFACE DOMINANT)

FIGURE 17

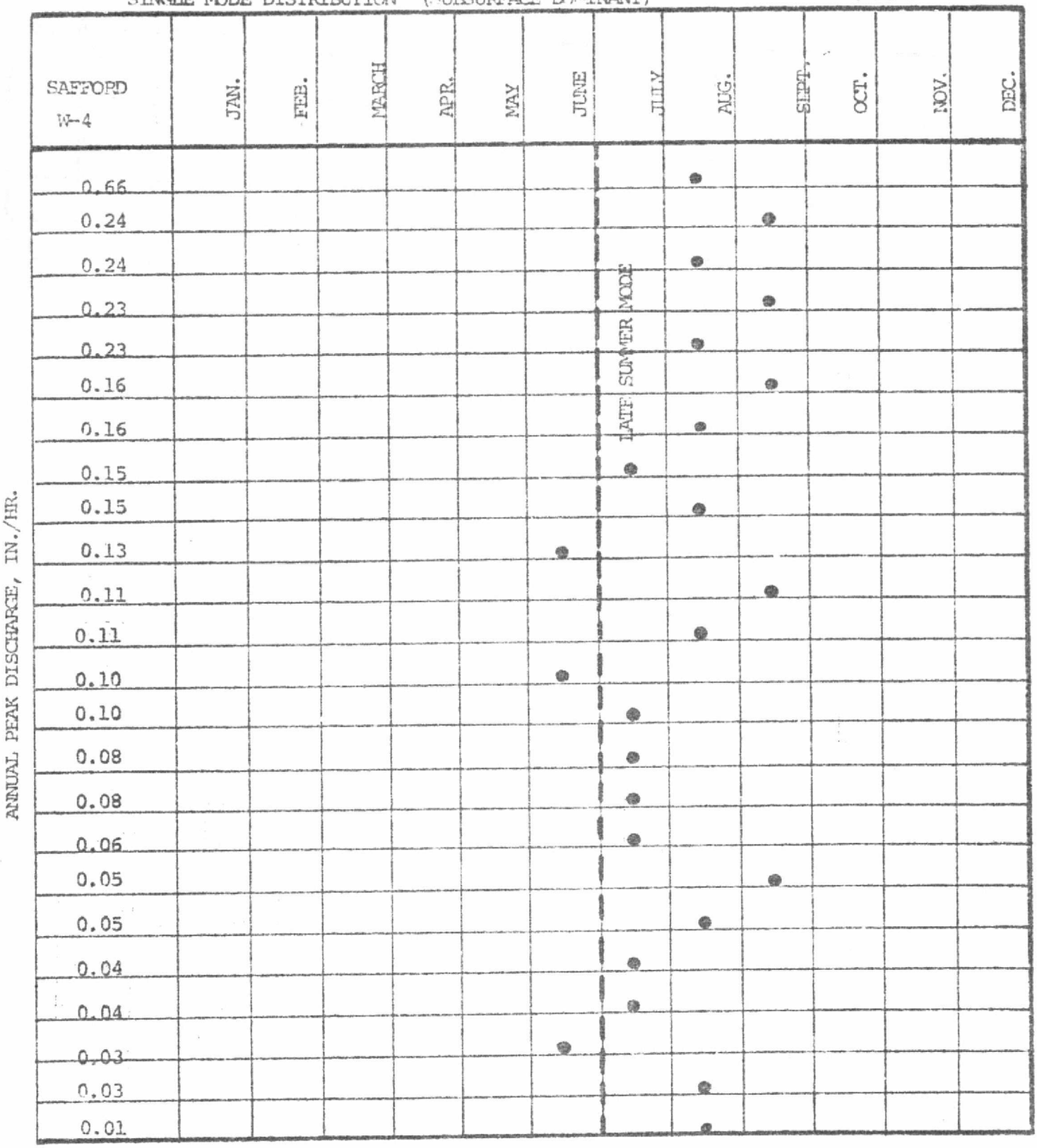

FIGURE 18 NO STRONG MODAL TENDENCY (TRANSITION)

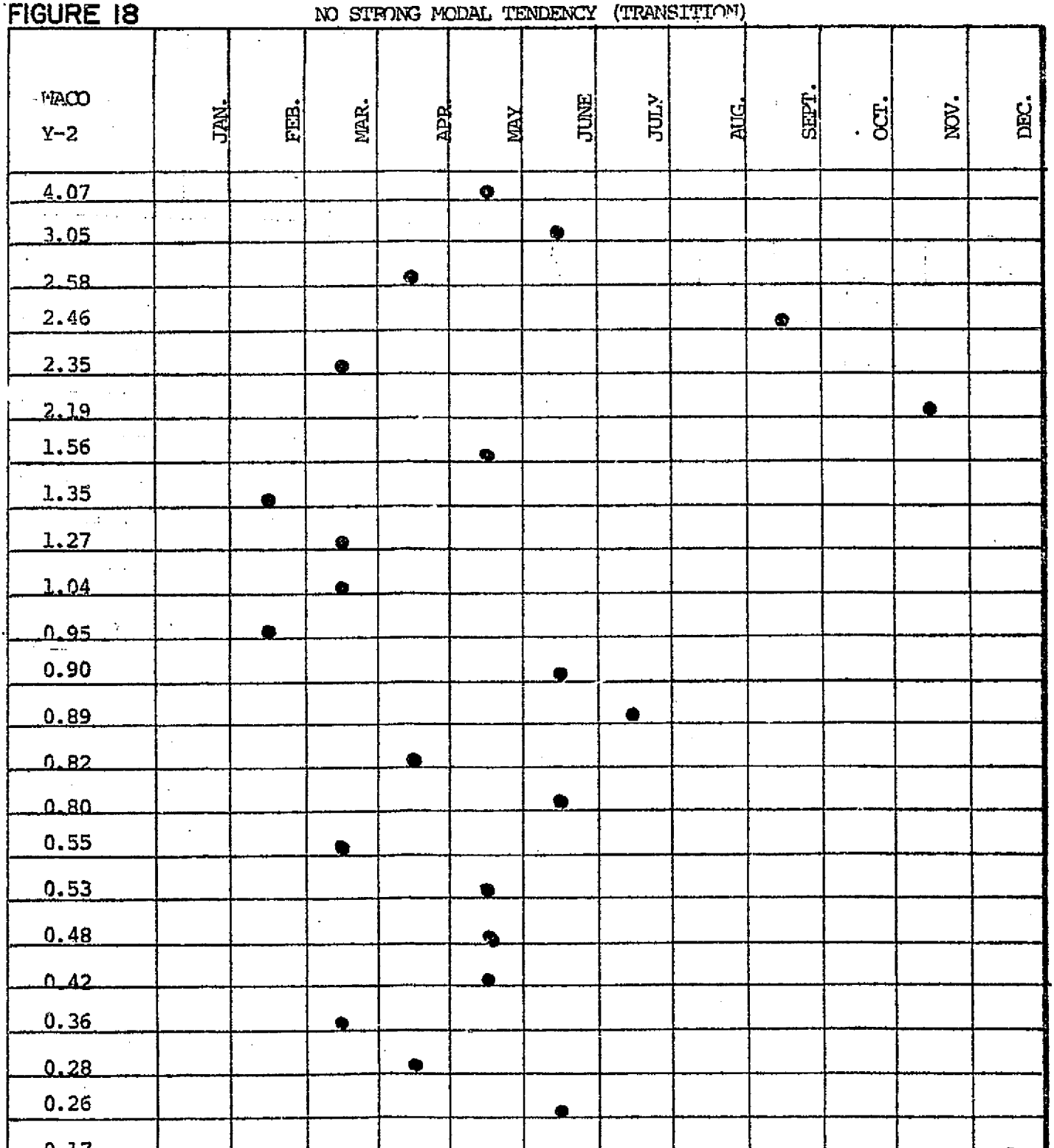

FIGURE 19 OCCURRENCE ENVELOPE

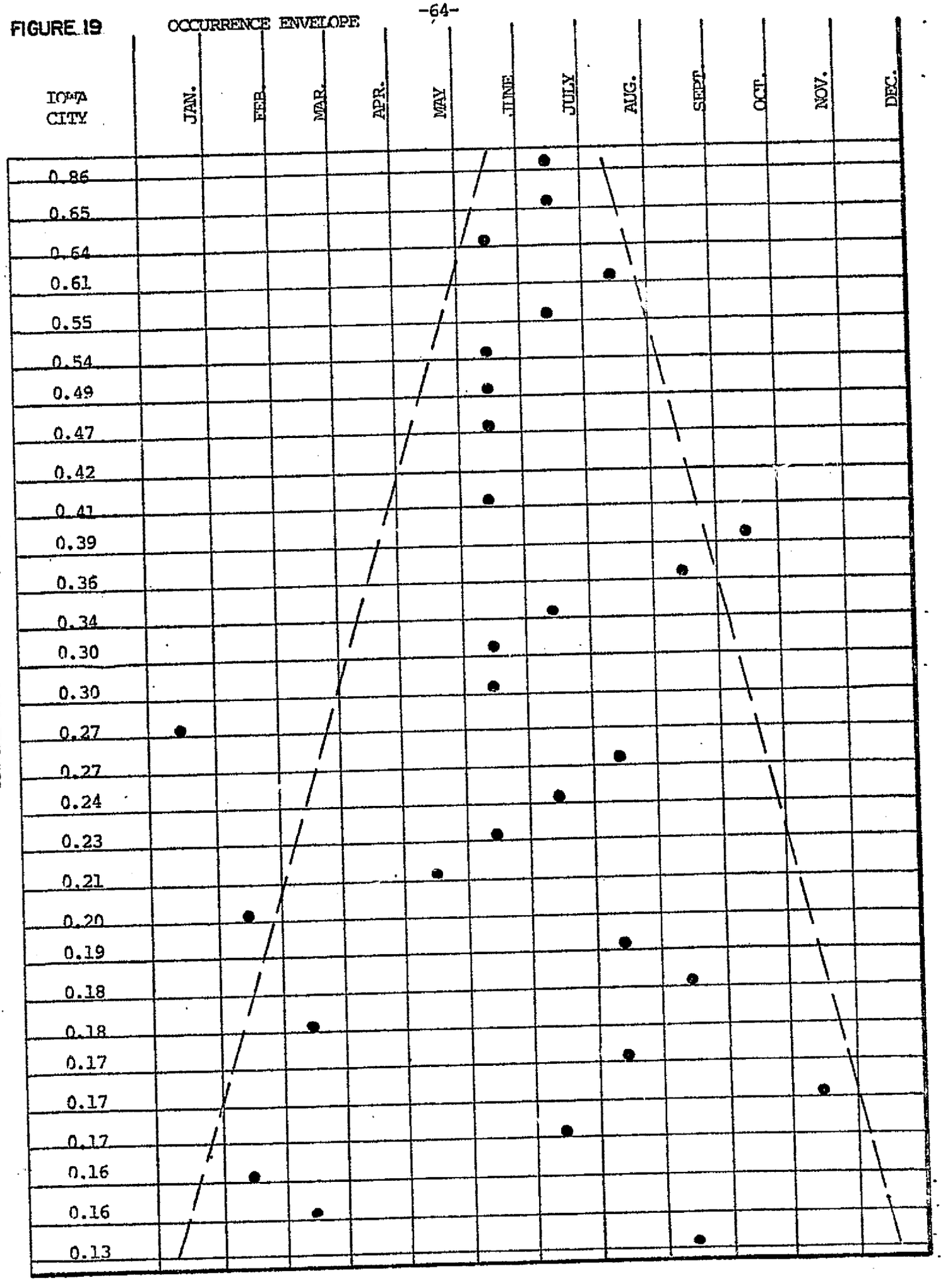

Since the analysis above considered discharge events of all recurrences, a subsequent analysis was undertaken to chart the behavior of the large recurrence flows only. Table 16 supplies the months of occurrence of the four largest discharges for the selected watershed sample.

TABLE 16 FLOW RATE RECURRENCE RANK

	1	2	3	4
Safford, Arizona #W-1	Sept.	Aug.	Aug.	July
Safford, Arizona #W-4	Aug.	Sept.	Aug.	Sept.
Safford, Arizona #W-5	July	Aug.	Aug.	July
Albuquerque, N.M., W-1	Aug.	Sept.	Aug.	June
Albuquerque, N.M., W-3	Aug.	Sept.	Aug.	July
Hastings, Nebraska W-3	July	May	July	May
Hastings, Nebraska W-5	July	June	June	June
Coshocton, O., #5	June	Aug.	June	July
*Coshocton, O., #10	June	Sept.	July	April
*Waco, Texas, C	March	Aug.	April	June
*Waco, Texas, W-2	May	June	April	Nov.
*Waco, Texas, Y-2	May	June	April	Sept.
*Stillwater, Okla., W-4	April	Oct.	July	May
Iowa City, Iowa	July	July	June	Aug.
Fennimore, Wisconsin, W-4	Aug.	Aug.	Aug.	July

Those watersheds which showed no seasonal trend are starred. The Coshocton, Waco, and Stillwater basins, as noted earlier, are in transition regions and show no seasonal skewness. From the data above it would appear that, except for transitional regions, peak flows tend to occur during a particular season. Therefore, the watershed conditions extant in that season should be reflected in the hydrologic model.

This hypothesis was tested further by performing a similar analysis for discharge volume rather than rate. Table 17 gives the month of

occurrence of the maximum two hour discharge volume. Again, the four highest events for the period of record are presented.

TABLE 17 FLOW VOLUME RECURRENCE RANK

	1	2	3	4
Safford, Arizona, W-1	Sept.	Aug.	Aug.	Sept.
Safford, Arizona, W-4	Aug.	Sept.	Aug.	Sept.
Safford, Arizona, W-5	July	Aug.	Aug.	Aug.
Albuquerque, N.M., W-1	Aug.	Sept.	Aug.	Aug.
Albuquerque, N.M., W-3	Sept.	Aug.	June	Aug.
Hastings, Nebraska, W-3	May	June	July	July
Hastings, Nebraska,W-5	June	June	July	May
Coshocton, O. #5	June	Aug.	June	March
*Coshocton, O, #10	June	Sept.	July	April
*Waco, Texas, C	March	Aug.	April	Dec.
*Waco, Texas, W-2	May	April	June	Nov.
*Waco, Texas, Y-2	May	April	March	June
*Stillwater, Okla., W-4	April	May	July	Oct.
Iowa City, Iowa	July	Aug.	July	July
*Fennimore, Wisconsin, W-4	Aug.	July	July	Jan.

The starred watersheds once more exhibit a weaker seasonal tendency. With the exception of the Fennimore basin, the rate and volume samples are the same. Comparison of the rate and volume table yields the following information:

1) Of the 60 sample points, 58% of the rate and volume peaks occur in the same month, and 80% occur within one month of each other.

2) Only seven of the samples did not occur in the same season.

Therefore, except in transitional regions, flood rates and volumes exhibit a propensity to occur in a particular three-month season, typically spring or late summer. A planning model, then, will be more likely to produce acceptable estimates if the condition present in these seasons are reflected.

3.2.3) Analysis of Sensitivity of Runoff to Surface Parameters

The purpose of this analysis is twofold:

1) to determine how accurately surface characteristics must be measured for input to models, i.e., what are acceptable errors in estimation of values of hydrologic parameters.

2) to develop a rationale for "averaging" surface parameters - for summing the values for each point on the watershed into some computationally manageable unit.

In the first phase of this effort, sensitivity to sub-surface drivers was analyzed via analog computer programs. This task, therefore, centered soley upon investigation of sensitivity to surface parameters. The strip model described earlier was employed, because it provided the capability to vary all surface drivers and determine changes in the resultant runoff. Computer runs were made to assess the sensitivity of discharge to slope and surface friction.

All computer runs assumed constant rain. The combination of triangular rain profiles and varying surface parameters is reserved for a subsequent phase of this effort. Also, the computer runs assumed a strip of fixed total length and a fixed duration and intensity of rain. Thus the results presented hereinafter are to be considered as indicative only. The generalization of the results to strips of arbitrary length, and rains of arbitrary intensity and duration is reserved for later phases of this effort.

1. The Effect of Slope on Runoff Peak: 30 runs

A series of computer runs were made to determine the effect of various slopes typical of rural watersheds (0.01 - 0.20) on both a single-plane strip and a two-plane strip. The first series assumed a strip of unit width, constant surface friction (n = .05) and length (l = 305m) and variable slope. A constant rainfall (P = 8cm/hr) was mathematically applied to the strip and the runoff hydrograph recorded for slope values of .01, .05, .15 and .20. The results show that the value of slope impacts the timing of the occurrence of the discharge peak, i.e., the time of concentration. As expected, higher slopes produce a shorter t_c; this, in turn affects the design duration of the planning rainfall. Figure 20 shows, for example, that the 20% slope produces a time of concentration of approximately 16 minutes where a 5% slope gives a t_c of 20 minutes. At a given recurrence interval, say 50 years, and for a given regional rainfall formulation, say Oxford, Mississippi, this change in slope results in an approximate decrease in peak rate of 11%. For the same set of assumptions, however, a change in slope from 5% by the same proportion to 1.25% gives a 38% decrease in peak rate. The conclusion is that slope must be measured more critically for flatter basins (S < 5%). In addition, the results (Figure 20) show that the duration of the peak is a function of slope, asymptotically approaching 20 minutes. As shown in Figure 21, for slopes less

FIGURE 20 SENSITIVITY TO SLOPE 1 PLANE S-VARIABLE N-.05 L-1000' EACH PLANE

UNIFORM RAIN: RATE = 3.1"/HR

40 MIN. DURATION

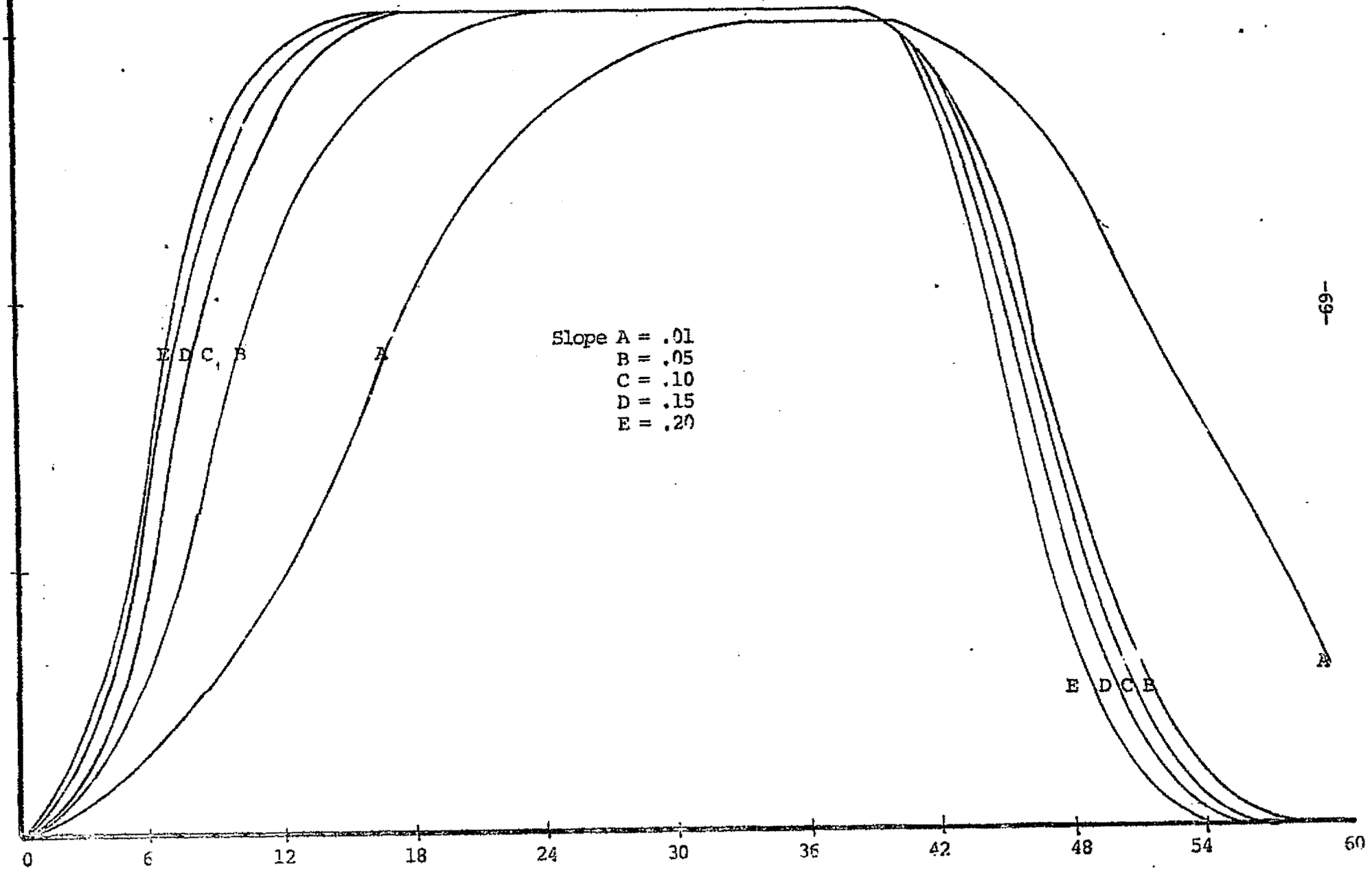

FIGURE 21

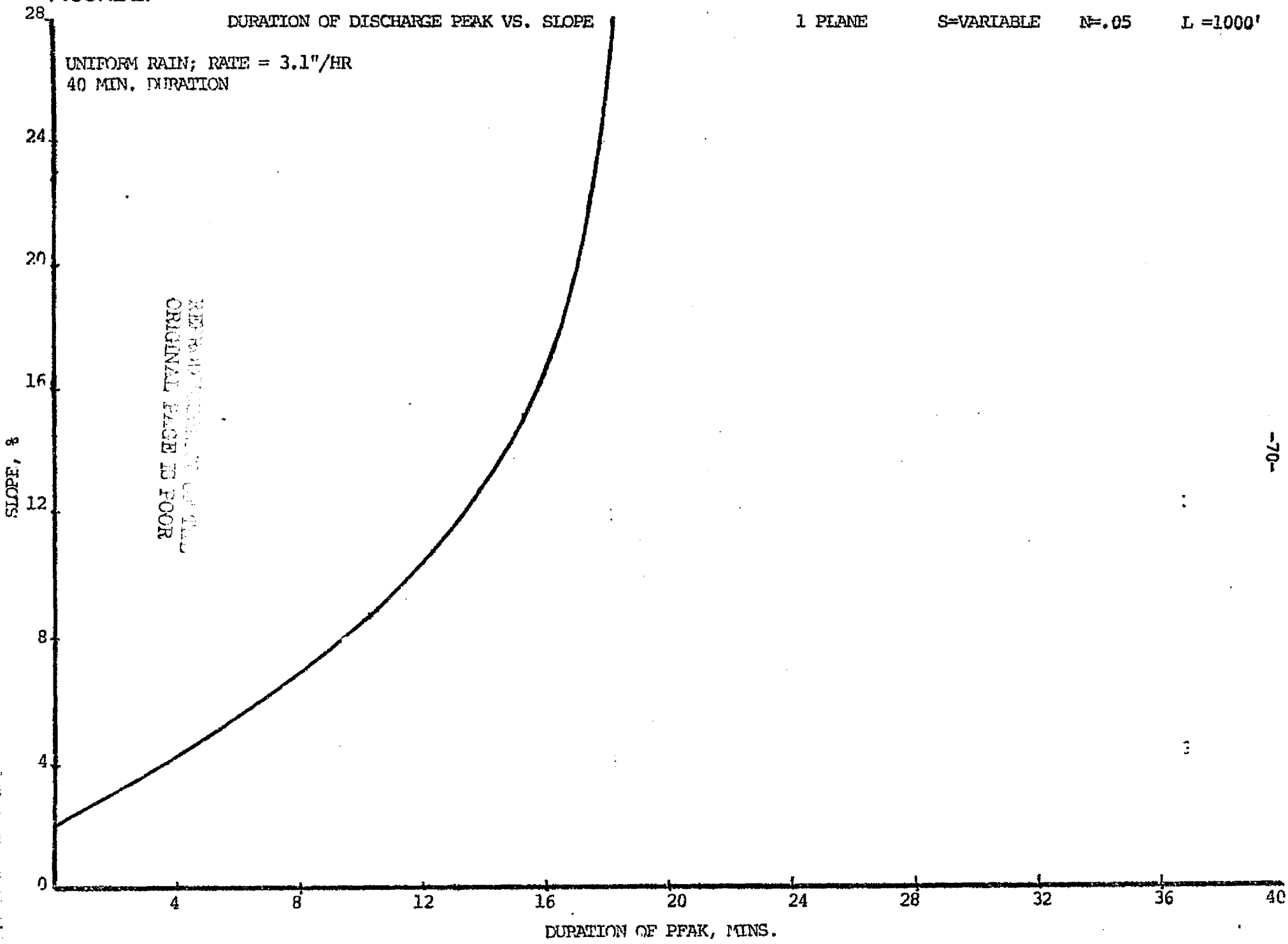

FIGURE 23

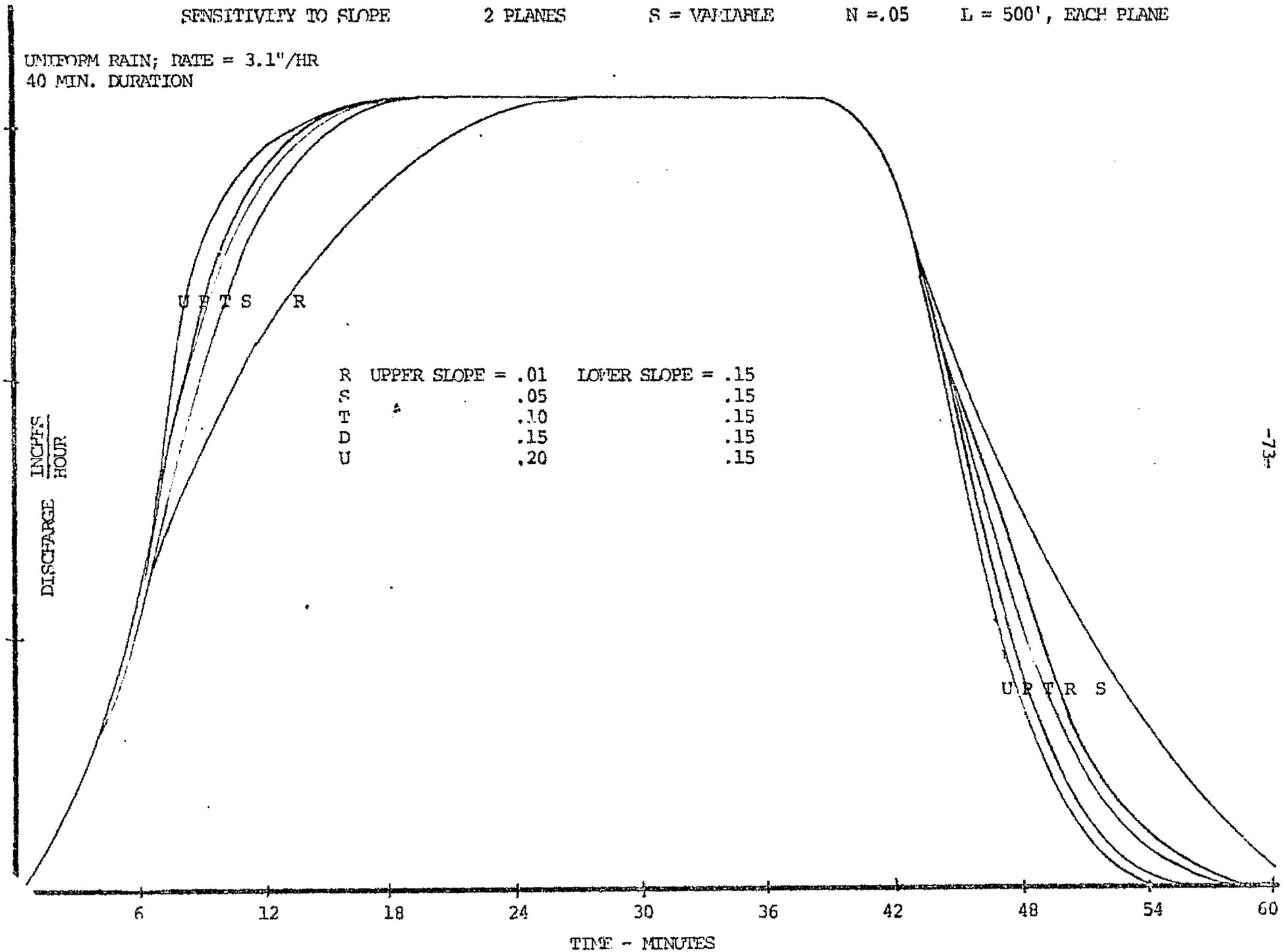

FIGURE 24 SENSITIVITY TO SLOPE 2 PLANES S = VARIABLE N = .0, L = 500', EACH PLANE

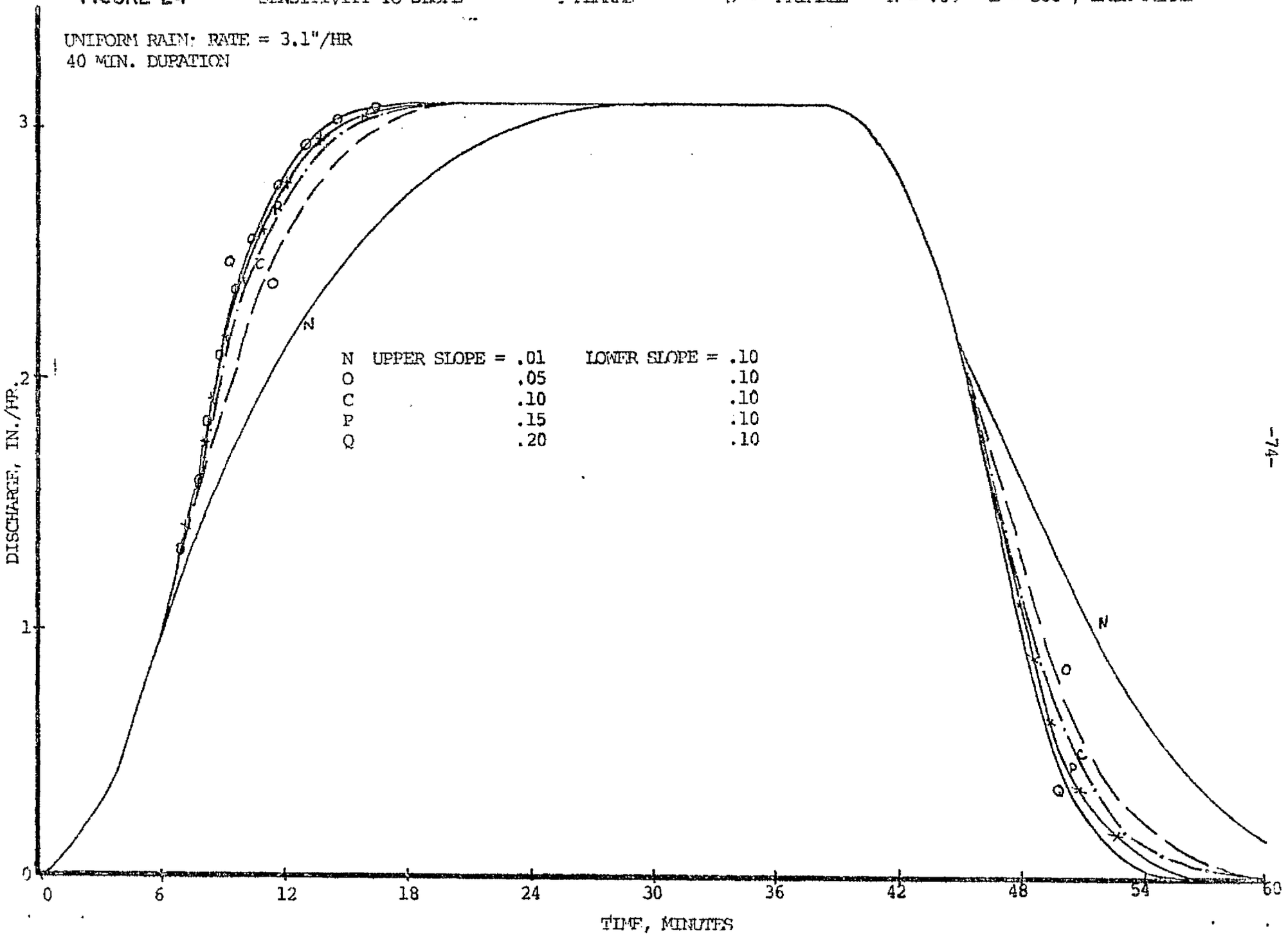

FIGURE 25 SENSITIVITY TO SLOPE

2 PLANES S = VARIABLE N = .05 L = 500', EACH PLANE

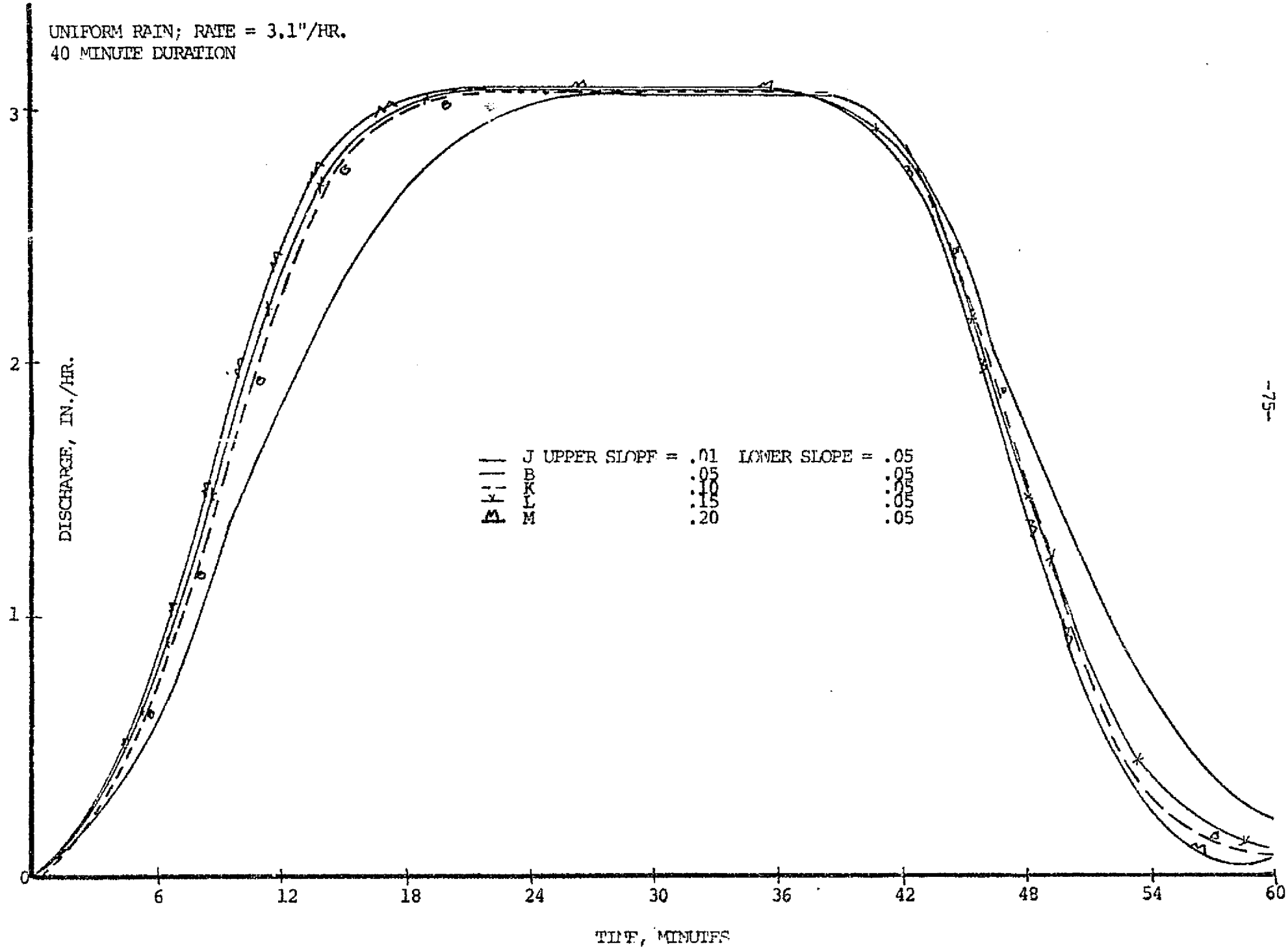

FIGURE 2.6

SENSITIVITY TO SLOPE

2 PLANES S = VARIABLE N = .05 L = 500', EACH PLANE

UNIFORM RAIN; RATE 3.1"/HR.
40 MINUTE DURATION

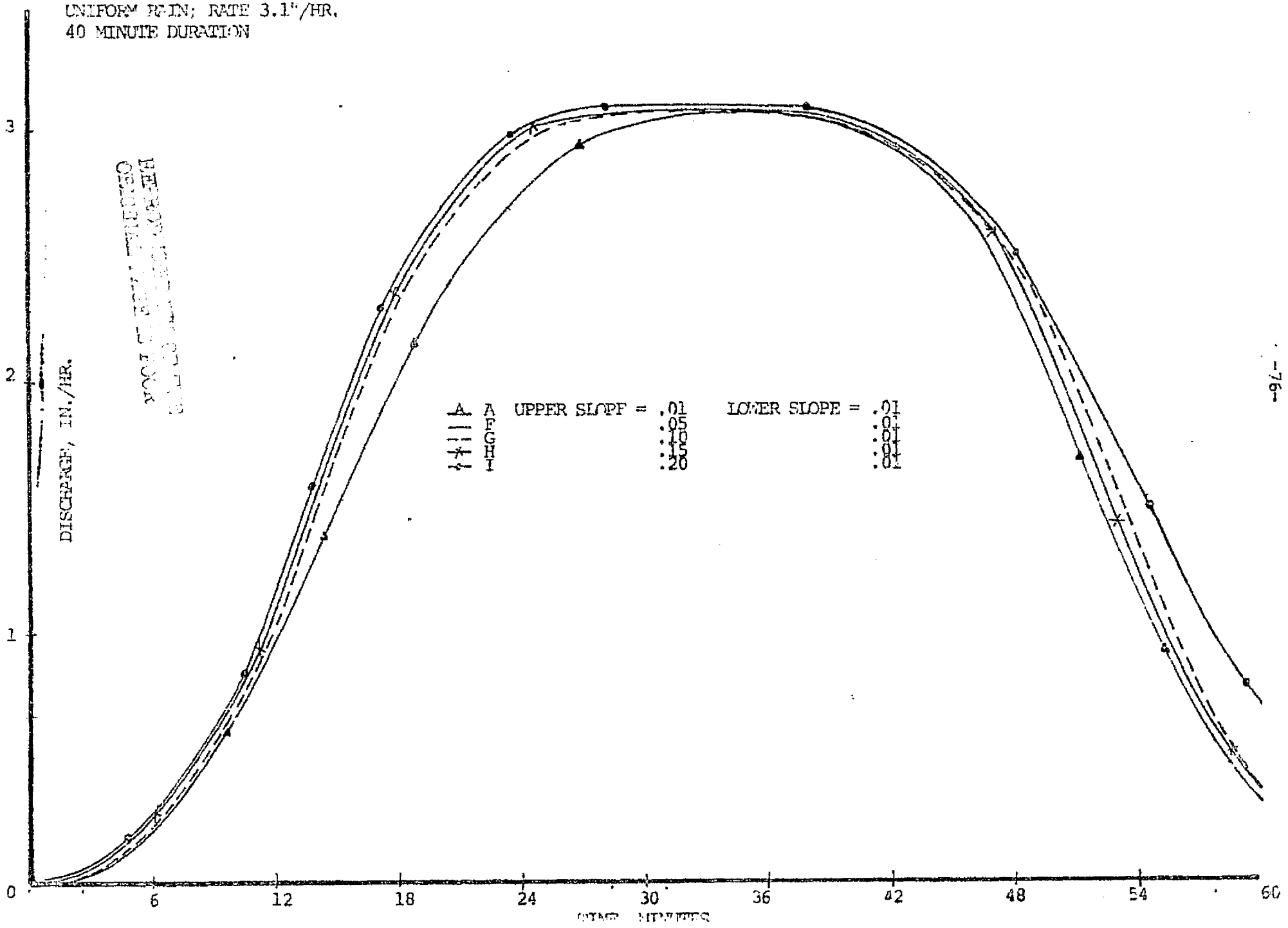

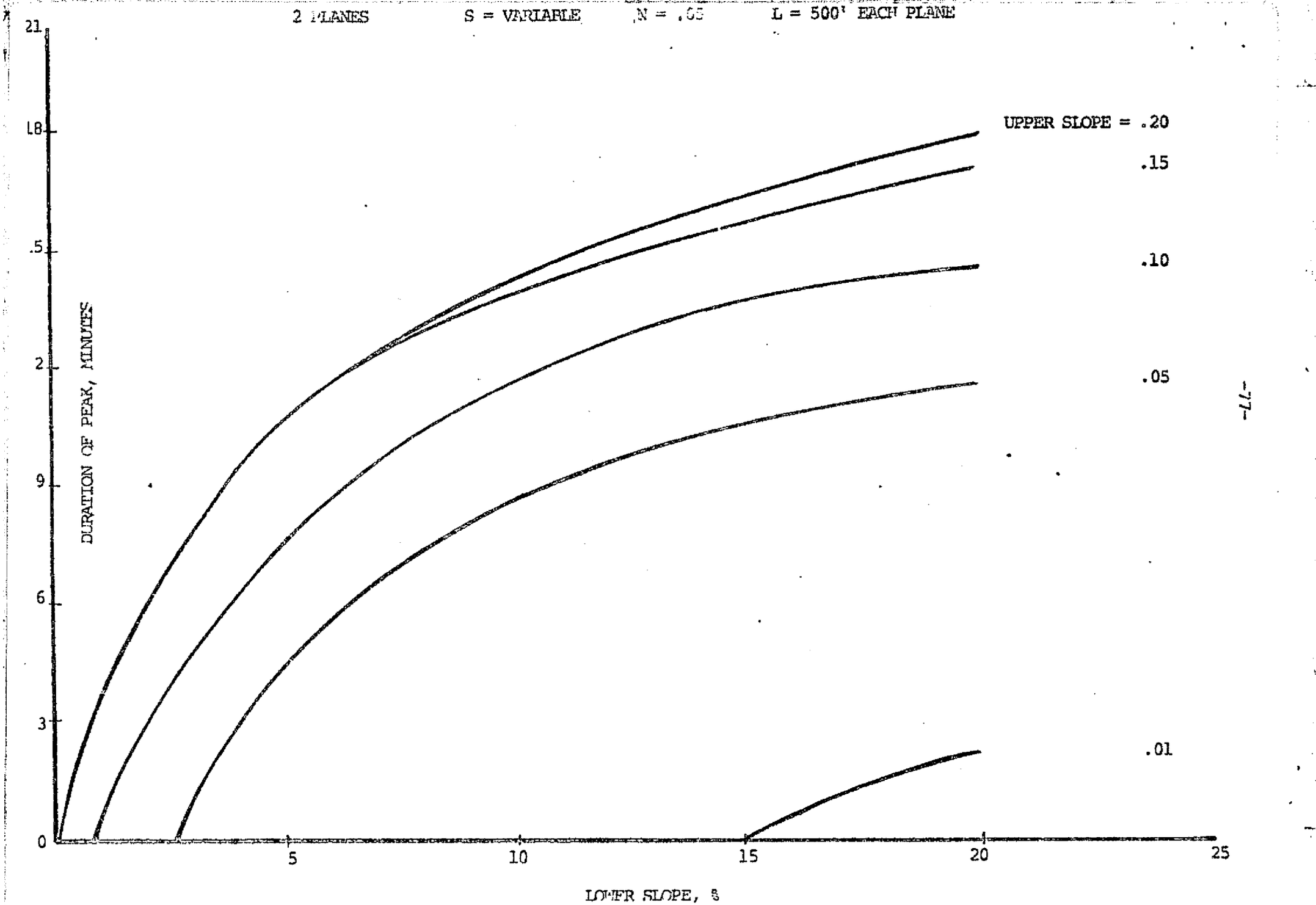
2 PLANES
S = VARIABLE
N = .03
L = 500' EACH PLANE
21
18
.5
2
9
6
3
0
DURATION OF PEAK, MINUTES
UPPER SLOPE = .20
.15
.10
.05
.01
5
10
15
20
25
LOWER SLOPE, S

gressively increasing number of straight planes. Figures 28 and 29 present the results.

The approximation of the watershed profile by a single plane produced errors of [illegible]% in the peak rate duration. The inclusion of a second [illegible] greatly increased accuracies. Further approximation did not, however, produce significant improvement. This suggests that only major changes in watershed topography need to be accounted for. Small fluctuations (<5%) in slope can be smoothed over without loss of accuracy.

2. The Effect of Surface Friction on Runoff Peak:

The surface runoff models uses Manning's "n" as a measure of flow resistance due to surface roughness. Overland flow was modelled for both the one and two plane cases with varying surface roughness. In the single plane run, the strip chosen was identical to that used in the slope sensitivity runs. All parameters were held constant (slope = .05; l = 305m; P = 8cm/hr) while Manning's "n" was varied, (n = .01 to .10) representing surface covers from concrete to heavy forest. Surface friction was found to affect peak discharge rate as shown in Figure 30. The time of concentration chosen for the planning rain will vary from 9 (Graph A) to 39 minutes (Graph E) depending on the Manning's "n" selected. Errors in discharge resultant from inaccurate surface friction estimation will be most severe for low values of Manning's "n". It may be con-

FIGURE 28 SENSITIVITY TO NUMBER OF PLANES 3000' ARC

UNIFORM RAIN; RATE = 3.1"/HR.
40 MINUTE DURATION

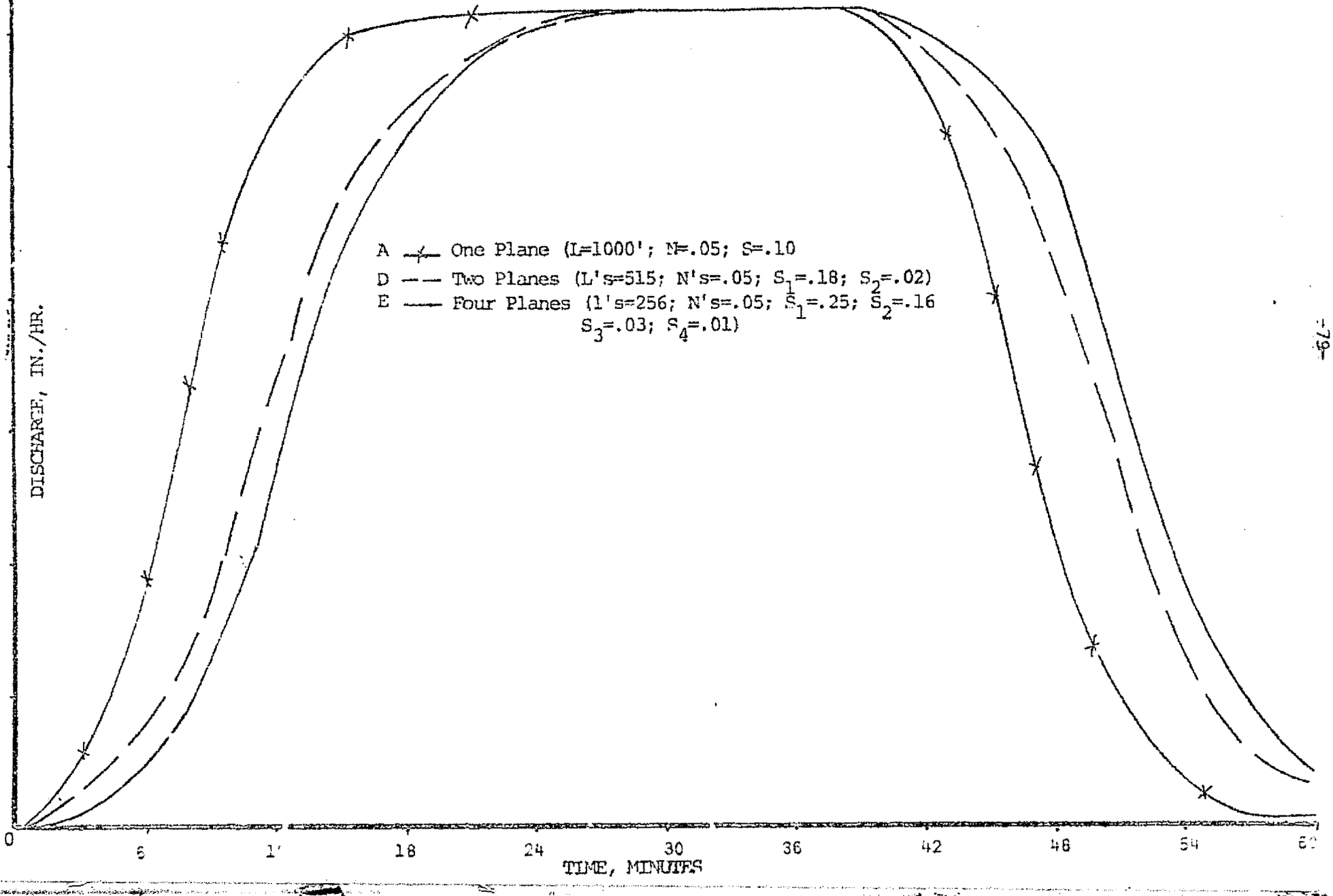

FIGURE 29 SENSITIVITY TO NUMBER OF PLANES 4000' ARC

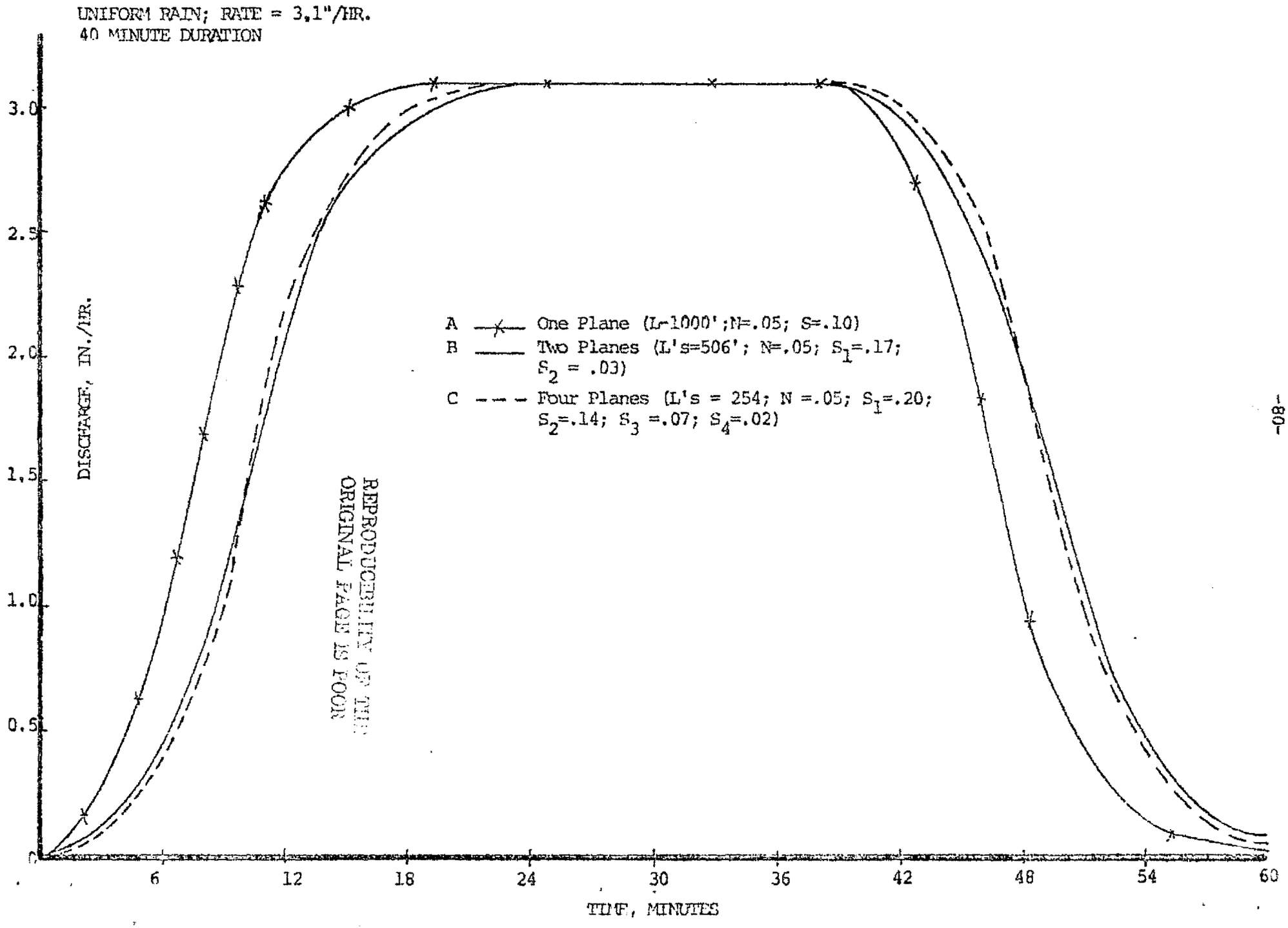

FIGURE 30

SENSITIVITY TO MANNING'S "N"

1 PLANE S = .05 N = VARIABLE L = 1000'

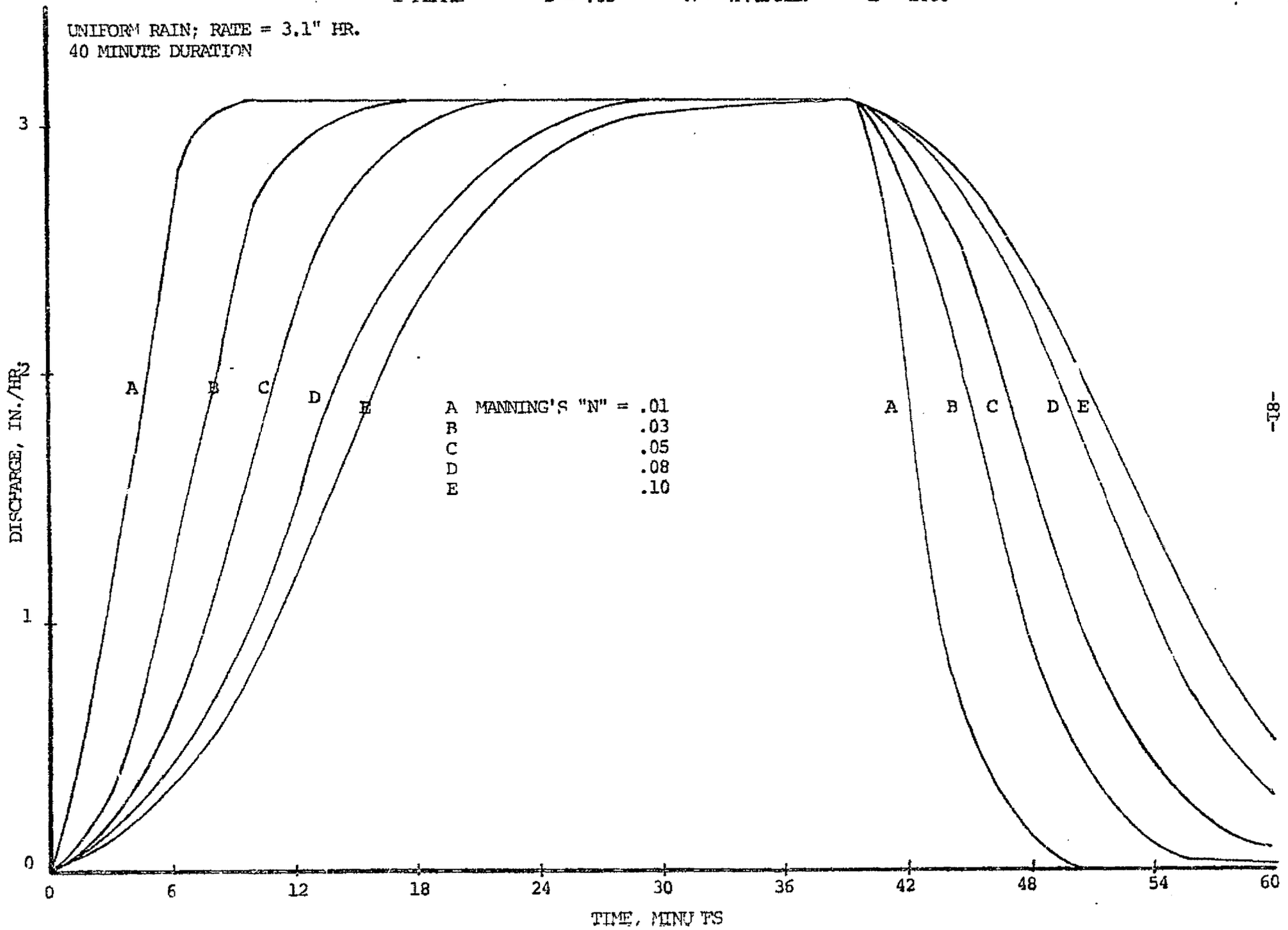

cluded then, that the more developed a watershed is, the more critical is the quantification of surface roughness. Further, peak duration were found to depend on surface roughness as shown in Figure 31. Peak duration is sensitive to surface roughness principally for more resistive surfaces ($n > 0.04$). For rural watersheds, a realistic range of Manning's "n" is from 0.03 to 0.10. In this region, a 25% estimation error will result on the average in about a 50% inaccuracy in runoff duration.

In the two-plane runs, the single strip was again divided at the midpoint. Both sections were given identical slopes and lengths, and various combinations of "n's" were modelled. The steady uniform rain was applied. Figures 32 through 37 show the sensitivity of the two plane model to surface roughness. Results similar to those of the single plane simulation were found. The impact of surface friction measurement upon estimation of t_c is most critical for low values of Manning's "n".

To date, computer analysis has been conducted for a basin strip of average dimension and for a typical rainfall input. The principal findings were:

a) Duration of runoff peak is most sensitive to slope at values less than about 10%. When slope of watersheds are greater than 10%, an average value can be approximated. In flat basins, though, more detailed ground truth should be consulted. The same sensitivity

FIGURE 31

DURATION OF PEAK FLOW VS. MANNING'S "n"

SINGLE PLANE, n = VARIABLE, SLOPE = .05, LENGTH = 1000'

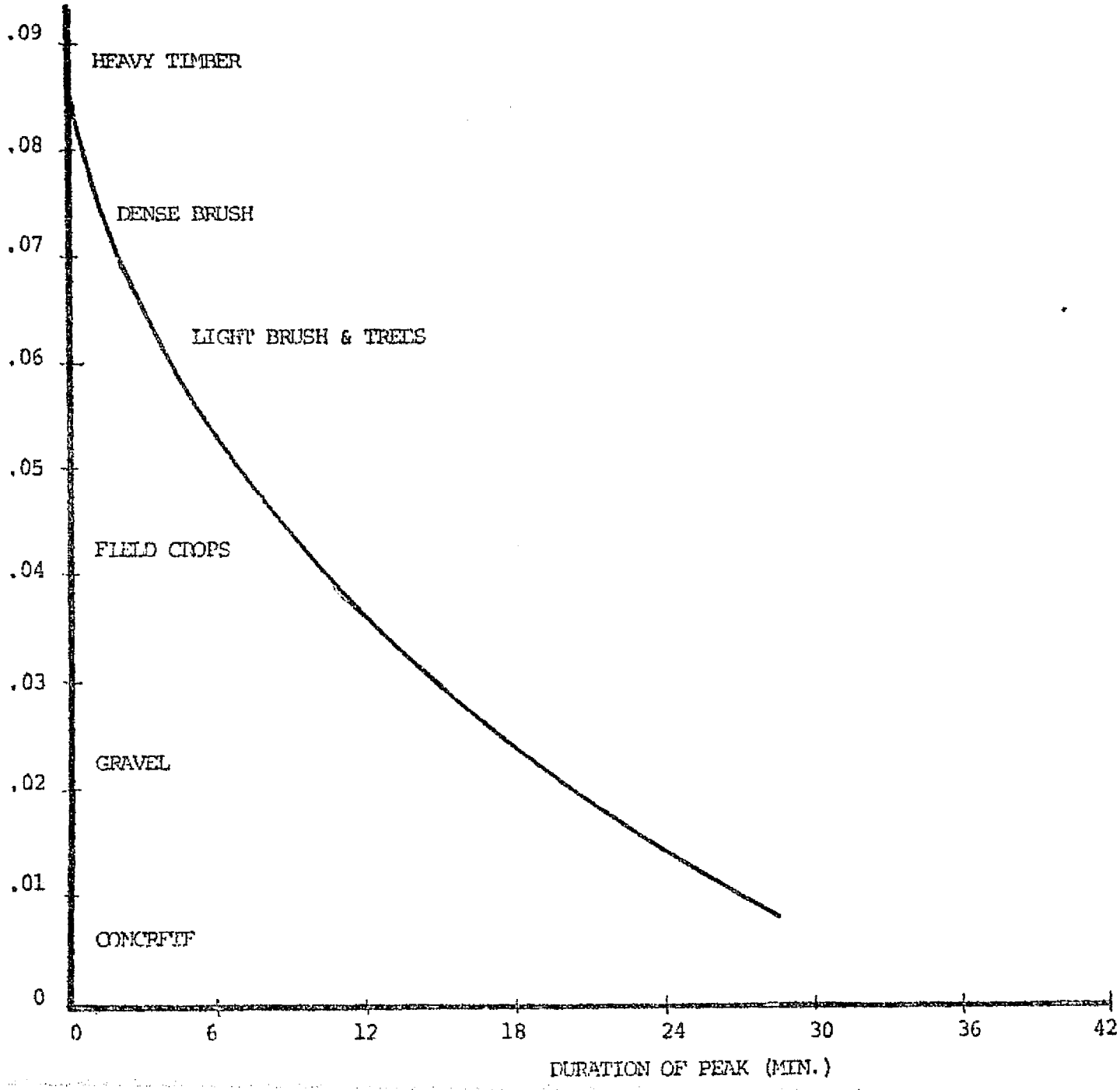

FIGURE 32

SENSITIVITY TO MANNING'S "N"

2 PLANES S = .05 N = VARIABLE L = 500' EACH PLANE

UNIFORM RAIN; RATE = 3.1"/HR,
40 MINUTE DURATION

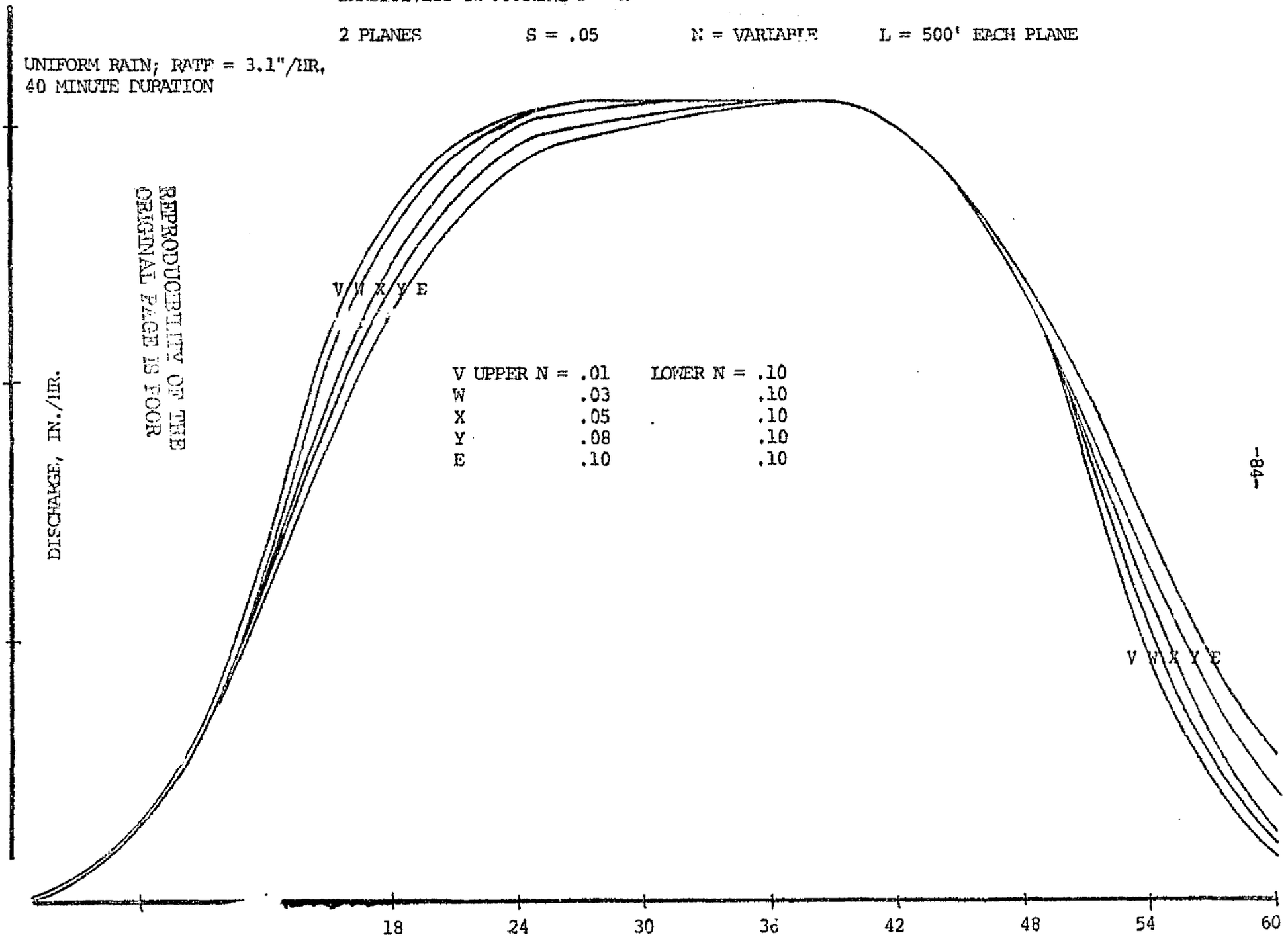

FIGURE 33

SENSITIVITY TO MANNING'S "N"

2 PLANES S = .05 N = VARIABLE L = 500' EACH PLANE

UNIFORM RAIN; RATE = 3.1"/HR.
40 MIN. DURATION

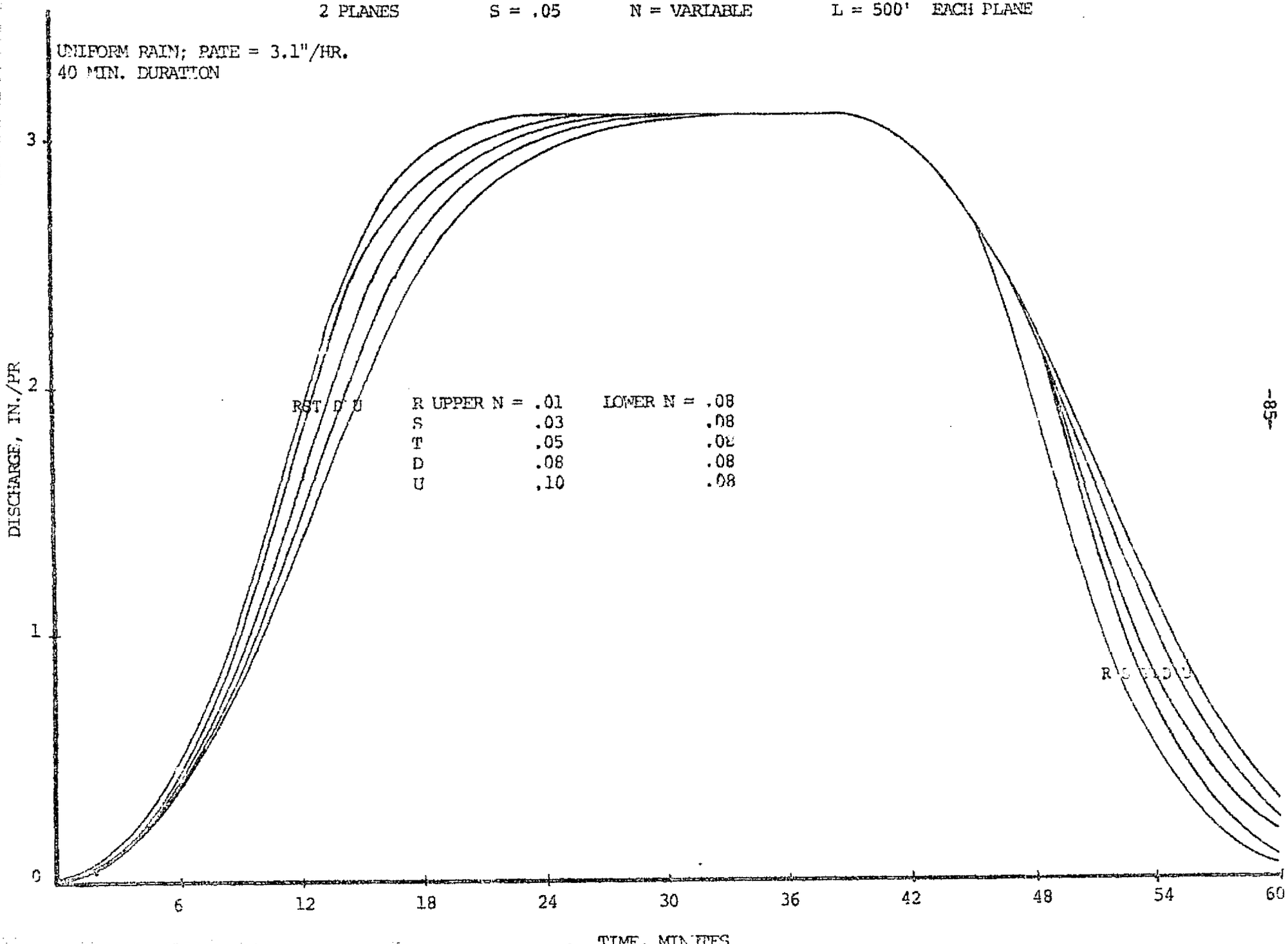

FIGURE 14 SENSITIVITY TO MANNING'S "N"

2 PLANES S = .05 N = VARIABLE L = 500' EACH PLANE

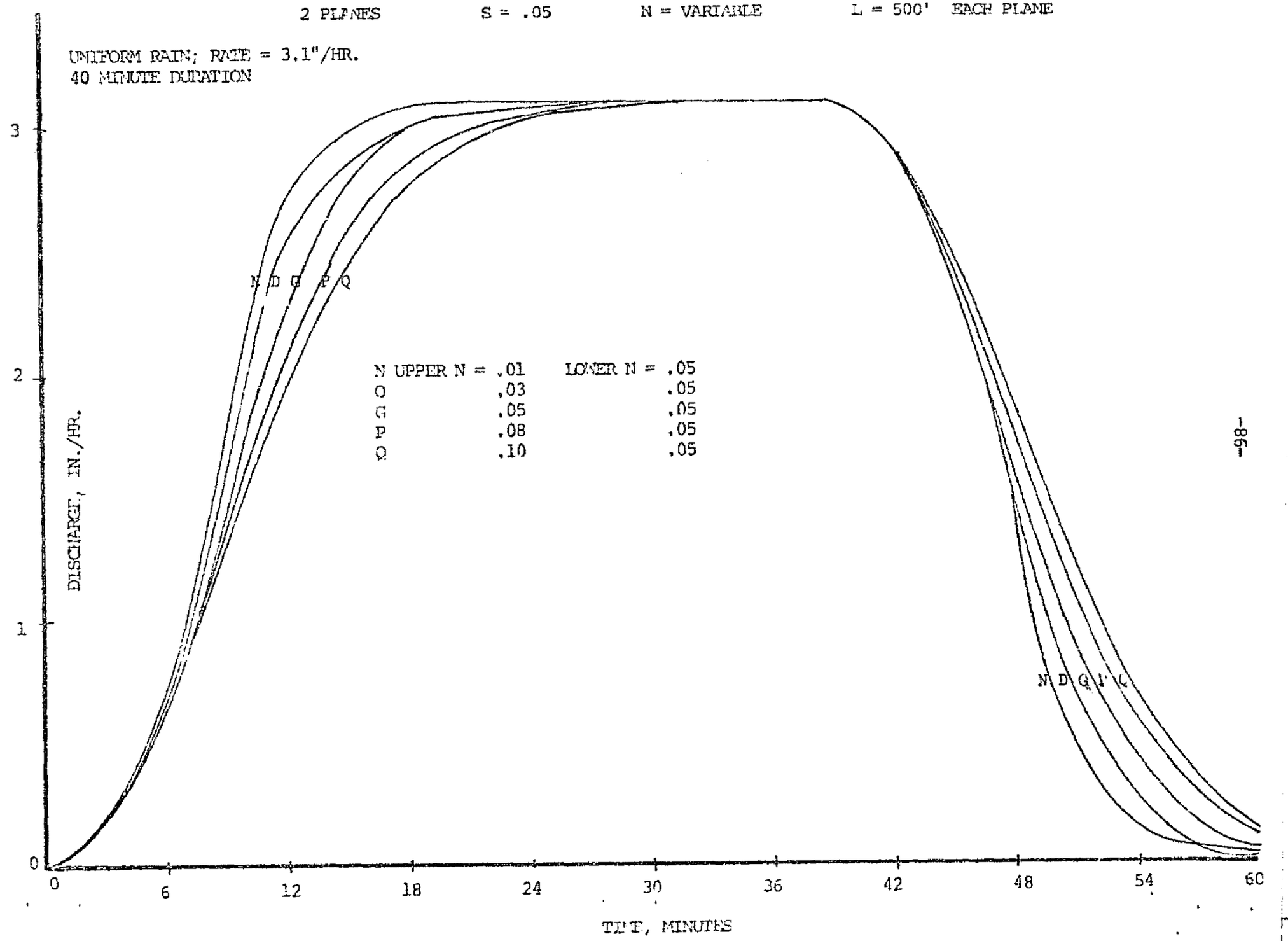

FIGURE 35

SENSITIVITY TO MANNING'S "N"

2 PLANES S = .05 N = VARIABLE L = 500' EACH PLANE

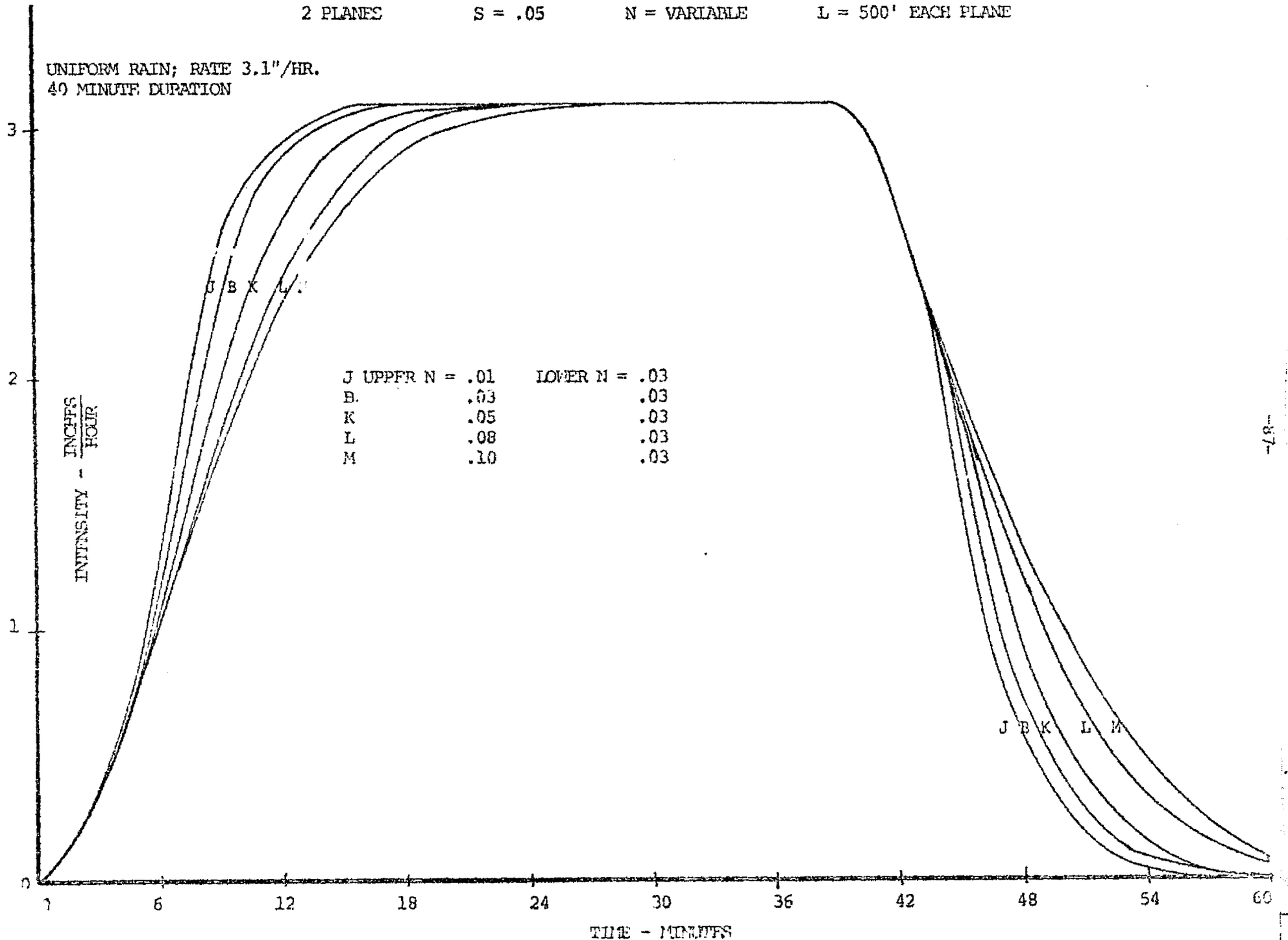

FIGURE 36 SENSITIVITY TO MANNING'S "n"

2 PLANES S = .05 N = VARIABLE L = 500' EACH PLANE

UNIFORM RAIN; RATE = 3.1"/HR.
40 MINUTE DURATION

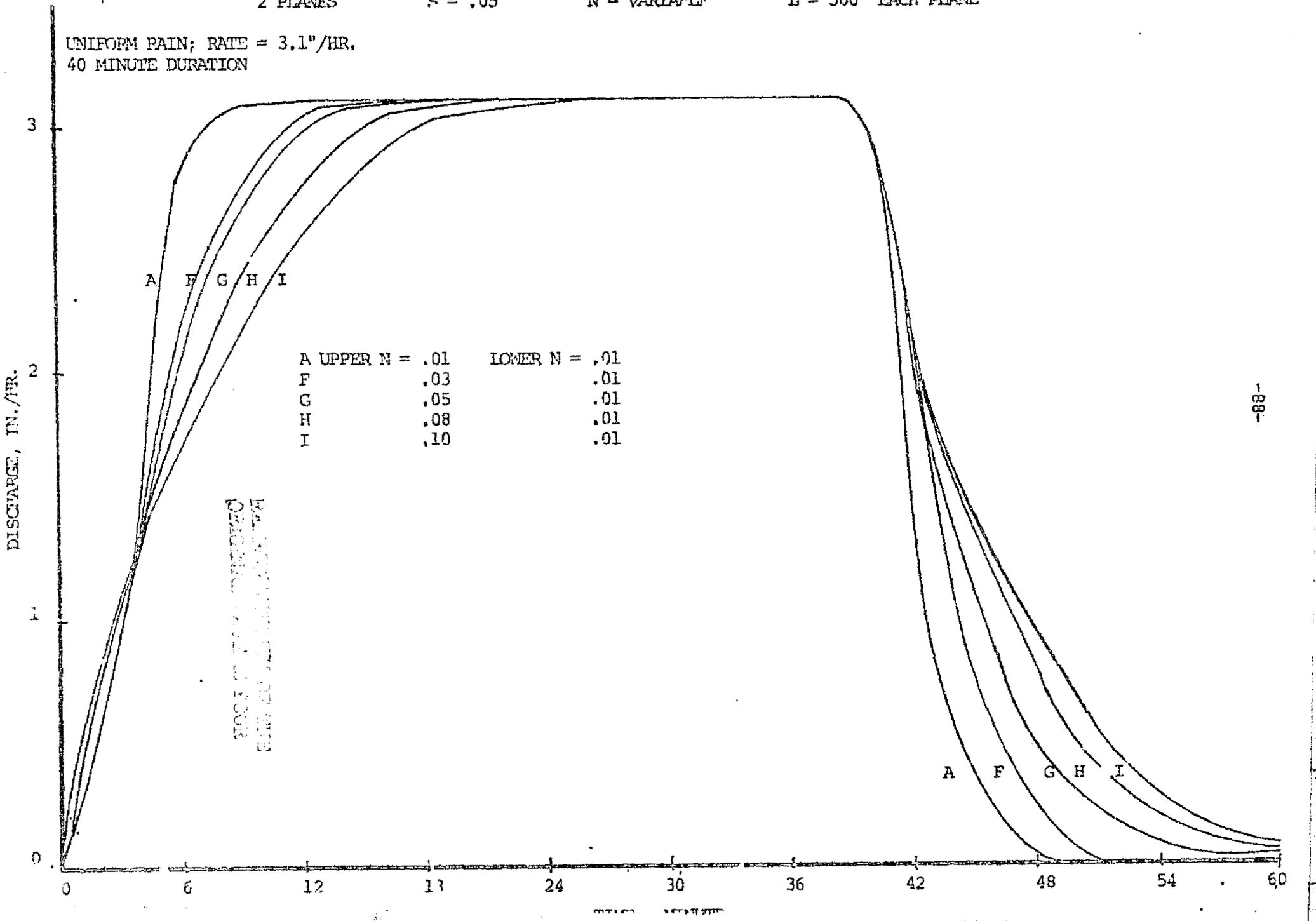

	UPPER N =	LOWER N =
A	.01	.01
F	.03	.01
G	.05	.01
H	.08	.01
I	.10	.01

FIGURE 37 DURATION OF PEAK VS. n 2 PLANES, S = .05, n = VARIABLE, L = 500' EACH

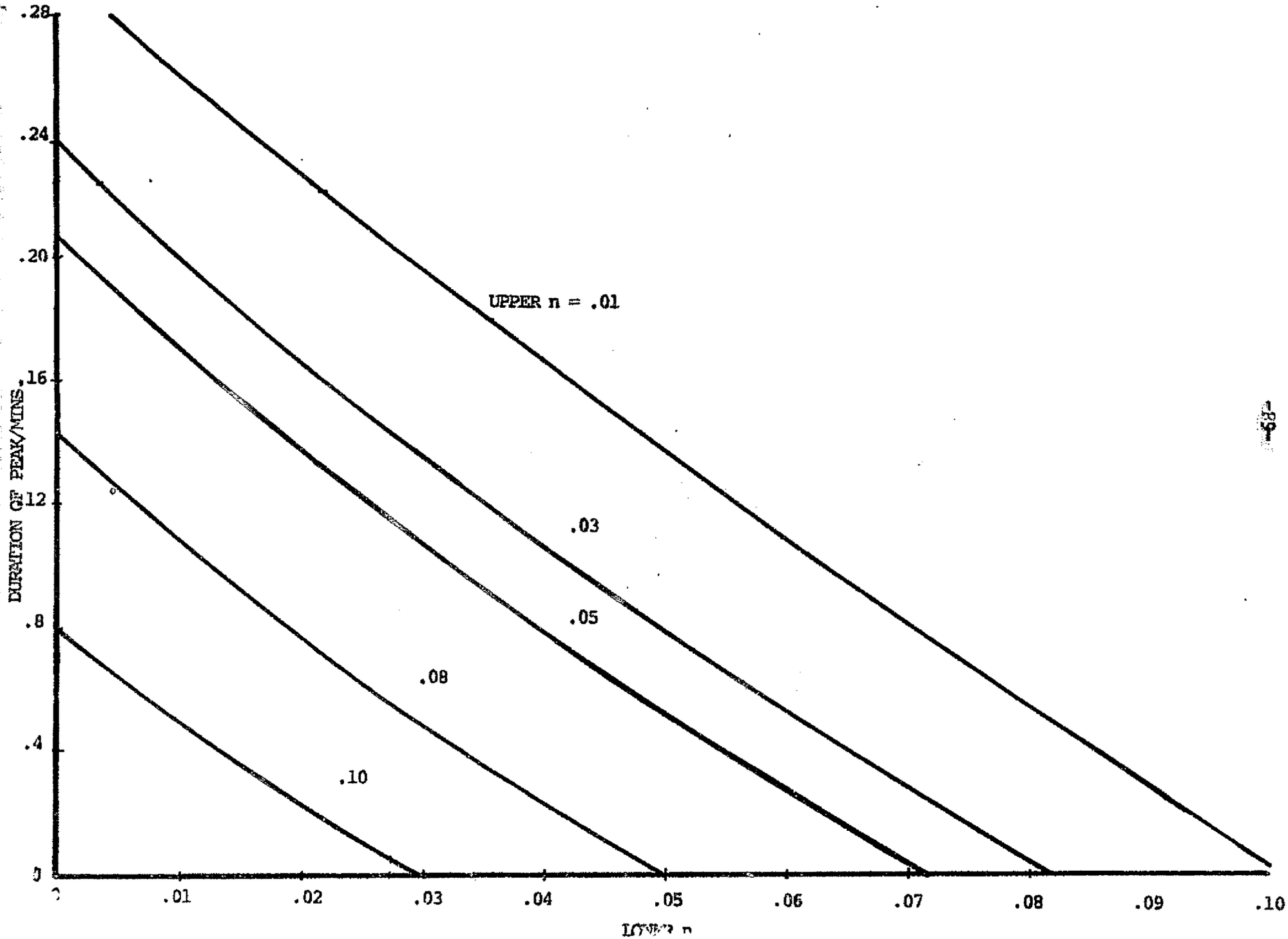

applies to estimates of time of concentration - the critical region consists of the lower slopes.

b) Irregular watershed slopes can be approximated by straight planes where slope variations are less than about 5%; otherwise, each strip should be divided with the outflow of the uppermost becoming the input to the lower.

c) The runoff peak rate is most sensitive to surface friction in basins with lower resistivities ($n < 0.04$), while the duration of the peak is most sensitive to higher friction. It follows that a remotely-sensed estimate of surface cover needs to be adequate enough to separate it into classes with similar values of Manning's "n". Referring again to Table 11, it becomes patent that a remote sensor should be able to separate forests from fields, fields from soil, and soil from urban areas, for example.

From the above, the following criteria can be established for the selection of model parameters:

1) The rainfall input should be of triangular shape, have duration equal to the time of concentration, and be of recurrence equal to fifty years.

2) The model parameters should reflect the conditions extant in the basin during the flood-probable season.

3) The slope module should be particularly accurate for flat basins; the surface friction factor should be differentiable among classes with large differences in Manning's "n".

3.3) Development of Routing Module

In large watersheds, or in those composed of several tributary streams, the assumption that all areas of the basin contribute to the outflow hydrograph simultaneously leads to errors. The hydrograph of each sub-watershed can differ from those of its neighbors in temporal distribution, magnitude and duration. The overall outflow from the basin is the combination of these hydrographs, appropriately added to account for the time lag required for runoff from each to reach the basin outlet. Figure 38 illustrates the differences between simple and complex basins.

Complex watersheds typically contain more than one predominant channel. The outflow from each sub-area does not drain directly into the main channel; rather, some flows first to secondary streams. The contribution of certain sub-areas is delayed. Figure 39 illustrates the effect. An effective hydrologic model accomplishes mathematically what has been done graphically in the Figure: it computes the hydrograph of each sub-watershed or sub-area and sums them according to a time-delay (routing) function. The routing model can provide the

C-2

FIGURE 38

ILLUSTRATION OF SIMPLE AND COMPLEX WATERSHEDS

COMPLEX WATERSHED
NEAR MUSCODA, WISC.

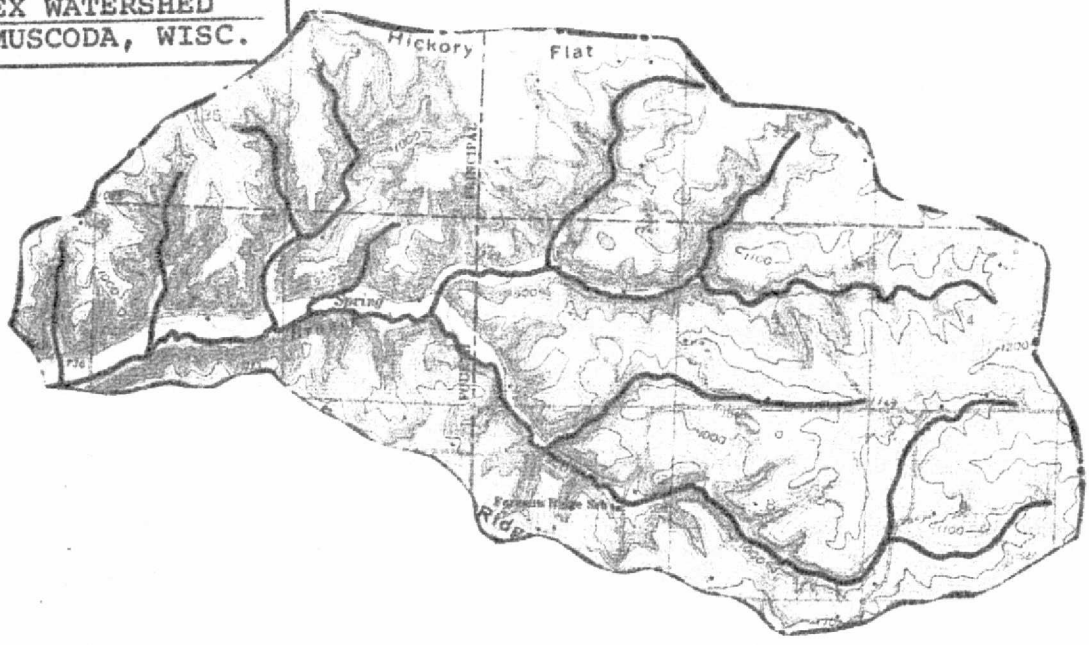

SIMPLE WATERSHED
NEAR MUSCODA, WISC.

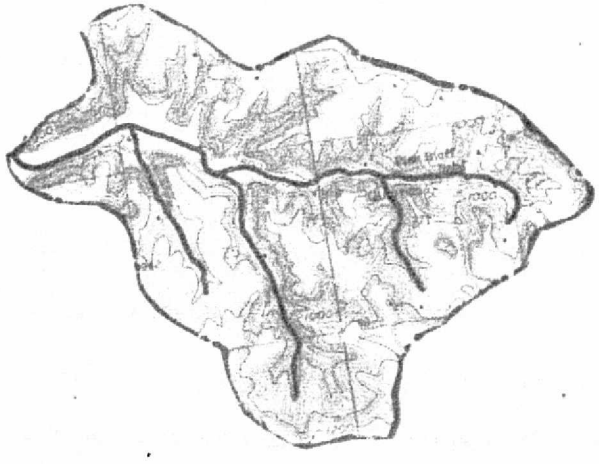

FIGURE 39 SUMMING OF DELAYED HYDROGRAPHS

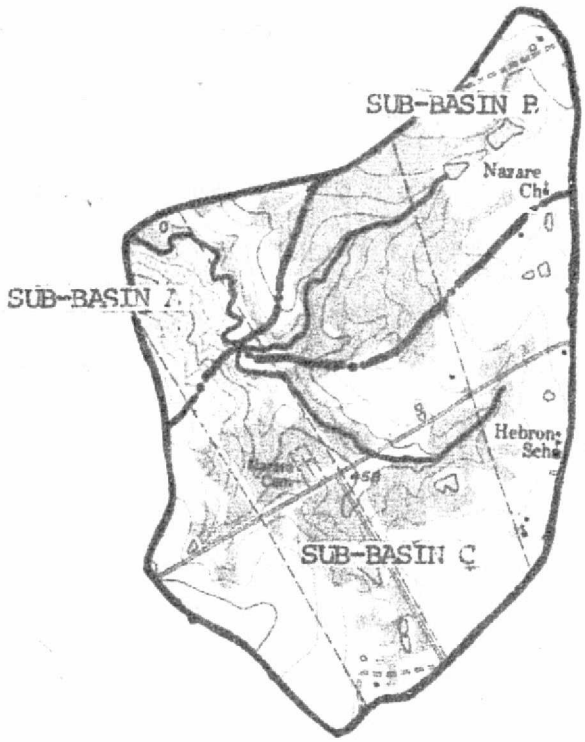

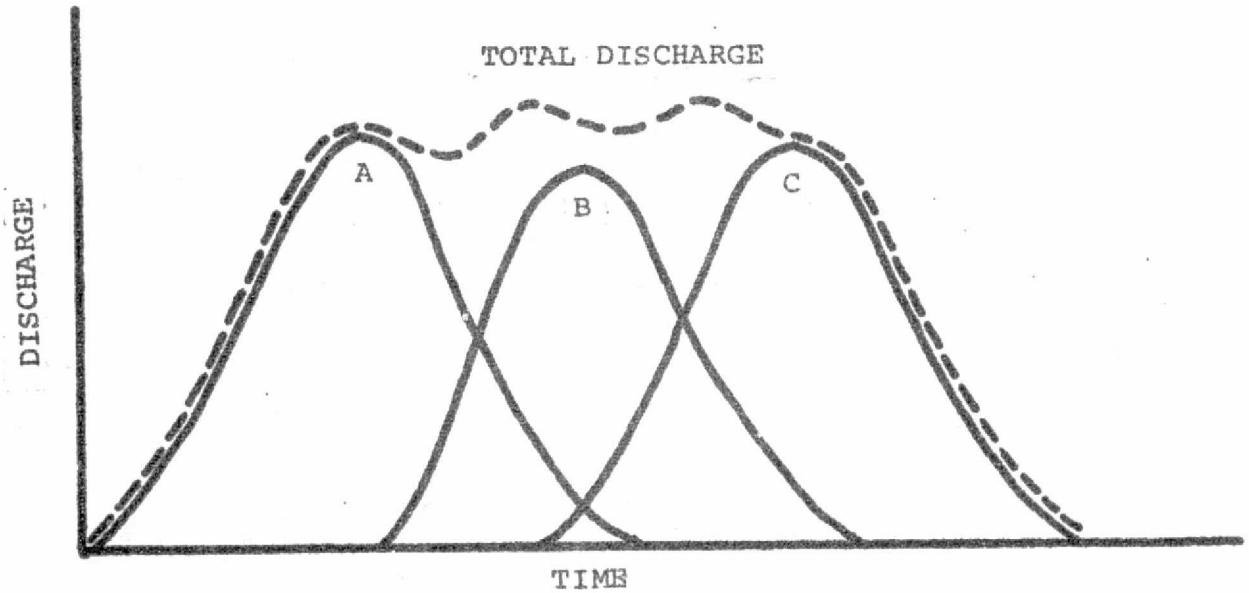

water resource planner a time picture of the buildup of the peak flow event, whereas the simple model generally yields only its maximum rate.

The approach to developing the routing module of the peak-rate model was to approximate a watershed by a series of unit strips and then to sum the hydrographs according to a time delay function. This technique was graphically summarized in Figure 39. The model, therefore, consists of an overland flow component (unit strips) and a channel flow component (lag time function). In line with the intent of this effort, the model was designed to keep the computing hardware to a minimum.

The model approximates overland flow on a unit-width strip and outputs the discharge hydrograph. The overland flow component assumes outflow to be a function of depth at the discharge point:

$$Q = \alpha \, h_o^m \qquad (1)$$

Where: Q = outflow rate, l^3/time
h_o = depth of outfall, l
m, α = constants

It also holds that the outflow at steady state will equal the rain rate times the area:

$$Q = iL \cdot 1 \qquad (2)$$

Where: i = effective rainfall rate, accounting for infiltration losses
(width = 1)

Therefore: $\alpha h_o^m = iL$; or (3)

$$h_o = \left(\frac{iL}{\alpha}\right)^{1/m} \qquad (4)$$

The average depth over the strip will equal the summations of the depths at each point divided by the total length:

$$\bar{h} = \frac{\int_o^L \left(\frac{i\ell}{\alpha}\right)^{1/m} d\ell}{L} \qquad (5)$$

Where: $\bar{h}$ = average depth

ℓ = length between 0 and L

$$= \left(\frac{i}{\alpha}\right)^{1/m} \left(\frac{1}{L}\right) \int_o^L \ell^{1/m} d\ell \qquad (6)$$

If the release of runoff at the outfall adheres to the Manning relation, then m = 5/3:

$$\bar{h} = \left(\frac{i}{\alpha}\right)^{3/5} \left(\frac{1}{L}\right) \int_o^L \ell^{3/5} d\ell \qquad (7)$$

$$= \left(\frac{i}{\alpha}\right)^{3/5} \left(\frac{1}{L}\right) \ell^{8/5} (5/8) \Big|_o^L \qquad (8)$$

$$= \frac{5}{8} \left(\frac{iL}{\alpha}\right)^{3/5} = 5/8\ h_o \qquad (9)$$

$$\frac{h}{h_o} = \frac{5}{8} \qquad (10)$$

The storage of water on the strip equals the average height times the area:

$$S = \bar{h}L = \frac{5}{8} h_o L \qquad (11)$$

Where: S = storage

Differentiating both sides yields:

$$\frac{dS}{dt} = \frac{dh_o}{dt}\left(\frac{5}{8} L\right) \tag{12}$$

The change in storage on the strip will also equal the inflow rate minus the outflow:

$$\text{Inflow} = (\text{rain rate}) \times (\text{area}) = iL \tag{13}$$

$$\text{Outflow} = (\text{Manning release}) = \frac{1.49 \sqrt{S} h_o^{5/3}}{n} \tag{14}$$

Where: S = slope
n = friction factor

$$\frac{dS}{dt} = \text{Inflow} - \text{Outflow} \tag{15}$$

From equation (12);

$$\frac{dS}{dt} = \frac{dh_o}{dt}\left(\frac{5}{8} L\right) = \text{Inflow} - \text{Outflow} \tag{16}$$

Therefore:

$$\frac{5L}{8} \frac{dh_o}{dt} = iL - \frac{1.49 \sqrt{S}}{n} h^{5/3} \tag{17}$$

or,

$$\frac{dh_o}{dt} = \frac{8}{5} i - \frac{2.38 \sqrt{S}}{n} h^{5/3} \tag{18}$$

Equations (14) and (18) define the overland flow component of the model. It was programmed to run in an iterative fashion on the larger-capacity hand calculators (Hewlett-Packard HP-65). A sample output appears in Figure 40. The required inputs are slope, surface friction factor, flow length, and rainfall rate. The first three are potentially measurable from remote sensors.

FIGURE 40. *SAMPLE OUTPUT OF ECO PEAK RATE MODEL*

CONSTANT AND TRIANGULAR RAINFALL INPUTS

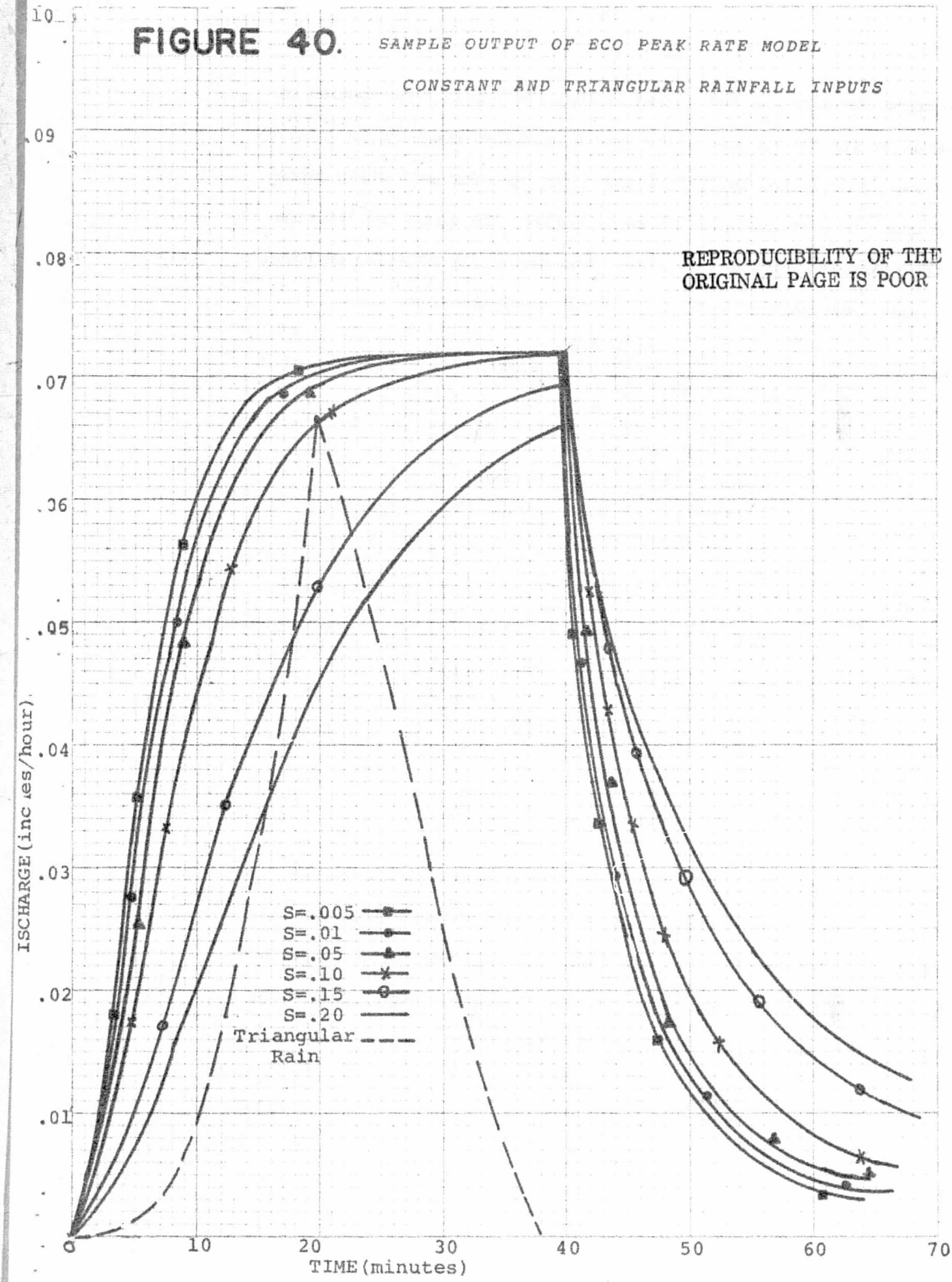

A routing function was then added so that the runoff contribution of several strips can be accumulated and a watershed modelled in totality. This was accomplished by introducing a lag time for each strip depending upon its distance from the basin outlet, the slope and friction of the channels, and the rain rate. The particular equation employed was taken from Overton (Reference 5) and is of the form:

$$\text{Lag Time } (T_L) = \frac{5}{8i}\left(\frac{niL}{1.49\sqrt{s}}\right)^{0.63} \text{ (secs.)} \qquad (19)$$

Where: i = rain rate, ft./sec.
n = Manning's "n" for the channel
L = length from outlet to strip, ft.
s = channel slope, ft./ft.

The output of a strip with length from the outlet of 100 feet, surface friction factor of .05, slope of .05 and rain rate of .00007 feet per second will have its lag time computed as follows:

$$T_L = \frac{5}{8\ (.00007)}\left(\frac{(.05)\ (.00007)\ (1000)}{1.49\ \sqrt{.05}}\right)^{.67} = 506.1 \text{ secs.}$$

$$= 8.4 \text{ minutes}$$

The outflow hydrograph from this strip, as computed by the overland flow component, will be delayed by 8.4 minutes and then added to the discharge of the remainder of the basin to yield the overall basin hydrograph. Figure 41 graphically depicts this modelling process. The complete form of the routing model is, therefore:

$$Q = \frac{1.49\ \sqrt{s}\ h_o^{5/3}}{n} \qquad (14)$$

FIGURE 41 Lagging Strip Hydographs

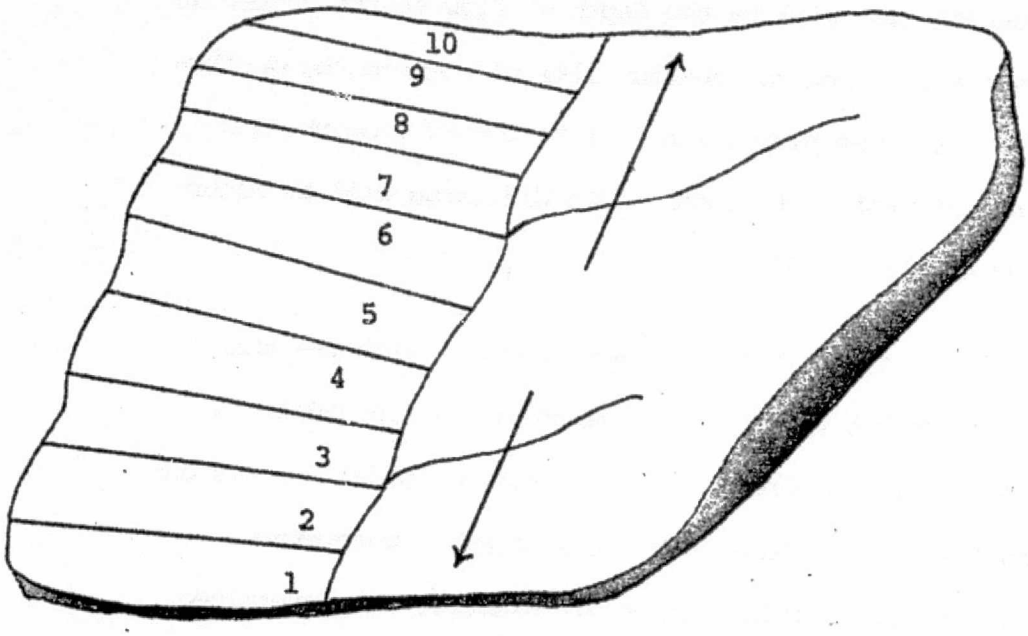

Rain Rate (q) = .000023 ft./sec. = .000007 m/sec.
Friction Factor (n) = .05
Slope (s) = .05
Length (L) = variable

$$\text{LAG TIME} = \frac{5}{8}\, q \left(\frac{nqL}{1.49\sqrt{s}} \right)^{0.6} \quad \text{(m secs.)}$$

TIME DELAY FOR
STRIP 1 = 2.5 minutes
STRIP 2 = 4.8 minutes
STRIP 3 = 6.6 minutes
STRIP 4 = 8.0 minutes
STRIP 5 = 9.3 minutes
STRIP 6 = 10.5 minutes
STRIP 7 = 11.7 minutes
STRIP 8 = 12.7 minutes
STRIP 9 = 13.7 minutes
STRIP 10= 14.6 minutes

$$\frac{dh_o}{dt} = \frac{8}{5} i - \frac{2.38 \sqrt{s}\ h}{n}^{5/3} \qquad (18)$$

$$T_L = \frac{5}{8} i \frac{niL}{1.49 \sqrt{s}}^{.63} \qquad (19)$$

The output of equation (18) will be the depth of flow at the outlet at time = t. This value is input to equation (14) to compute the outflow rate, also at time = t. The hydrograph will be formed from the Q's for all t's. Its contribution to total basin discharge will be determined, in turn, by equation (19).

Previously, sub-surface sensitivity had been examined with the analog computer and surface sensitivity through the simple strip model. A final type of sensitivity required a complete routing model for its analysis. The sensitivity of discharge to physiographic parameters, namely basin shape and areal distribution of rainfall, was determined through the use of the newly developed model.

A simulation was run to quantify the effect of watershed shape upon peak discharge rates. Five hypothetical basins of 400 hectare area were modelled, each having a different shape. Figure 42 shows the shapes and their corresponding discharge outputs for a constant rainfall input. As expected, those basins with large percentages of their total area close to the outlet produced higher discharges. The shape factor in this example accounted for up to a 20% difference in outflow peak.

The time to peak rate was also affected, though not significantly. These findings confirm our earlier assertion that watershed shape is

FIGURE 42

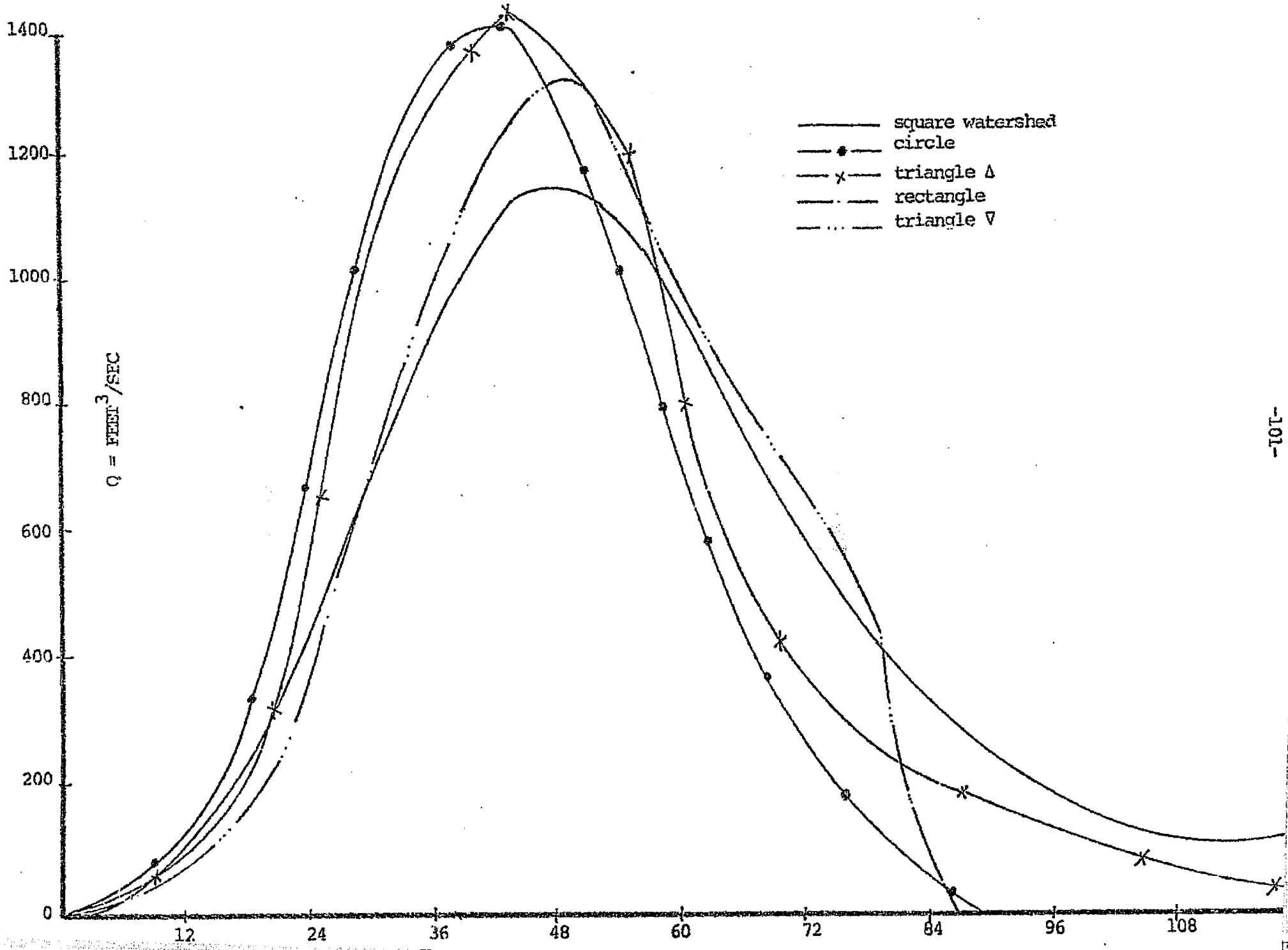
SENSITIVITY OF ALCN TO WATERSHED SHAPE
square watershed
circle
triangle Δ
rectangle
triangle ∇
Q = FEET³/SEC
1400
1200
1000
800
600
400
200
0
12
24
36
48
60
72
84
96
108

a driver of peak flow events. Since shape is a discharge driver, a planning model should be capable of accounting for it. The routing model provides the capability. The watershed will be simulated by a number of strips which can have different lengths (as well as slope and Manning's "n"), so any shape can be approximated.

A second simulation was performed to ascertain the sensitivity of outflow to the areal extent of rainfall. To this end, a square basin of 400 hectares was assumed, and different rainfall rate combinations applied over its area. A high (15cm/hr.) and low (7.5cm/hr.) rate were simulated for a 30 minutes duration. The basin was divided in thirds and the high rain was effectively moved from the outlet to the ridge line. Figure 43 gives the results.

Higher peaks accrued from harder rains nearer the outlet. This is the same effect observed in the shape simulation in that higher peaks result when a greater percentage of the rain can reach the outlet quickly. Further, it is possible to get a dual rather than single peak resultant from the position of the rainfall relative to the outlet as shown in the Figure. Though the particular combination of rain rates and positions which produce the maximum outflow will vary with basin size and shape, when basins to be measured are very large or when rainfall characteristically occurs only over small areas the effects of the "worst case" should be accounted for.

Again the routing model is particularly applicable to modelling variable rain rate. Each unit strip can be given a separate rainfall input. Where detailed rainfall network data exists, then, it can be modelled very closely.

FIGURE 43

SENSITIVITY OF FLOW TO AREAL DISTRIBUTION OF RAINFALL

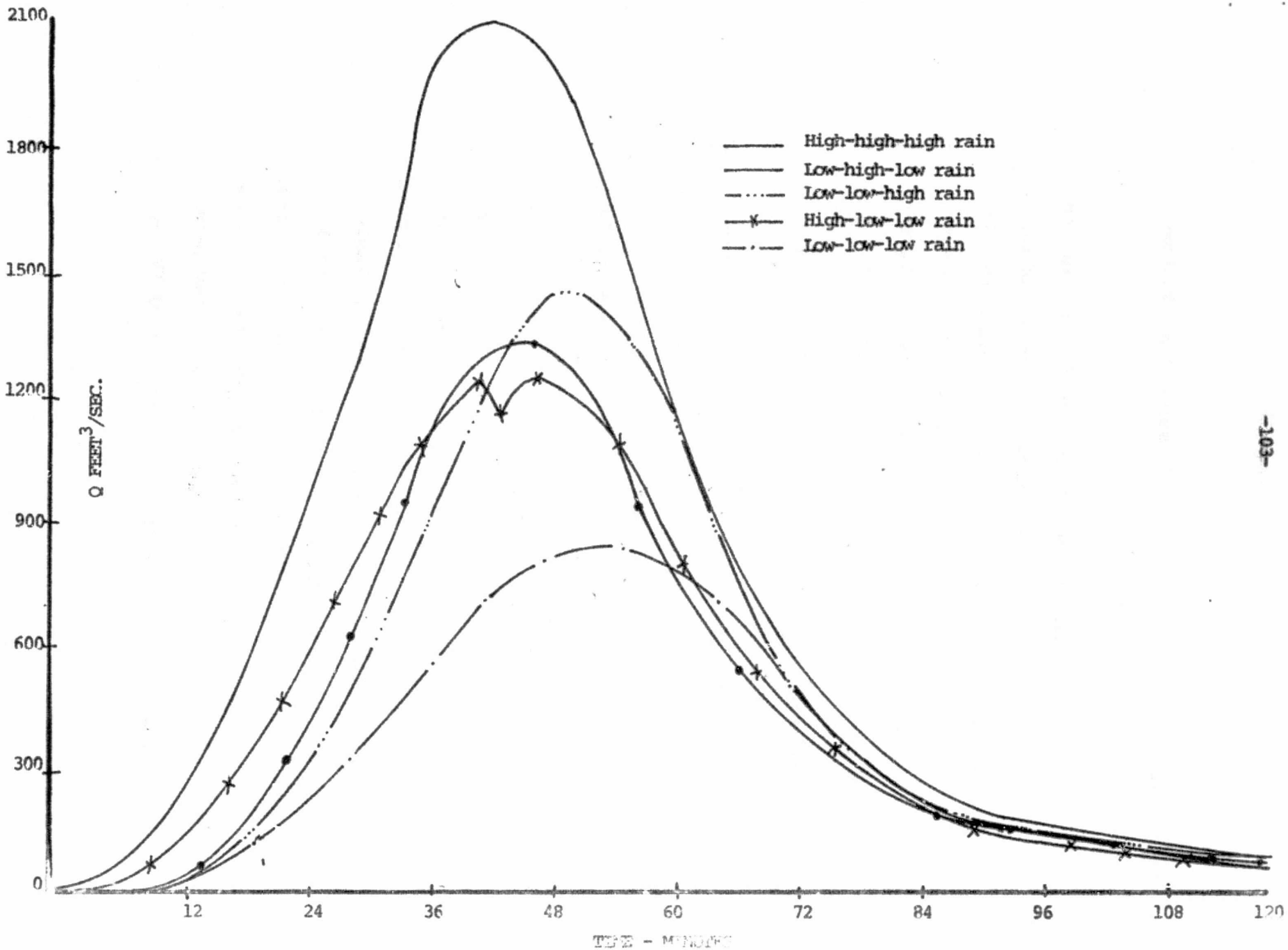

The following summarizes the findings and results of the development of the planning model:

1) The peak rate model has been further verified by extension of the test sample to 31 watersheds. The results of the model were found to be a significant improvement over similar commonly-used models. Most of the model parameters can potentially be measured from remote sensing stations - slope, surface cover, and physiographic measurements.

2) The analysis of rainfall characteristics and their seasonal modifiers has allowed two conclusions. First, though no direct relation exists between the "x" year rain and the discharge of like recurrence, enough evidence exists to permit estimation of a "planning rain." The rationale for its selection has been presented. These rains formed the inputs to the peak rate model and produced reasonable results. Second, it will behoove the water resource modeller to consider the seasonal perturbations to rainfall-runoff phenomena. Individual geographic regions will have varying peak flow characteristics. These factors provide valuable clues to construction of the planning model data set. Satellite remote sensing offers an improvement over conventional sources of ground truth in this regard. Should it be determined that the model should reflect late summer conditions in a basin, for example, LANDSAT imagery from that period can be acquired and analyzed. The most readily available

source of aerial photographs, on the other hand, "sees" a particular area only once every several years.

3) A routing model has been synthesized for modelling of "complex" basins. It offers two principal features. First, a great deal of flexibility is provided for approximation of watersheds with internally variable hydrologic parameters. The number and physical characteristics of the strips can be tailored to closely approximate conditions extant in the watershed to be modelled. Second, ample opportunity for remotely-sensed input is provided. Slope, surface friction, strip and channel dimensions are potentially measurable from remote sensing stations. The model has been successfully applied to assessment of the sensitivity of runoff to basin shape and areal distribution of rainfall.

CHAPTER IV

HYDROLOGIC ANALYSIS OF LANDSAT IMAGERY

This task included three principal components:

1) Analysis of the state of the art of techniques for measuring surface characteristics of hydrologic significance and of their cost, implementation time, equipment and skill requirements.

2) Evaluation of the specific hydrologic information content of the four LANDSAT bands and determination of which bands or combinations of bands are best suited to measuring each model input.

3) Quantitative hydrologic analysis of a complete watershed using LANDSAT imagery and available ground truth.

4.1) Analysis of the State of the Art of Measurement of Hydrologic Parameters from Remotely-Sensed Data

This investigation focused upon measurement methods for those remotely sensible hydrologic factors of most immediate value to watershed modelling:

1) Physiographic Basin Measurement

2) Surface Cover Identification & Classification

3) Soils Classification

The analysis could be carried to significant depth thanks to the simultaneous availability of an effort sponsored by Goddard Space Flight

Center, Dr. Vincent Salomonson, NAS5-20567, "User Requirements and User Acceptance of Current and Next-Generation Satellite Mission and Sensor Complement, Oriented Toward the Monitoring of Water Resources," of December, 1975, with which the burden of this research was shared.

4.1.1) Measurement of Physiographic Basin Parameters from Remotely Sensed Data

Various physiographic measurements which serve as direct inputs to hydrologic models are possible from LANDSAT imagery: the measurement of watershed area, overland flow lengths, drainage density; and the estimation of channel dimensions.

Watershed areas are defined by the ridge line, i.e., the contour within which all rainfall drains to the same outflow point. In regions where relief is pronounced, ridge lines can be directly discerned from aerial photography or satellite imagery. Where slopes are not so steep, topographic and slope maps are valuable interpretive aids. With the boundary delineated, area can be measured with a planimeter or calibrated grid. Flow lengths can also be directly measured. The watershed's shape, which has been shown in this effort to be one of the drivers of discharge, can also be discerned.

Figure 44 illustrates the method for the definition of the watershed area. The uppermost set of images demonstrates how the ridge lines can be identified from pronounced relief. Shown is a western California watershed of 72,320 hectares. The left-hand image shows that a significant contrast exists between the northeastern (light) and southwestern

FIGURE 44 DELINEATION OF WATERSHED AREA FROM REMOTELY SENSED DATA

LANDSAT BAND 5

June 1972

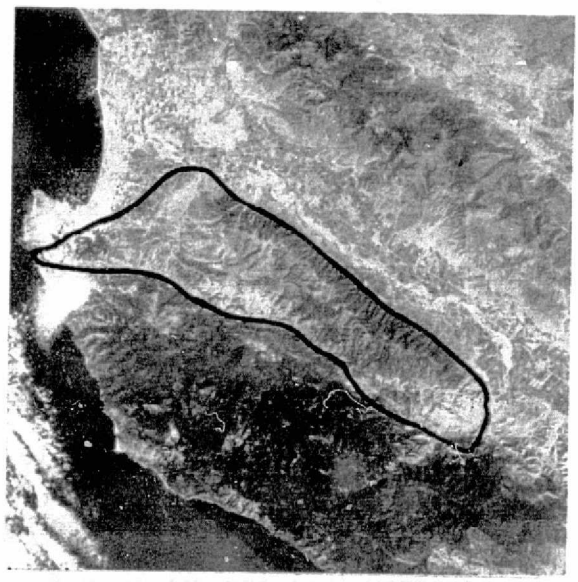

Monterey, California

1:1,000,000 Scale

LANDSAT BAND 5

June 1973

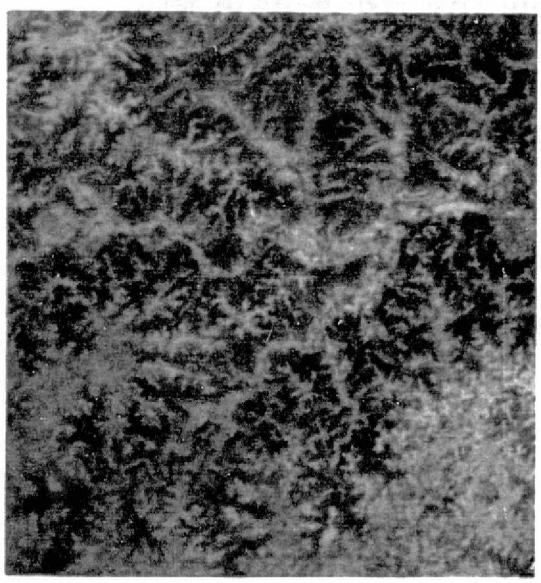

LaCrosse, Wisconsin

1:400,000 Scale (approx.)

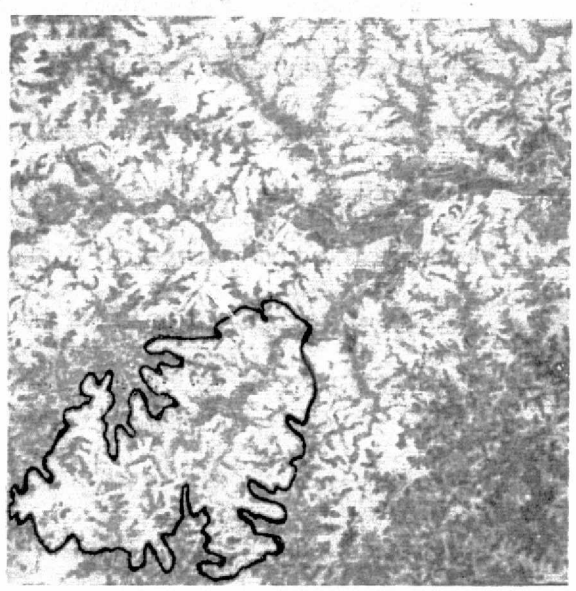

(dark) slopes of the steep ridges comprising the basin boundary. In the right-hand image, a contour is drawn around the ridge line defined by the reflectance difference. The area can then be measured by overlaying a calibrated grid and counting the divisions within the line.

The lower pair of images shows an area where slopes are less than 10%, so that relief is not apparent. What is apparent, however, are several streams, each with associated drainage structure. The streams appear dark in the Band 5 image while the land shows up light. By following the streams visually it can be determined which ones drain to the same point, thereby approximately defining the watershed. The boundary location can be refined by interpolating the distance between streams which drain away from each other. The line on the right hand lower image was drawn by dividing the distance between streams in half. This approximation of the ridge line resulted in area measurement errors of order 5% or less.

It is possible to determine physiographic data from LANDSAT imagery to an accuracy comparable to that available from medium-scale maps. Figure 45 shows a section of an U.S.G.S. 1:250,000 scale topographic map of an ARS test watershed at Chickasha, Okla. The elevation contours give the altitude of points around the central stream. By connecting the points of highest elevation, the watershed boundary can be obtained. The area of the basin was measured by planimeter from the map to be 54,857 hectares.

FIGURE 45 Comparison of LANDSAT Imagery and Topographic Map for Determination of Watershed Boundary and Area

U.S.G.S. Topographic Map

1:250,000 Scale

LANDSAT MSS5 Image
4X Magnification; 1:250,000
20 October 1973

The lower illustration is a LANDSAT image enlarged four times to match the scale of the topographic map. This watershed is relatively flat, so ridge lines could not be relied upon to define area. The boundary was instead determined by using the drainage divide and vegetation shade changes as guides. The watershed area was mensurated by a polar-planimeter to be 56,470, a 3% overestimate with respect to the topographic map.

Should the appropriate clues not be present, the satellite image can be projected onto a topographic map and aligned using identifiable features (roads, lakes) as landmarks. The ridge line derived from the topo map can then be transferred to the image.

The length of channels affects the ratio of overland to channel flow. Their particular arrangement within the watershed determines the amount of time that precipitation spends running over the land versus in the channel, and therefore the lag time involved in transmitting flow to the basin outlet. The length of the channels is a variable entering the computation of basin time of concentration in certain hydrologic models. In others, drainage pattern and density are compared with basin area to develop time delay histograms for overland flow, because it determines the lag time for the contribution of each watershed sub-area to reach the outflow point. Watersheds with higher drainage densities have more channel length per unit area and, therefore, water will travel a shorter distance overland before reaching a stream. Since channel flow is generally faster than surface flow, a watershed with high drainage density will reach its outflow peak quicker than one of equal area with a lower ratio.

Figure 46 demonstrates the importance of drainage density in hydrologic phenomena. The upper image is a 400 square mile section of Band 5 LANDSAT image, photographically enlarged approximately 2.5 times. It shows a number of watersheds with a high ratio of stream length to unit area. Streams appear light and land surface dark. A representative drainage density for the area is approximately 1 kilometer per square kilometer. The exact value for each basin can be measured by first determining basin area as earlier described and then computing stream length within the area with a map wheel or similar measuring device.

The lower image is an area of like dimensions from a higher and drier location. It is apparent that much more surface area per unit stream length exists in this watershed than in the previous image. Stream length was measured by map wheel from the image to be 210 kilometers. Drainage density here is approximately 1 kilometer per 5 square kilometers.

Figure 47 demonstrates the utility of the several LANDSAT bands for measuring channel parameters. The images show a Minnesota watershed as seen in each band. To measure total stream length, best results are achieved using Bands 4 and 5, because higher order (smaller) streams are visible which cannot be seen in the other bands. On the other hand, to measure channel width, Bands 6 and 7 are preferable because the contrast between the stream and the surrounding vegetation is much improved. The main channel is particularly visible, appearing light amongst darker vegetation.

FIGURE 46

DELINEATION OF DRAINAGE PATTERN AND MEASUREMENT OF DRAINAGE DENSITY FROM REMOTE SENSING IMAGERY

HIGH DENSITY DENDRITIC PATTERN

COLBY, WISCONSIN ; MSS 5

JUNE 1973

1:400;000 Scale (approx.)

LOW DENSITY DENDRITIC PATTERN

NEAR TOPEKA, KANSAS ; MSS 4

JULY 1973

1:400,000 Scale (approx.)

FIGURE 47 USE OF MULTIBAND IMAGERY IN IDENTIFICATION

DRAINAGE PATTERN AND DENSITY

ROCHESTER, MINNESOTA SCALE 1: 350,000 (approx.)

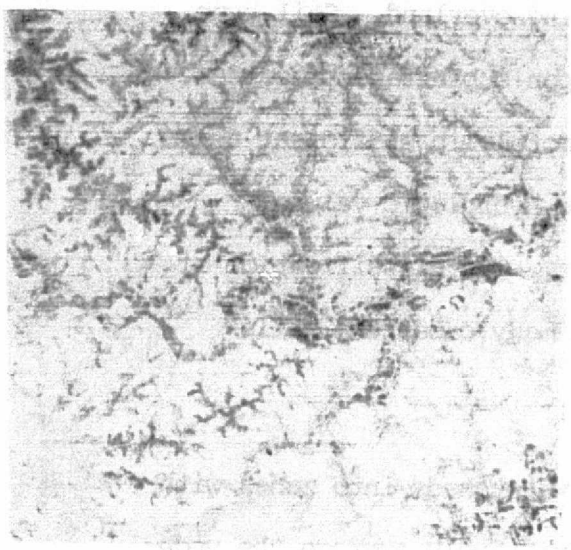

BAND 4

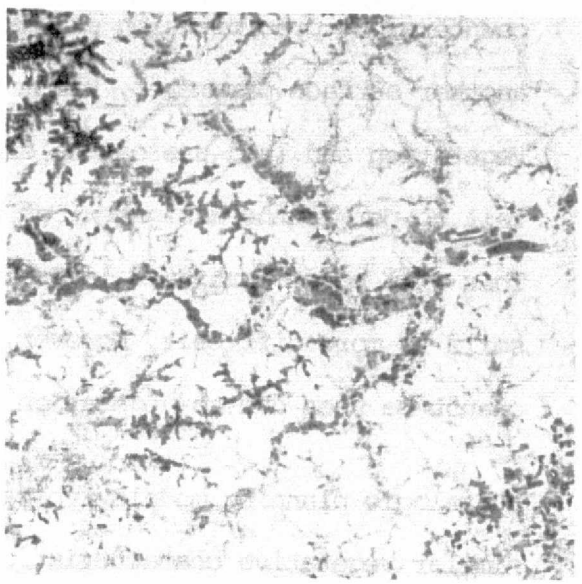

BAND 5

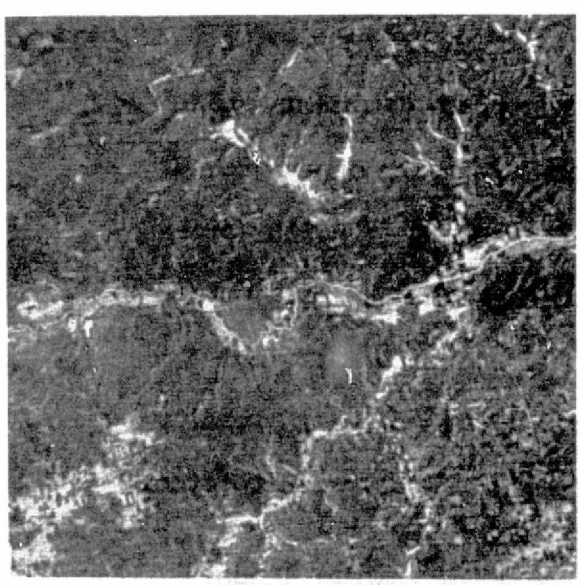

BAND 6

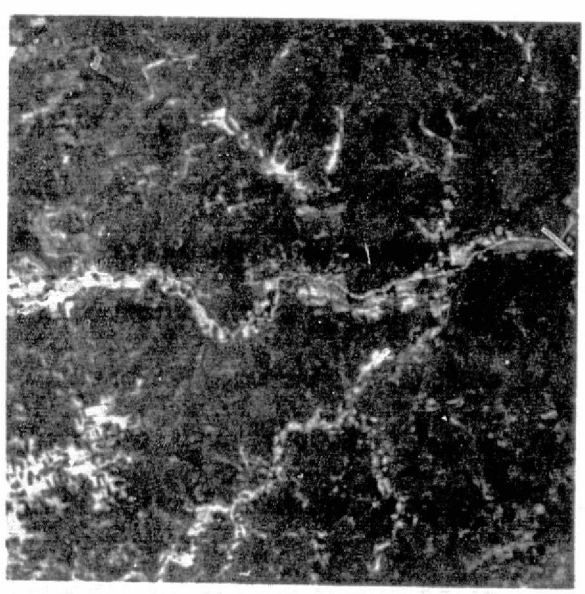

BAND 7

4.1.2) Measurement and Classification of Surface Cover from Remotely Sensed Imagery

The type and distribution of surface cover influence the friction encountered by precipitation excess while running overland. Soil type, another surface parameter, has more impact upon subsurface processes. Vegetation and land use can be classified remotely in sufficient detail to permit the assignment of quantitative hydrologic values. This will be demonstrated later in the report. The classification of soils is more difficult, however, because in many cases the soils cannot be seen due to vegetation cover.

Hydrologic planning models typically divide watersheds into zones with similar vegetative characteristics, or, alternatively average the vegetation factors across a catchment and utilize a "lumped" parameter. Moreover, vegetation class and density are used as indicators of water retention and infiltration.

Figure 48 indicates the ability of LANDSAT imagery to determine different vegetative cover on the watershed as compared with other ground truth sources. The upper photo indicates a section of 1:24,000 (original scale) USGS topographic quadrangle including the ARS test watershed in Blacksburg, Virginia. In the lower aerial photo (original scale 1:45,000) the field structure and hydrologic land use is readily apparent and with limited ground truth can be successfully interpreted.

Field structure can be likewise interpreted from the LANDSAT image. Note particularly the odd-shaped field near the center of the aerial and satellite photos. Classification from LANDSAT data will generally

FIGURE 48

U.S.G.S. Topographic Map

Scale 1:24,000

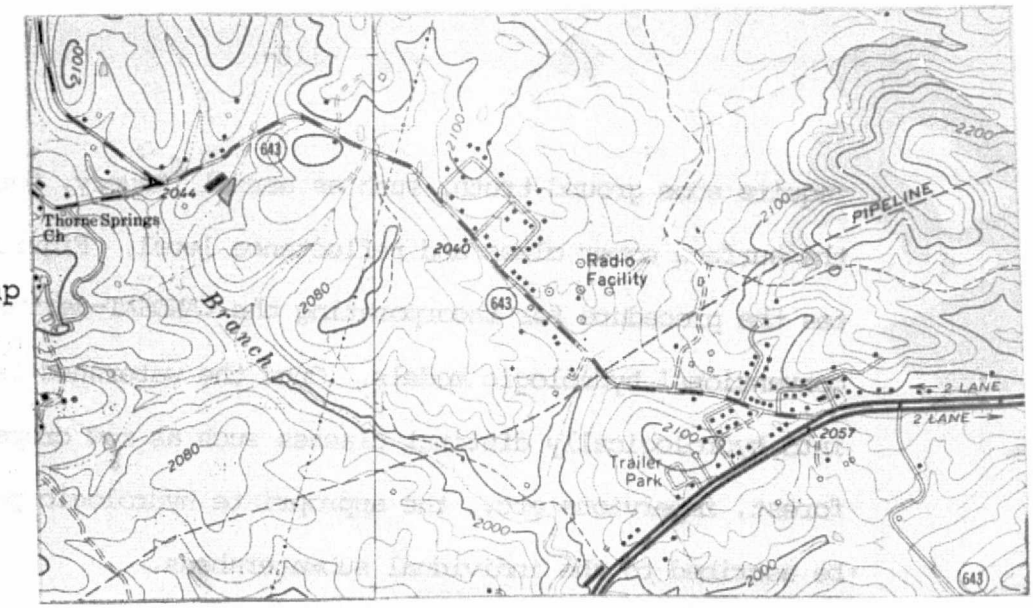

Aerial Photograph

Scale 1:45,000

(approx.)

LANDSAT Band 5

Scale 1:125,000

(approx.)

require some ground truth, such as aerial imagery, for correlating the surface cover class and reflectance level. Figure 49 illustrates the procedure for incorporating the LANDSAT-derived data into conventional hydrologic models. Once the watershed is partitioned into hydrologically distinct classes such as row crops, fallow, forest, impervious etc., the appropriate hydrologic parameters can be ascribed to the individual subwatersheds.

The technique is illustrated for a hypothetical watershed for three important parameters; Manning's "n", which is a measure of the impedance of the watershed to overland flow; Holtan's "a", which is a measure of the ilfiltration potential of the watershed; and the SCS curve number, which is directly used to determine the fraction of a given rainfall event which appears as direct runoff.

4.1.3) Remote Classification of Soils

Hydrologic models typically group soil into homogeneous hydrologic classes of different permeabilities, porosities, etc. Areal extent of soil type is used to determine infiltration rate and potential moisture content. Soil permeability, porosity, and conductivity serve as inputs to the infiltration and evapotranspiration components of the models.

Soils classification must in many cases rely upon inference rather than direct measurement since the soils are often obscured by vegetative cover. Soil association must typically be inferred from knowledge of the surficial vegetation. Some interpretation is possible directly from the imagery since soil wetness affects photo-

FIGURE 49

ASSIGNMENT OF HYDROLOGIC PARAMETERS TO VEGETATION CLASS

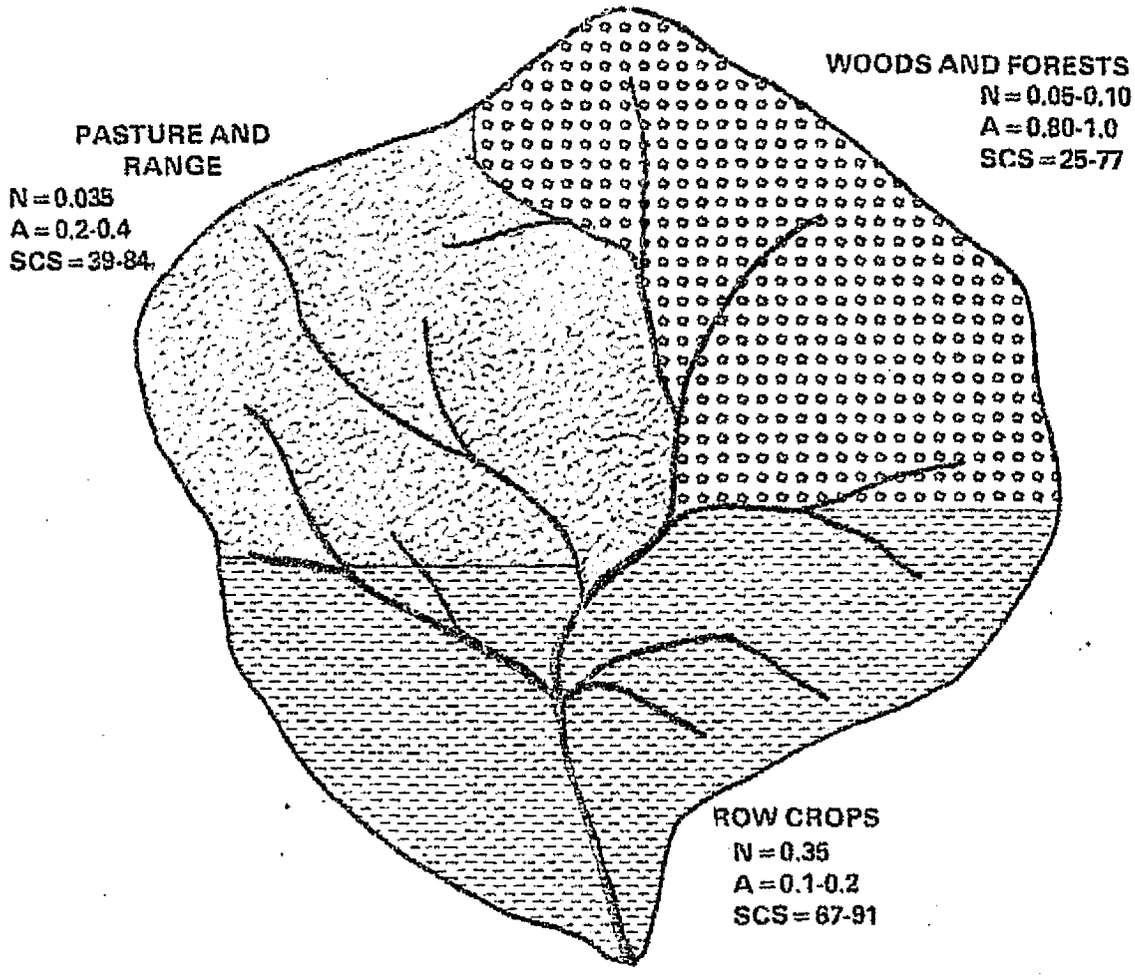

VALUES OF HYDROLOGIC PARAMETERS

MANNING'S "N"		HOLTAN'S "A"		SCS CURVE NUMBER	
SMOOTH ASPHALT	0.013	FALLOW	0.10-0.30	ROW CROP	
CONCRETE (TROWEL FINISH)	0.013	RAW CROPS	0.10-0.20	(STRAIGHT)	67-91
ROUGH ASPHALT	0.016	SM. GRAINS	0.20-0.30	(CONTOUR)	65-88
CONCRETE (UNFINISHED)	0.017	HAY (LEGUMES)	0.20-0.40	SM. GRAIN	
SMOOTH EARTH (BARE)	0.018	HAY (SOD)	0.40-0.60	(STRAIGHT)	65-88
FIRM GRAVEL	0.020	PASTURE		(CONTOUR)	61-84
CEMENTED RUBBLE MASONRY	0.025	)bunch grass)		LEGUMES OR	
PASTURE	0.030-0.035	TEMPORARY		ROTATION	
CULTIVATED AREA	0.035-0.040	PASTURE (SOD)	0.40-0.60	NATIVE PAS-	
SCATTERED BRUSH, HEAVY WEEDS	0.045	PERMANENT	0.80-1.0	TURE OR	39-84
LIGHT BRUSH & TREES	0.050-0.060	PASTURE (SOD)		RANGE	
DENSE BRUSH	0.070-0.100	WOODS & FORESTS	0.80-1.0	WOODS	25-79
HEAVY TIMBER	0.100				
IDLE LAND	0.030				
GRASSLAND	0.032				

graphic darkness in MSS Band 7. Ancillary data such as vegetation type, geographic location, slope and proximity to water bodies facilitates classification and mensuration.

Figure 50 shows a section of the SCS Soil Survey for Marshall County, Mississippi. The survey provides a map of general soil associations and an acre-by-acre county-wide soil classification. The figure depicts the soil association map: it alone is generally marginal for hydrologic modelling since hydrologic parameters vary widely within a soil association.

The lower figure is a LANDSAT Band 7 image of the same area taken August 1973. The differences in shade allow broad soil association classification. A clear correspondence exists between reflectance in the image and soil association as shown in the SCS maps. Additional detail useful in finer classification, is however not readily apparent. Therefore, in models not specifically designed for remote sensing input, additional ground truth, such as the soil survey, is required to assign values to subsurface inputs.

4.2) Specific Hydrologic Analyses of LANDSAT Imagery

4.2.1) General Principles

The objective of this task was to determine the extent to which information directly applicable to hydrologic models can be gleaned from the satellite data. The task consisted of an assessment of the information content of the MSS bands and of the quantitative hydrologic analysis of selected test basins, specifically:

FIGURE 50

Photointerpretation of Remote Sensing Imagery for Soil Classification

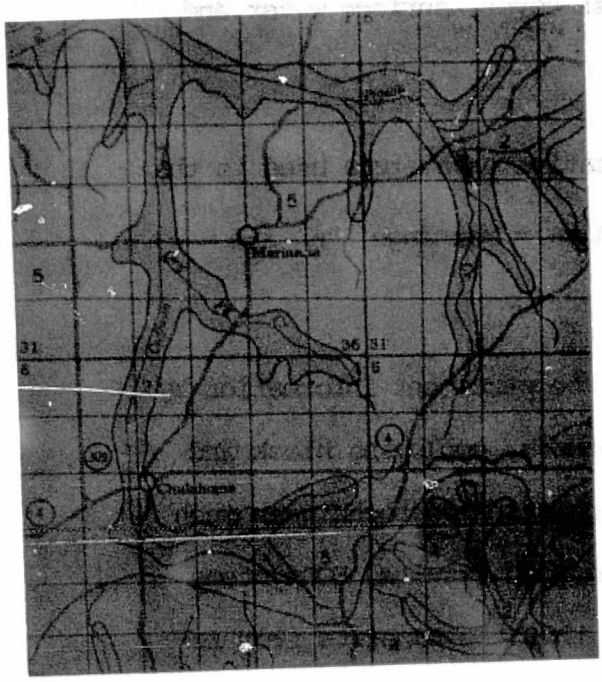

Soil Conservation Service Soil Association Map

Scale 1: 190,000

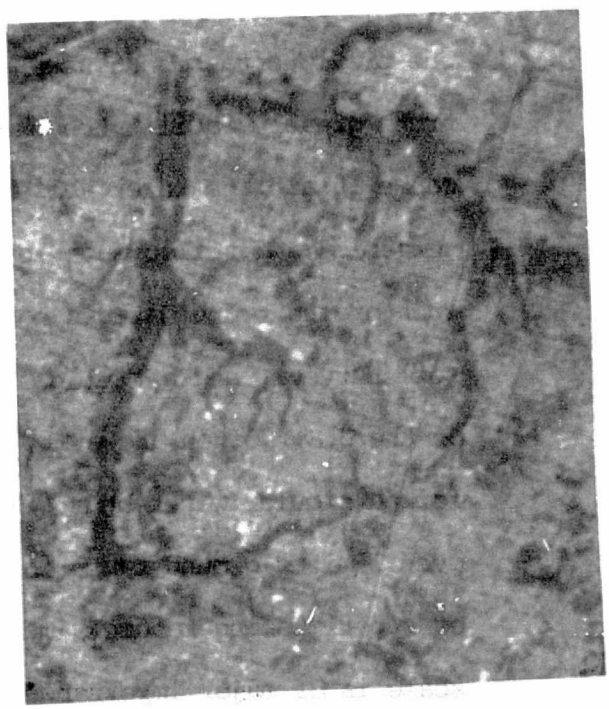

LANDSAT Band 7 August 1973

Scale 1: 190,000 (approx.)

1) the identification of hydrologic features of watersheds, namely, stream courses, forest cover, surface water and impermeable areas.

2) The assignment of two quantitative parameters used in the routing model for the two basins - Mannings' "n" and Holtan's "a".

The effort focused upon extraction of the pertinent information by relatively simple, low-cost, visual methods, employing black and white Landsat imagery. Though more sophisticated techniques such as computer-aided analysis have yielded good results, ECOsystems' familiarity with small users indicates that the benefits from remotely-sensed data will be realized earlier if simple yet adequate information-extraction procedures can be identified.

The previous task indicated that at least a minimal level of ground truth greatly facilitates the interpretation of remote imagery, because it assists in establishing a correlation between surface observables and reflectance levels. The degree of availability of such ground truth data is not the same everywhere. Topographic maps, soil surveys, and aerial photography can be obtained for large areas of the U.S. Often, however, all three do not exist simultaneously for particular watersheds. In spite of this unevenness of coverage, even limited ground truth is valuable. Therefore, the capability of superimposing Landsat imagery onto ground truth data at the same scale is of major importance to successful extraction of hydrologic parameters.

To accomplish this function, an image viewing system was assembled, capable of projecting single or multi-band LANDSAT imagery onto a work surface. The satellite imagery was magnified up to forty times and could be traced or overlayed upon ground truth maps or photographs. The system developed is a low-cost, highly reliable visual analysis tool of the type readily accessible to practicing hydrologists.

4.2.2) Analysis of Hydrologic Information Content of LANDSAT Bands

Two of the ARS experimental watersheds were selected for visual photointerpretation of LANDSAT images. Those chosen - the Thorne Creek basin near Blacksburg, Virginia, and Watershed W-10 near Oxford, Mississippi - were singled out due to the availability of adequate ground truth in the form of topographic maps, soil surveys and aerial photography. These aids were applied to verify the interpretation from LANDSAT imagery.

The same methodology was used for both basins. Using the projection device, the imagery in each band was overlayed on a topographic map upon which the basin boundary had been drawn. The LANDSAT image was matched in scale, position and orientation to the map using prominent physical features (roads, rivers, etc.) as reference points. Once matched, selected portions of the LANDSAT image were visually compared to the ground truth to establish "training samples" of reflectance correspondences. Next, the ground truth was removed, and the photointerpreters attempted to identify all surface features and to measure those requiring quantification.

4.2.2.1) Analysis of the Blacksburg Watershed

Figure 51 reproduces an aerial photograph of the Blacksburg watershed at the scale of approximately 1:60,000. The basin is 1235 hectares in area; it contains primarily agricultural fields, plus small stands of forest. Urbanization is insignificant. The following describes the results of the photointerpretation in each LANDSAT band, and compares the detail discernible in LANDSAT imagery to that available in other sources.

Band 7 (0.8 - 1.1 μm)

a. Surface Water - The Blacksburg watershed contains no standing water areas of significant size. The LANDSAT scene in which it appears does contain a large (~1,000' width) river: this was readily discernible and used to align the imagery with the ground truth map.

b. Streamcourses - Without the topo map, identification of small streams was extremely difficult. When the LANDSAT image was overlayed on the map, some stream patterns became more apparent - approximately 20% of the streams in the watershed were detectable.

c. Vegetation - Vegetative detail is not readily detectable in Band 7. Agricultural fields could not be delineated. Most vegetation appeared a uniform gray shade. Correspondence with topo map information was fair. 55 hectares of land were identified as forest, whereas 71 are reported in the topo map.

FIGURE 51 AERIAL AND LANDSAT IMAGES OF BLACKSBURG WATERSHED

AERIAL PHOTOGRAPH
Scale: 1:60,000 (approx.)

LANDSAT BAND 5
26 OCTOBER,1973 Scale: 1:125,000 (approx.)

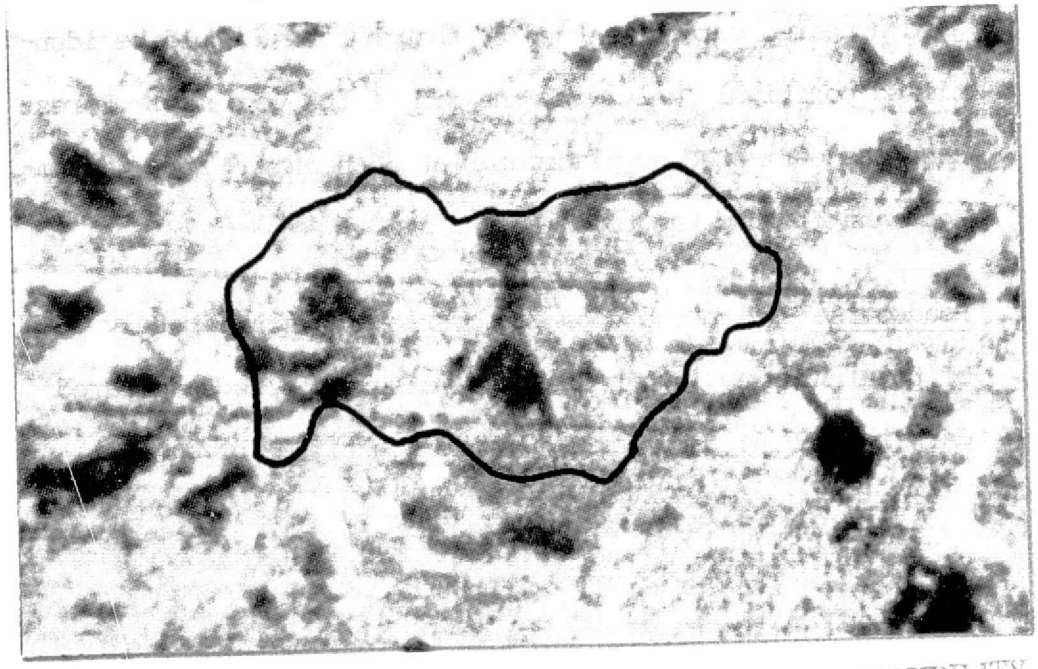

d. Impermeable Areas - The only impermeable areas readily identifiable were roads. Primary four lane highways appeared dark, secondary roads were partially visible. Some railroad right of way could be seen. Approximately 25% of total highway miles could be seen.

Band 6 (0.7 - 0.8 μm)

a. Surface Water - The large river in the scene was visible, though not quite as dark as in Band 7. This river again was used to align the imagery.

b. Streamcourses - No streams could be discerned within the watershed without the aid of the topographic map. When overlayed, however, approximately 20% of total stream length could be identified, appearing a slightly darker gray than their surroundings.

c. Vegetation - The more heavily vegetated areas of the watershed appeared darker in Band 6, though forest could be identified positively only with the aid of the topo map. Forest area was estimated by planimeter at 56 hectares from the images and 71 from the topo map.

d. Roadcourse - With the topo map overlayed, approximately 35% of total highway length could be measured. Roads appeared dark in Band 6; they could also be identified by shape.

Band 5 (0.6 - 0.7 μm)

a. Surface Water - The large river was visible in Band 5: contrast was not as good as in Bands 6 or 7. Visibility was sufficient to use the river for alignment, however.

b. Streamcourse - With the image projected on the map, more streamcourse became visible in Band 5 than from the preceding two bands. Approximately 22% could be measured visually.

c. Vegetation - Band 5 appears to offer the most vegetative detail. Color ranges from dark to very light and some field shapes are distinguishable. Forest area was measured by planimeter as 52 hectares.

d. Roadcourse - Road detail was minimal without the ground truth. Contrast is not as good as it is in areas where roads are cut through forests. When overlayed, though, the image revealed sections of primary road. Approximately 5490 meters of the 12,505 meters present could be discerned.

Band 4 (0.5 - 0.6 μm)

a. Surface Water - Surface water is obscured in Band 4. The large river was only faintly visible and could not be used to locate the watershed.

b. Streamcourse - No streams could be measured even with the topo map as reference.

c. Vegetation - Vegetative detail is significantly worse than in Band 5. Most cover classes appear an almost uniform gray shade, with a few fields having high reflectance. One such field could be located and correlated to a ground truth aerial photo. Forest acreage was not measurable.

d. Roadcourse - Only occasional sections of road could be seen and only in combination with the topo map. Though two sections were used to align the map, no significant quantitative measurements could be taken.

4.2.2.2) Analysis of the Oxford Watershed

Figure 52 shows the Oxford, Mississippi test basin. The watershed consists of 2227 hectares in north central Mississippi. The land is low-lying, characterized by a preponderance of forest cover with some open fields and no urbanization.

Band 7 (0.8 - 1.1 μm)

a. Surface Water - According to the 1970 USGS maps and the ASCS aerial photography, the watershed contains 105 ponds. Of these, 22 are larger than 1 acre in area. In LANDSAT Band 7, 11 ponds were visible, ranging from 1.25 to 8.0 acres. 49% of the total standing water area was visible. The visibility of the water bodies was not directly related to the size of the water bodies, i.e., some ponds of area 1 to 2 acres were clearly discernible while other larger ones were not. Distinctively shaped ponds were successfully used to align the LANDSAT imagery and the topo map.

FIGURE 52

AERIAL AND LANDSAT IMAGES OF OXFORD WATERSHED

AERIAL PHOTOGRAPH 11-22-74
SCALE 1:60,000

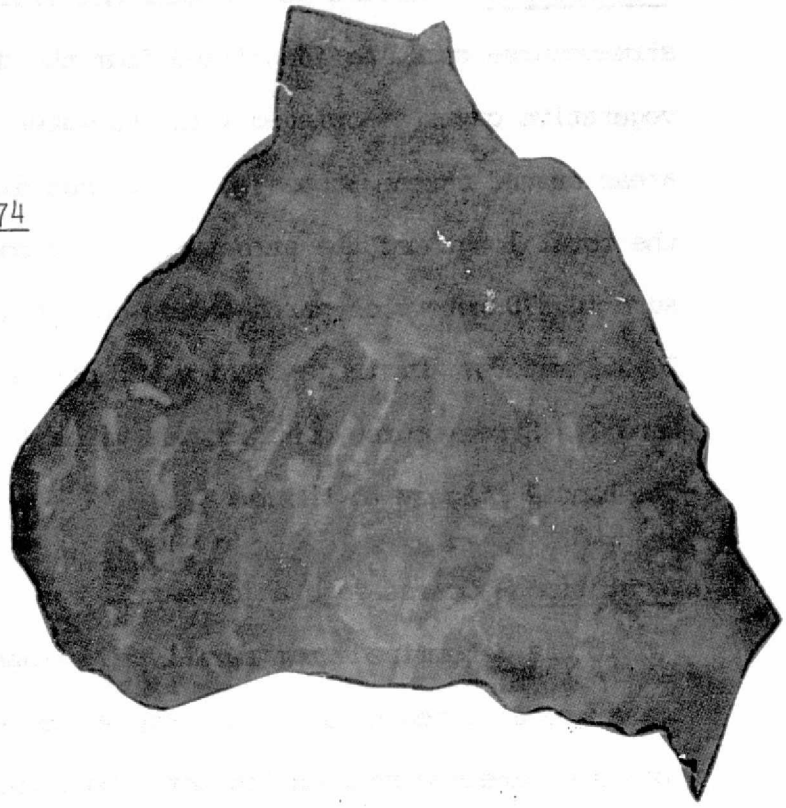

LANDSAT IMAGE 8-21-73
BAND 5 SCALE 1:60,000(approx.)

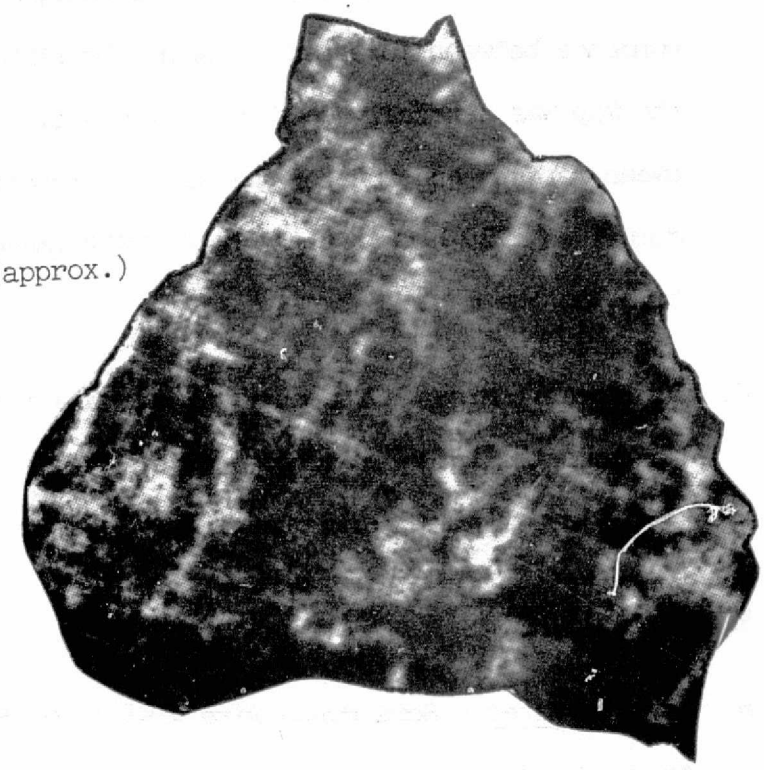

b. Streamcourse - Streams per se were not visible, but the streamcourse could be identified from the differences in vegetative cover associated with the water route. Wide areas around streams appeared light, but did not follow the total length of the streams. It was possible to measure 10,370 meters of streamcourse out of a total of 20,283 meters. Drainage density was not measurable on Band 7. Streamcourse contrast was valuable in aligning the Band 7 imagery to the map.

c. Vegetation - Coarse vegetation detail was visible on Band 7. It was determined from aerial photographs that the forest cover appeared a medium gray while less heavily vegetated areas were much lighter. Only two gray shades could be easily separated by visual analysis. The correspondence between forested areas on the LANDSAT images and the map was generally good but not exact. The borders between forests and non-forests matched imperfectly. Forests comprised 1730 hectares on the LANDSAT images and 1321 hectares on the map.

d. Impermeable Areas - The only impermeable areas clearly visible were the larger roadbeds. Visibility of roadways in Band 7 was minimal - no quantitative measures could be made.

Band 6 (0.7 - 0.8 μm)

a. Surface Water - Some ponds were visible on Band 6 but contrast was poorer. Six ponds were identified ranging from

1.25 to 8.0 acres. These six were a subset of those identified in Band 7, i.e., five of the intermediate size ponds were obscured. These six ponds represented 41% of total surface water area.

b. Streamcourse - The appearance of streamcourses on Band 6 was similar to Band 7, but the amount of detail visible was reduced. General contrast was slightly poorer than that of Band 7. 8450 meters out of 20283 meters total streamcourse were measurable. The streams themselves were not visible, though a canal approximately 50 feet wide was identified. In Band 6 the streamcourses and ponds were used to align the image.

c. Vegetation - Forest and non-forested areas were visible, although agreement with the map was imperfect. The heavily vegetated areas were basically a single shade of gray. The detail was slightly better than in Band 7. Forest area was estimated from Band 6 as 1704 hectares, a 29% discrepancy with respect to the USGS map.

d. Impermeable Areas - Roadcourses were far more apparent in Band 6 than in Band 7. The roads in the scene are of secondary and tertiary size. The roads themselves were not visible but the contrast between forest and clearing around the road was apparent. Approximately 50% of the ridge lines corresponding to the path of the roads was visible. 7320 meters of a total of 12810 meters of roads were identified.

Band 5 (0.6 - 0.7 μm)

a. Surface Water - Surface water was invisible on Band 5. No ponds could be identified.

b. Streamcourse - The streamcourse in Band 5 was presented less contrast than in either Band 6 or Band 7. It was more difficult to locate the basin since streams and ponds were not satisfactory guides. Though the contrast was severly reduced, more streamcourse was visible than in Band 6 and Band 7, once the imagery had been registered with the map. Band 5 provided an improved estimate of total channel length over either bands 6 or 7.

c. Vegetation - Subtle differences in vegetative cover were apparent. Forests were darker than fields, but greater differentiation was possible within the forest class. In this respect more detail is present than is given in the map, and the correspondence of forest area is greater.

d. Impermeable Areas - Roadcourses have high reflectance in Band 5 and contrast is marked. Tertiary roads are visible to a great extent, and were used to align the watershed imagery. Without the roads, location of the watershed would have been extremely difficult. Approximately 80% of the ridge-line corresponding to roadcourses was discernible.

Band 4 (0.5 - 0.6 μm)

a. Surface Water - No standing water was visible in Band 4.

b. Streamcourse - Streamcourses were lighter than forest but contrast was not as sharp as in Bands 6 and 7. About 6% of total streamcourse was detectable in Band 4.

c. Vegetation - Overall contrast is poorer than Bands 5, 6, or 7. Light and dark correspondence with ground truth was similar to Bands 6 & 7, but visibility was severly inhibited. Forest area, therefore, was not measured in Band 4.

d. Impermeable Areas - Some but not all secondary and tertiary roads were visible in Band 4. Total length visible was visible was 10,980 meters. Roadcourses appear light and were used to align the imagery, but contrast is much worse than in Band 5. About 30% of the ridge line corresponding to roadcourse was clear.

In additional analysis, the photointerpreter took a single surface characteristic - forested area - and attempted to quantify it in bands 5 and 7 and in two multi-band combinations. The forested areas were mapped and subsequently compared to ground truth data (USGS topographic map) to check classification accuracies. Figures 53a through e depict maps of forested areas constructed from Landsat imagery by utilizing the reflectance levels of the bands. It is clear that Band 7 greatly overestimates forest area. This is consistent with the single band analyses presented earlier. Band 5 can differentiate more detail among surface covers and therefore yields a better estimate. Satisfactory results (15.1% inventory error) also came from the intersection of Bands 5 and 7.

FIGURE 53 REMOTE CLASSIFICATION OF FORESTED AREA

OXFORD, MISS., WATERSHED

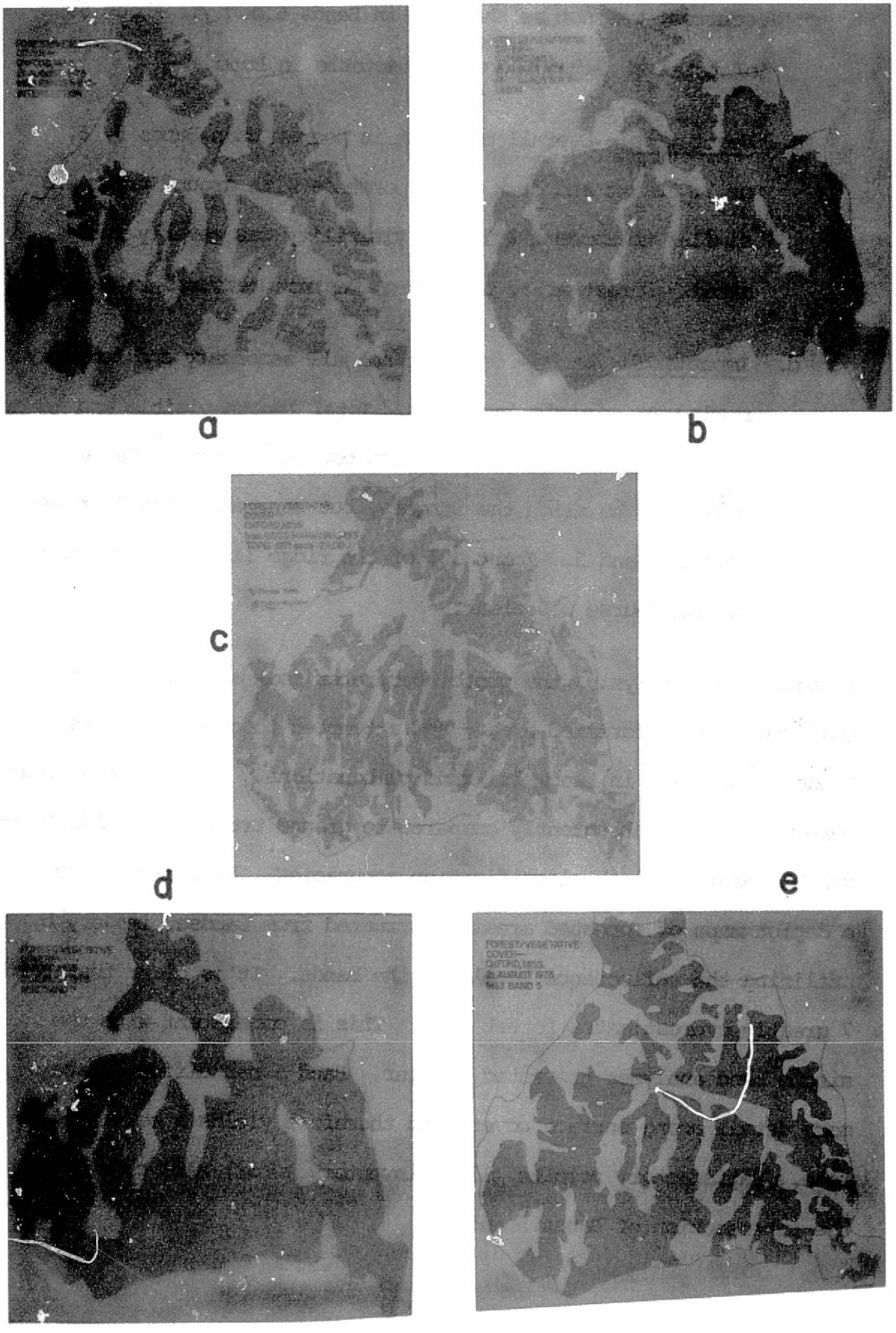

Table 18 presents the omission and commission errors calculated from the forest area estimates. In the inventory mode (errors calculated by taking the difference between observed and actual areas and dividing the result by actual area), Band 5 yielded an error of only 1%.

4.2.2.3) Conclusions from the Analyses

Table 19 summarizes the findings made on the Oxford and Blacksburg watersheds. The following conclusions can be made regarding the relative value of each band limited, of course, to the examples analyzed.

1) Band 7 appears to be best for identification and measurement of surface water area. This is because of the very low reflectance of standing water in the 0.8 - 1.1 μm range and consequent high contrast with its surroundings. Though no significant urbanization exists in either basin, analysis of the remainder of the LANDSAT scene showed Band 7 to be good also for identification of urban land use.

2) Band 5 offers much more information about vegetation than the other bands. Where vegetative cover typically appears only as one or two shades of gray in other bands, Band 5 often yields twice that number.

3) The information derivable from Band 6 is correlated with that of Band 7; likewise, Band 4 is correlated with Band 5. In both cases, the detail in the former has proven inferior. Band 4, however, was found useful in the measurement of road-courses.

TABLE 18

FOREST/VEGETATIVE AREA COMPARISON

	Band 7	Band 5	Intersection 5 & 7	Union 5 & 7
Total Area Measured	1730 Ha.	1309 Ha.	1123 Ha.	1911 Ha.
Omission Error	6.1% (81 Ha)	9.3% (123 Ha)	2.8% (37 Ha)	2.1% (28 Ha)
Commission Error	31.1% (411 Ha)	21.2% (281 Ha)	18.9% (250 Ha)	38.3% (506 Ha)
Inventory Mode Error	31%	1.01%	15.1%	44.5%

Actual area = 1296 Ha. (from U.S.G.S. 1:24,000 Scale Topographic Map)

NOTE: The U.S.G.S. map is not necessarily accurate. Thus the results quoted should be considered as indicative, but not conclusive

TABLE 19 COMPARISON OF MEASURED HYDROLOGIC SURFACE CHARACTERISTICS TO USGS TOPO. MAPS

	STREAMCOURSE VISIBLE (ft.)		FOREST VISIBLE (Ac.)		ROADCOURSE VISIBLE (ft.)		SURFACE WATER VISIBLE (Ac.)	
	Blacksburg	Oxford	Blacksburg	Oxford	Blacksburg	Oxford	Blacks-burg	Oxford
BAND 4	*	10,000	*	1792	*	36,000	0	0
BAND 4	14,000	36,000	129	3232	18,000	12,000	0	0
BAND 6	12,000	28,000	138	4210	14,000	24,000	0	33
BAND 7	12,000	34,000	135	4273	10,000	0	0	39
USGS. MAP	58,000	163,000	175	3265	41,000	42,000	0	80

TABLE 20 COMPARISON OF HYDROLOGIC PARAMETERS ESTIMATED FROM LANDSAT TO THOSE ESTIMATED FROM GROUND TRUTH DATA

	Holtan's "a"		Manning's "n"	
	Va.	Miss.	Va.	Miss.
BAND 4	*	.59	*	.053
BAND 5	.42	.75	.033	.071
BAND 6	.43	.86	.033	.084
BAND 7	.43	.87	.033	.084
BAND 5 & 7	-	.70	-	.065
MAP	.44	.76	.034	.072
A.R.S. RECORDS	.42	.56	.039	.060

* No quantitative measurement possible

The final step of the analysis was aimed at determining the accuracy of the measurements of Manning's "n" and Holtan's "a" from LANDSAT imagery. These two parameters were first computed from the ARS records. The two coefficients were calculated from the information extracted from each band. For the Blacksburg watershed, the best estimate came from Band 5, though it was only marginally better than the values obtained from the other bands. All estimates are satisfactory for modelling purposes. The best single band for the Oxford watershed was Band 4: the Band 5 and 7 intersection was an improvement over other single-band figures. Results are given in Table 20.

The overall conclusion is that since each band provides an information increment, the sum of the information present in each should be applied to determining the model's parameters. This can be accomplished by analysis of each band individually, as was done for the Oxford and Blacksburg basins, or by compositing the information into a "synergistic" image, as will be described in the next section.

4.3) Quantitative Hydrologic Analysis of LANDSAT Imagery

The results of the preliminary visual analysis of the Blacksburg and Oxford watersheds were sufficiently promising as to warrant its extension to a detailed study of a third basin, possessing high-quality recent ground truth. The objective was to determine how many surface features could be identified and measured; to assess the accuracies

achievable in areal measurement in the inventory and land use modes; and to ascertain the hydrologic information content of composite imagery. The Muddy Branch Creek in Montgomery County, Maryland, was selected for this study, for the following reasons:

1) A set of multi-temporal ground truth is available in the form of high-altitude color infrared aerial photographs of high quality. These were obtained through the cooperation of the Maryland Department of State Planning. The photography was taken within two months of the LANDSAT pass analyzed.

2) Soil Surveys and 1:24,000 scale topographic maps are available.

3) The watershed is gaged.

4) The watershed is sufficiently large - approximately 5000 hectares - to contain a variety of land uses, thus presenting a good test of the remote sensing capability to identify a diverse set of surface covers.

5) Other local studies of this watershed for other purposes are available: thus a good inventory exists of physiographic and hydrologic data.

6) The watershed is rapidly urbanizing and subject to frequent flooding, resulting in high monetary losses.

7) The basin is sufficiently close to permit detailed on site visual examination if required.

Figure 54 shows a map of the Muddy Branch watershed. The surface cover contains fields and meadows, some of which are cultivated, and some fallow, plus other several land uses. The areas immediately adjacent to the main stream are predominantly forested. The northeastern end of the watershed contains part of the city of Gathersburg and therefore, residential and industrial land uses. Several lakes are present, ranging from one-half to approximately 5 hectares in area. Figure 55 is an aerial photograph showing the location of these surface covers.

The two bands containing the most hydrologic information, MSS 5 and 7, were first analyzed individually: the accuracies of measurement of important hydrologic parameters from Landsat imagery were determined by comparison with the accuracy achievable from aerial photography. The analysis technique was visual. Thirty-five millimeter sections containing the Muddy Branch Watershed were cut out of LANDSAT 9" X 9" images, suitably mounted and projected by means of the device described earlier. "Training" correspondences between surface cover and visible color were established; the basin was then classified using only the Landsat imagery. The findings of the photointerpreters are presented following.

Band 7 (0.8 - 1.1 μm) Black & White

Vegetation detail was not good. Contrast among vegetated areas was low. Forests and fields were a medium shade of gray with forests appearing only slightly darker. Thus, forested area was generally overestimated, similar to what had occurred for the Oxford basin. The photointerpreter measured the forest area by planimeter to be 2591 hectares, as com-

FIGURE 54

MAP OF MUDDY BRANCH WATERSHED

Scale: 1:63,000 (approx.)

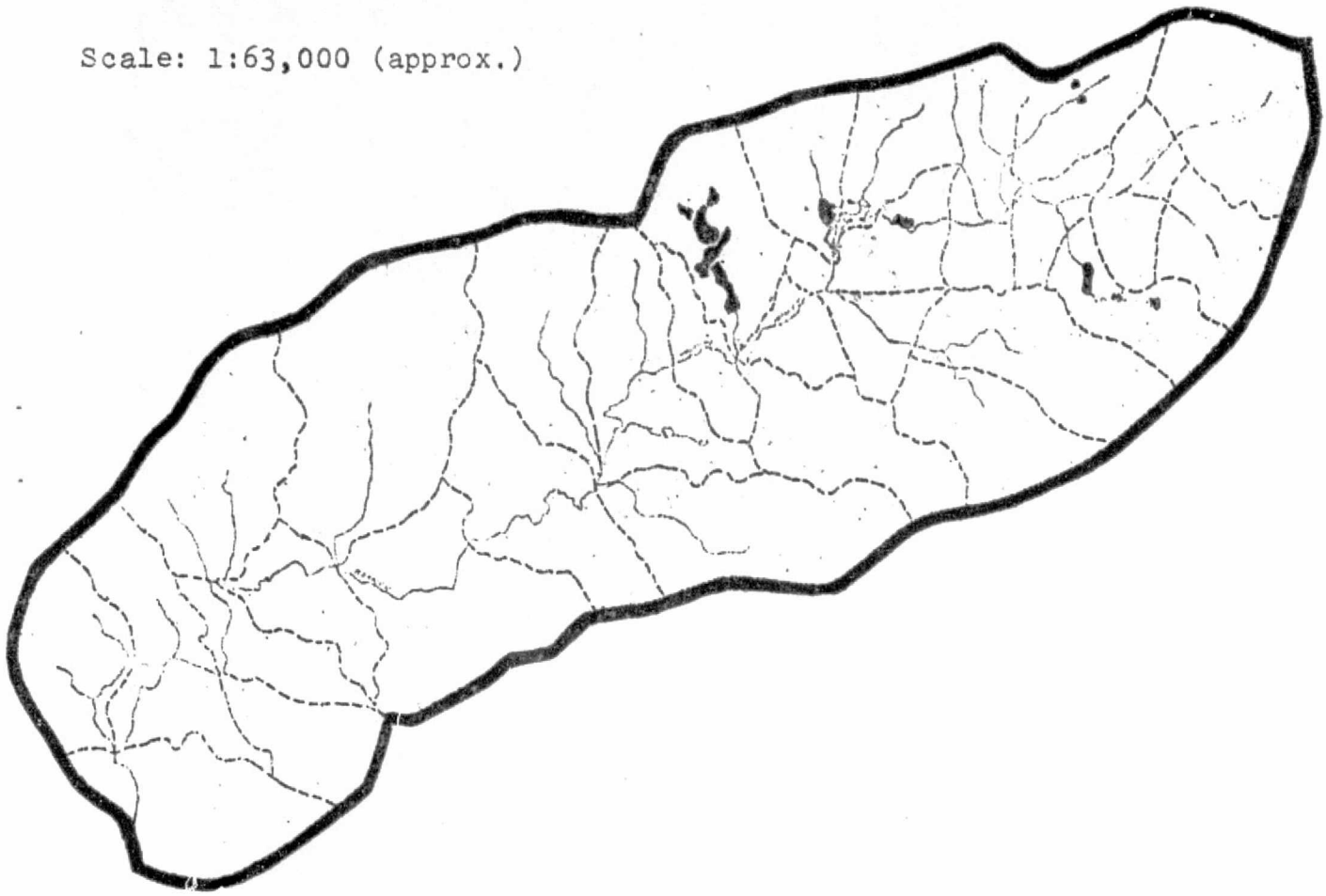

Source: Storm Water Management--A Comprehensive Study of the Muddy Branch & Seneca Creek Watersheds, Cornell, Howland, Hayes & Merryfield, Clair A. Hill & Associates, April, 1975.

FIGURE 55 CLASSIFICATION OF AERIAL PHOTOGRAPHY GROUND TRUTH

MUDDY BRANCH WATERSHED

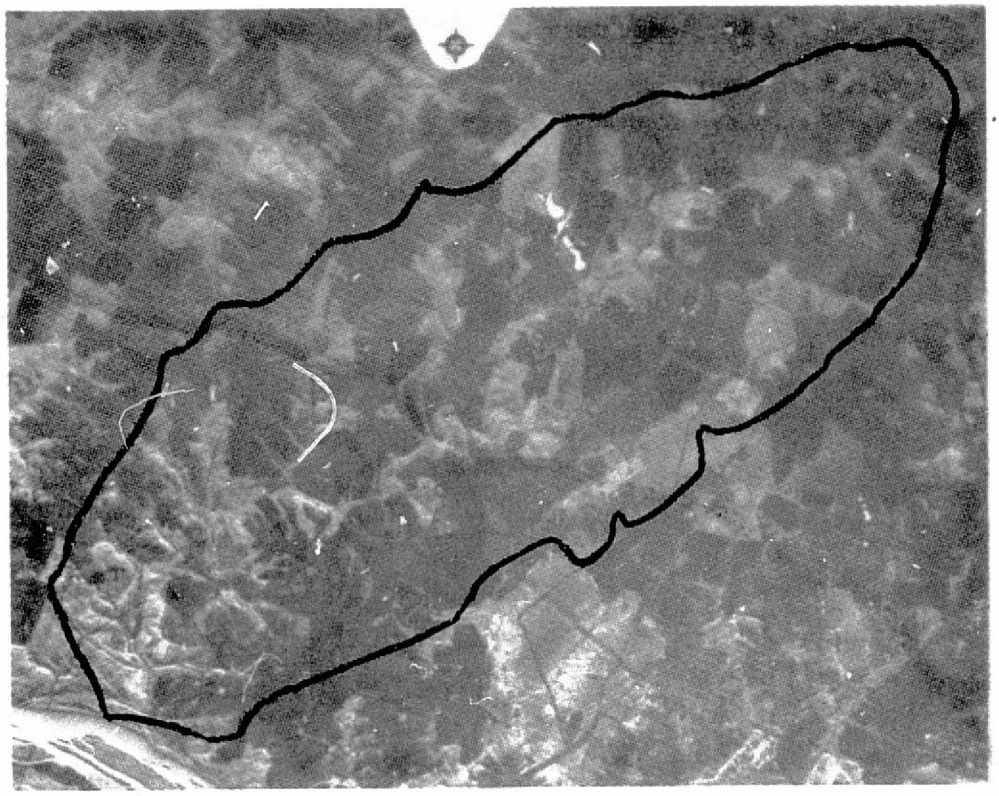

pared with 1519 measured from the aerial photographs. Band 7 is much better suited for identifying and measuring surface water. Forty-one lakes are present in the watershed. Eleven could be seen easily; two more were discernible when the topographic map was overlayed. These thirteen, comprise 67% of the total surface water. Roads were not particularly visible on Band 7. A major interstate highway which traverses the watershed could be seen, as could a second major artery: no others were visible. Streamcourse visibility was minimal and could be identified only with the aid of the topographic map. When overlayed, 5490 meters of streamcourse out of a total of 79,300 were discerned.

Band 5 (0.6 - 0.7 μm) Black & White

The river banks of the Potomac River which appears within the scene containing Muddy Branch Creek were not sharp. Impermeable areas - standing water and urbanization were also depressed. No lakes or ponds could be seen. Only the large interstate highway was visible. Conversely, vegetation detail was substantial. It was possible to more accurately differentiate between fields and forested areas. Area was measured by planimeter to be 1703 hectares, a overestimate with respect to ground truth. Differences in vegetative shade could be used to delineate certain other physical features of the watershed. Power line cuts could be easily seen; as could the location of a building situated in a small cleared area. Streamcourses per se could not be discerned, but were apparent insofar as they were correlated to forested areas.

Single-band analysis of Muddy Branch thus produced results congruent with the earlier findings; Band 7 is most useful for identification of surface water and urban uses while Band 5 is most suited to vegetation classification.

Multi-band Imagery Analysis

Multi-band images were prepared for analysis using a diazo processor. LANDSAT 9" X 9" black and white images were transferred to a sheet of transparent film and encoded in shades of a single color. A Band 5 image, for example, was reproduced in shades of magenta. Band 4 and 7 diazo images were produced in yellow and cyan, respectively. This color combination places the individual images 120 degrees apart on the "color wheel" and thereby heightens the contrast and readability of the composite.

The individual transparencies of the three bands were then combined into a layered sandwich. The images were registered using the reference marks available on the Landsat imagery. Tests with calibrated test sheets demonstrated registration errors to be significantly less than a pixel. The advantages of thus producing diazo composites were found to be:

1) The information contained in all the spectral bands is made visible simultaneously.

2) It is well-known that the eye is more amenable to separation of color than of shades of gray. In fact, the addition of color provides a marked improvement in visual

analysis over black and white images. The three primary hues combine in the composite to produce a large number of distinguishable colors.

3) The diazo films can be developed and combined to stress different colors and shadings. This permits the interpreter to "tune" the composite images to accent the contrast of desired features. For example, a composite with a dark magenta component in Band 5 obscures vegetation contrast, but heightens surface water visibility.

4) The process is very inexpensive. A four-color composite can be generated for a total cost of approximately $1.00.

A slide-size section containing the watershed was cut out from the composite and projected as previously described.

The first composite analyzed was made from LANDSAT images taken in October, 1973. The ground truth aerophotos were taken in December, 1973 at a scale of 1:130,000. Five distinct land uses could be seperated: forests, fields, lakes, bare soil, and urban areas. The LANDSAT composite was visually interpreted and thematic maps prepared for each cover class. Description of the analysis and accuracies achieved follows.

FORESTED AREA

All vegetation appears red or red-orange; forests display a darker red shade. In the inventory mode, forest area was measured as 1242

hectares from the LANDSAT composite versus 1292 from the aerial photo. This estimate of forested area is significantly better than that obtained from single-band imagery.

FIELDS

On the aerial photograph, cropped and non-cropped fields were discriminable; in the LANDSAT composite the agricultural areas were too similar to ordinary meadows to be separable from these. Fields could usually be separated easily from forests due to their lighter red-orange shade. Some of the boundaries between fields and forests or bare soil were unclear and had to be estimated. Area of fields was measured as 2852 hectares from the LANDSAT imagery, a 6% underestimate compared with aerial photoground truth.

LAKES

Standing surface water showed the best contrast with its surroundings and was therefore the most easily identifiable surface element. Lakes down to an area of approximately one acre were visible, though all lakes extant in the basin could not be identified from the LANDSAT composite. Surface water appeared almost black in the composite and was typically surrounded by orange fields, illustrating the value of contrast for identification and mensuration. Percent total surface water area was overestimated slightly from the LANDSAT imagery due to the dominance of border pixels in the low Band 7 reflectance of water.

BARE SOIL

In the aerial photograph, land without vegetative cover showed up white. In the LANDSAT color composite, areas identified as bare soil presented two distinct colorations. Most areas appeared light blue: some displayed a much darker blue coloration. The reason for this difference is not completely clear; it appears that moisture content could be causing the effect. Both light and dark blue areas were summed in computing bare soil area. 575 hectares acres were measured from the composite versus 547 from the aerial.

URBAN AREAS

Two distinct shades were visible for developed urban areas. Some locations appeared pinkish while others were bluish. Both types were less uniform in color (i.e., appeared mottled) than any other cover class: this factor allowed their separation and identification. From the aerial photo, the type of urbanization (residential versus non-residential) could be seen and a correlation was attempted between land use and color. Though the relation did not always hold, there appeared to exist a correspondence between color intensity of development. Large-lot residential areas contain vegetation (and therefore appear pinkish) than more crowded sites possessing a less amount of natural surface cover. Total urban area was measured to be 557 hectares from the LANDSAT composite and 649 hectares from the aerial.

Figure 56 is a black and white reproduction of the October LANDSAT composite. The lower graphic presents a summation of the thematic

FIGURE 56

OCTOBER 1973 LANDSAT COMPOSITE IMAGE

MUDDY BRANCH WATERSHED

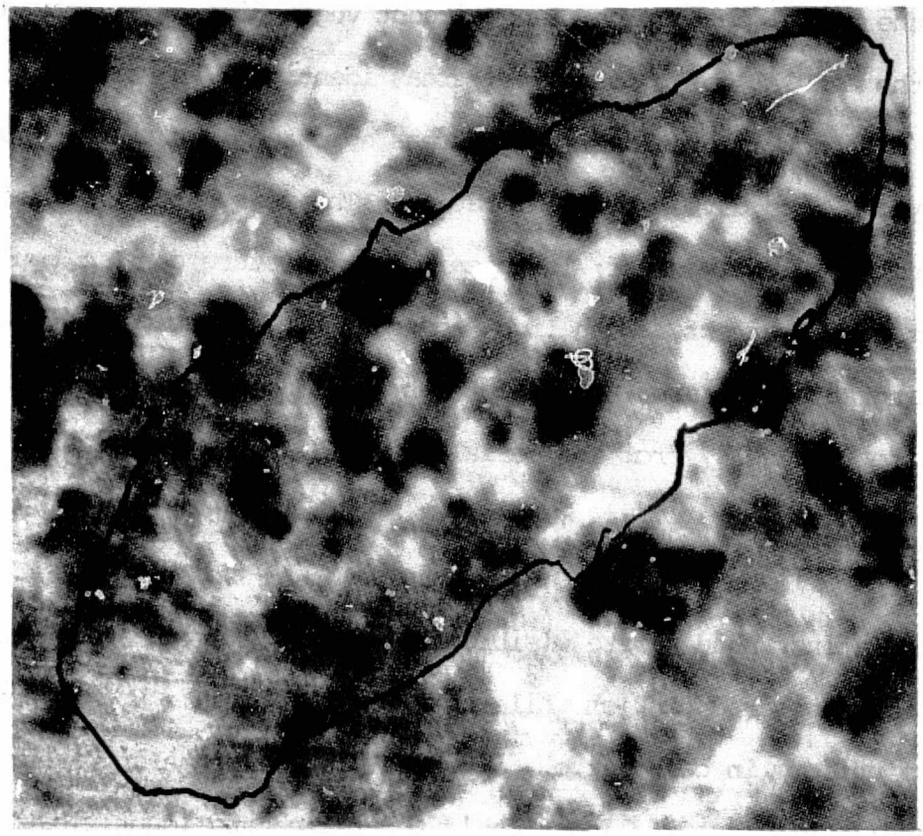

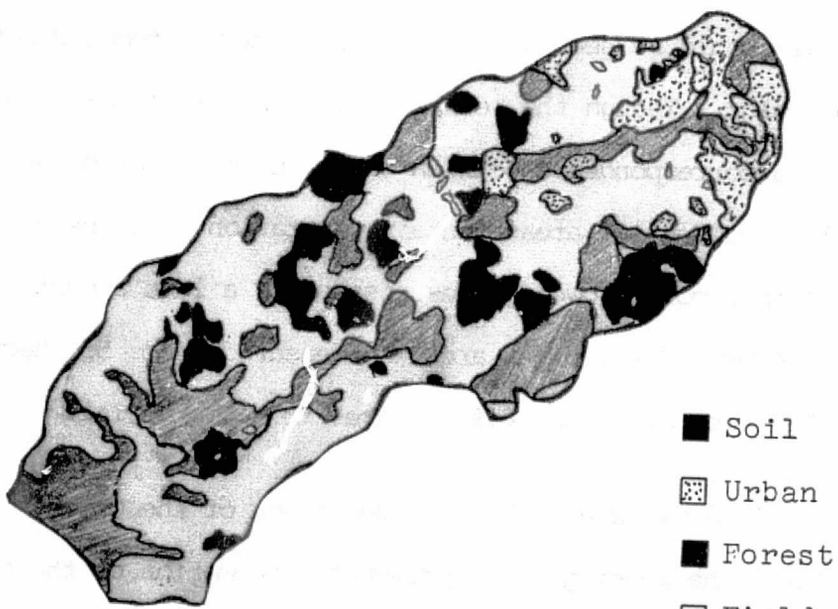

maps produced for each cover class. The areal extent of each land use was measured by overlaying a calibrated grid and counting the squares included in the particular cover class. The number of squares was then converted to hectares and errors calculated. Some areas had earlier been estimated with a planimeter, however, it was found that the grid technique produced commensurate accuracies while reducing analysis time. The results obtained in the inventory mode are reported in Table 21. They were calculated by subtracting actual area from measured area and dividing by actual area. The errors shown, therefore, represent differences in areal measurement rather than in location. Table 22 presents the results in the land use mode. As expected, these corresponding errors (area correctly classified minus actual area, divided by actual area) are higher than the inventory errors. However, in most hydrologic models, the parameter used is the percent of a watershed in each surface cover class: the inventory mode errors apply in this case.

Table 23 presents a breakdown of errors by category. Lakes, for example, were most often confused with fields. This was not due to their having similar reflectance characteristics, but rather to the fact that the border between the two was unclear. The lakes supplied very low reflectance and therefore dominated the border pixels. This led to confusion with the surrounding fields and consequent overestimation. Forest, field, urban and soil combinations exhibited similar behavior. Though their color shades in the composites were easily distinguishable, the boundaries were not as sharp as in the aerial photography. For example, two forested areas separated by a small tract of fields tend to be classified as all forest.

INVENTORY MODE ERRORS - MUDDY BRANCH BASIN

TABLE 21

INVENTORY MODE					
	AREA LANDSAT	% OF WATERSHED	AREA AERIAL	% OF WATERSHED	INVENTORY ERROR
Urban	1,376 acres	11	1,604 acres	12	- 14%
Forest	3,068 acres	24	3,192 acres	23	- 4%
Lakes	74 acres	1	72 acres	1	+ 3%
Soil	1,420 acres	11	1,352 acres	10	+ 5%
Fields	7,044 acres	54	7,480 acres	55	+ 6%

LAND USE MODE ERRORS - MUDDY BRANCH BASIN

TABLE 22

LAND USE MODE			
	COMMISSION ACRES	OMMISSION ACRES	LAND USE ERROR
Urban Area	156	472	- 24%
Forest	614	778	- 23%
Lakes	22	16	- 28%
Bare Soil	684	546	- 46%
Fields	1,088	1,548	- 20%

TABLE 23

ANALYSIS OF CLASSIFICATION ERRORS

	AERIAL (Hectares)	LANDSAT-1 (Hectares)	LANDSAT-1: HECTARES CLASSIFIED AS:					
			LAKES (a)	SOIL (b)	URBAN (c)	FOREST (d)	FIELDS (e)	SUM (a+b+c+d+e)
LAKES	27	28	-	1	0.3	1	11	14
SOIL	421	428	0	-	8	40	122	170
URBAN	614	480	0	7	-	46	136	190
FOREST	1231	1245	2	17	33	-	164	216
FIELDS	2186	2246	16	228	65	174	-	483

The percent areal composition of each class of cover of the Muddy Branch watershed was computed from the aerial photography and from the LANDSAT analysis. Table 21 shows that the largest difference between the two was one percent.

Manning's "n" and Holtan's "a" were again calculated on the basis of LANDSAT and ground truth data. Table 24 depicts the findings:

TABLE 24

	LANDSAT COMPOSITE	AERIAL GROUND TRUTH
Manning's "n"	0.037	0.037
Holtan's "a" *	0.489	0.480

* for non-urban areas only

The color composite clearly gave results equal to those of the aerial ground truth. The accuracies achievable from LANDSAT in the assignment of hydrologic parameters were found to be quite satisfactory.

The quantitative analysis of LANDSAT imagery for Muddy Branch watershed demonstrates that accuracies sufficient for hydrologic modelling can be obtained through relatively simple visual means. It was further determined from the investigation of the Oxford and Blacksburg watershed that two factors can improve classification results:

1) The quality of the data used as ground truth is important. The aerial photographs used for the Muddy Branch analysis were more recent, and therefore more reliable, than was the map data applied in the Oxford and Blacksburg investigation.

Moreover, aerial photography gives a picture of what is on the surface rather than a graphic representation, thus facilitates comparison to satellite imagery.

2) The application of the several MSS bands individually and in composite form provides far more discriminability and therefore better accuracies than does the use of a single band.

CHAPTER V

SUMMARY OF FINDINGS AND CONCLUSIONS

Three tasks were undertaken in this effort: 1) the validation of the peak-rate model on an expanded set of watersheds, 2) the development of a routing model for complex basins, and 3) the quantitative hydrologic analysis of LANDSAT imagery. The findings and results are described in the following.

5.1) Expanded Validation of the Peak-rate Model

A thirty-one watershed sample was selected with significant geographic and hydrologic diversity. The prediction supplied by the model was tested on each, and the output compared to the records and to forecasts computed by using three other conventional planning models. The remote sensing model gave improved variability and accuracies commensurate to the other three models. Mean errors for the remote sensing model were approximately 50%. The remote-sensing model in its current implementation applies to "simple" basins - composed of a single predominant channel, and devoid of significant sub-basins.

Additionally, some potential sources of modelling error were identified and therefore a number of pertinent questions were addressed. First, the "planning rain" had to be defined. Subsequent analyses led to the conclusion that this rain could be best approximated by one of triangular shape, having a duration approximately equal to the time of concentration of the basin and having a recurrence of approximately fifty-years. Second, seasonal characteristics of peak flow phenomena were investigated to ascertain what impacts they might have on a model.

It was discovered that different geographic regions exhibit varying seasonal properties, but that, within a region the characteristics are similar. Those basins located in subsurface-dominated areas, for example, show a propensity to produce peak discharge in a two to three month period in late summer hence requiring increased satellite coverage during this period. The model, therefore, should measure the physiographic (drainage density) and hydrologic (surface cover, soil moisture, etc.) conditions which exist in the critical season. Finally, sensitivities of surface parameters were examined. It was shown that the runoff rates were sensitive to slope primarily at low slopes. Further, it was found that sensitivity to surface function requires that a remote sensor be able to classify surface cover into categories with similar values of Manning's "n".

5.2) Development of a Routing Model

The need for a model to treat "complex" basins was identified above. A model was developed which approximates the watershed by a series of strips, each having its own set of surface and rainfall parameters. The output of these strips is summed using a simple time delay function which accounts for the length of overland flow and the hydrologic characteristics of the channel. The complete model was applied to analysis of the sensitivity of runoff to basin slope and areal extent of rainfall. It was discovered that both are significant and should be provided for by the planning model. The routing model met these criteria and also those of high remote sensing input potential and computational simplicity.

5.3) Hydrologic Analysis of LANDSAT Imagery

The final task was aimed at using remote sensing directly to determine hydrologic information content of the LANDSAT bands and to atatmpt to simply extract the necessary hydrologic data. Initially, the Oxford and Blacksburg test basins were examined. It was found that information sufficient to determine several of the important inputs to the model could be determined from LANDSAT data using relatively uncomplicated visual techniques. Moreover, it was determined that single bands contain useful but different data and hypothesized that a composite image would optimize the information value. This hypothesis was confirmed through in-depth analysis of the Muddy Branch basin. Surface features of the watershed were identified, measured, and checked against aerial photographs ground truth. The results showed inventory errors to be well within acceptable limits for modelling and useful for direct computation of model parameters.

APPENDIX A

STATISTICAL ANALYSIS OF FORECAST ERROR IMPROVEMENT

A set of tests was run to determine if the observed improvements were statistically significant. The procedure to be used is to first establish the equality or inequality of variances among the four models and given these results, to determine the significance of the difference among the means. First, the Cochran test for equality of vaiance was performed to test the null hypothesis that

$$\alpha^2_{\text{peak rate}} = \alpha^2_{\text{SCS, Cook, Rational}}$$

against the alternative that the variances are unequal.

The appropriate statistic is as follows:

$$G = \frac{\text{largest } S_i^2}{\sum_{i=1}^{k} S_i^2}$$

Where: G = test statistic number

S_i = sample variance of i^{th} sample

k = number of treatments (equal to 2 in this case since the models were tested in pairs)

The process for comparing the variances of the peak rate and S.C.S. models is given below.

$$S^2_{SCS} = 6,691.24$$

$$S^2_{\text{peak rate}} = 1,332.25$$

$$G = \frac{6,691.24}{8,023.45} = 0.83$$

The table value of G at the 95% confidence level is 0.7657.

$$G_{test} > G_{table}$$

The null hypothesis for the peak rate and SCS formulas can therefore be rejected, thus accepting the alternative hypothesis,

$$\alpha^2_{SCS} > \alpha^2_{peak\ rate}$$

Similarly, the equality of variance of the peak rate and Cook's model was tested.

$$S^2_{peak\ rate} = 1,332.25$$
$$S^2_{Cooks} = 22,290.49$$

$$G = \frac{22,290.49}{23,622.74} = 0.94$$

$G_{test} > G_{table}$ (= 0.7657 at 95% confidence level)

$\therefore$ we reject the null hypothesis, and conclude that

$$\alpha^2_{peak\ rate} < \alpha^2_{Cooks}$$

Further, the inequality of variances between peak rate and Rational was established

$$S^2_{peak\ rate} = 1,332.25$$
$$S^2_{Rational} = 26,634.24$$

$$\therefore G = \frac{26,634.24}{27,966.49} = 0.95$$

$G_{test} > G_{table}$ We rejected the null hypothesis in favor of the alternative hypothesis, and conclude that

$$\alpha^2_{\text{peak rate}} < \alpha^2_{\text{Rational}}$$

All the above analyses enable us to conclude that the variance of the peak rate model is less than the variances of the other models. The reduction of variance observed is therefore statistically significant at the 95% confidence level.

Knowing that the variances between the peak rate model and the other three are not equal defines the appropriate test for equality of the means. In this series, the peak rate model was tested individually against the three other models for significance of difference between the means. The test statistic used was:

$$T = \left[\frac{\bar{x}_1 - \bar{x}_2}{\frac{S_1^2}{n_2} + \frac{S_2^2}{n_1}} \right]$$

T = test statistic

$\bar{x}_{1,2}$ = mean errors of the two test samples

S_1^2, S_2^2 = variances of the samples

n_1, n_2 = number of each sample

In the first test, the peak rate model was compared with the SCS formula:

$$\bar{x}_{\text{peak rate}} = 54.1 \qquad \bar{x}_{SCS} = 62.5$$

$$s^2_{\text{peak rate}} = 1{,}332.25 \qquad s^2_{SCS} = 6{,}691.24$$

$$n_{\text{peak rate}} = 31 \qquad n_{SCS} = 31$$

$$T = \left[\frac{62.5 - 54.1}{\frac{6{,}691.24}{31} + \frac{1{,}332.25}{31}} \right] = 0.5$$

The number of degrees of freedom were computed by the formula:

$$\nu = \frac{\left[\frac{S_2^2}{n_1} + \frac{S_1^2}{n_2} \right]^2}{\frac{\left[\frac{S_2^2}{n_1} \right]^2}{n_1 - 1} + \frac{\left[\frac{S_1^2}{n_2} \right]^2}{n_2 - 1}} = 41.49$$

$\approx$ 42 degrees of freedom

The value of the table statistic at the 90% confidence level for 42 degrees of freedom is less than 1.311

$$\therefore \; T_{test} < t_{table}$$

The hypothesis of equality of means must therefore be accepted showing the peak rate model errors to be equal to the SCS model.

The second test compared the peak rate and Cook models.

$$\bar{x}_{Cook} = 99.2$$

$$s^2_{Cook} = 22{,}290.49$$

$$n_{Cook} = 31$$

By the same equation as previously given:

$$T = 1.63$$
$$\nu = 34$$

The table value of $t_{0.10}$ at 34 degrees of freedom is less than 1.311

$T_{test} > t_{0.05}$ ∴ Reject the null hypothesis and conclude that the mean peak rate model error is significantly less than that of the Cook formula.

Finally, the peak rate model was compared with the Rational formula.

$$x_{Rational} = 86.7$$
$$s^2_{Rational} = 26,634.24$$
$$n_{Rational} = 31$$

Therefore,

$$T = 1.09$$
$$\nu = 33$$

The significance of error improvement could not be established at thi confidence level.

BIBLIOGRAPHY

Precipitation; Meteorology

1) Rainfall Frequency Atlas of the U.S., Dept. of Commerce, Weather Bureau, 1963.

2) Rainfall Intensity - Frequency Regime Report #29, Vol. 1-5, Eastern U.S., Dept. of Commerce, Weather Bureau, 1958.

3) Climatic Atlas of the U.S., Dept. of Commerce, E.S.S.A., Environmental Data Service, 1968.

4) Probable Maximum Precipitation, Susquehanna River Drainage Above Harrisburg, Pa., Hydrometeorological Report No. 41, Dept. of Commerce, Weather Bureau, June, 1965.

5) Probable Maximum and TVA Precipitation Over the Tennessee River Basin Above Chattanooga, Hydrometeorological Report No. 41, Dept. of Commerce, Weather Bureau, June, 1965.

6) Probable Maximum Precipitation, Northwest States, Hydrometeorological Report No. 43, Dept. of Commerce, Weather Bureau, November, 1966.

7) Probable Maximum Precipitation Over South Platte River, Colorado, and Minnesota River, Minnesota, Hydrometeorological Report No. 44, Dept. of Commerce, Weather Bureau, January, 1969.

8) Probable Maximum Precipitation, Mekong River Basin, Hydrometeorological Report No. 46, Dept. of Commerce, Weather Bureau, May, 1970.

9) Meteorology of Flood-Producing Storms in the Mississippi River Basin, Hydrometeorological Report No. 34, Dept. of Commerce, Weather Bureau, July, 1956.

10) Meteorology of Hydrologically Critical Storms in California, Hydrometeorological Report No. 37, Dept. of Commerce, Weather Bureau, December, 1962.

11) Meteorology of Flood-Producing Storms in the Ohio River Basin, Hydrometeorological Report No. 38, Dept. of Commerce, Weather Bureau, May, 1961.

12) "Accuracy of Precipitation Measurements for Hydrologic Modeling," L.W. Larson & E.L. Peak, presented at A.G.U. Spring Meeting, 1974.

13) "Methods of Estimating Areal Average Precipitation," A.F. Rainbird, Report No. 3, World Meteorological Organization, Reprinted in 1970.

14) "Measurement and Estimation of Evaporation and Evapotranspiration," Technical Note No. 83, World Meteorological Organization, Reprinted in 1971.

15) Storm Rainfall in the U.S.; Depth - Area - Duration Data, U.S. Army Corps of Engineers, July 1973.

16) Climatological Data, and Local Climatological Data for Washington, D.C.; Maryland; & Delaware, Aug. 1972 to present, U.S. Dept. of Commerce, N.O.A.A.

17) Meteorological Drought, Research Paper No. 45, U.S. Dept. of Commerce, Weather Bureau, 1965.

Soils

1) Soil Survey Manual, Soil Conservation Manual, 1951.

2) Soil Survey, Dorchester County, Md., U.S.D.A. and Maryland Agricultural Experiment Station, 1963.

3) Soil Survey, Carroll County, Md., U.S.D.A. and Maryland Agricultural Experiment Station, 1969.

4) Soil Survey, Prince George's County, Md., U.S.D.A. (S.C.S.) and Maryland Agricultural Experiment Station, 1967.

5) Soil Survey, Marshall County, Miss. U.S.D.A. (S.C.S.) and Mississippi Agricultural Experiment Station, 1972.

6) Soil Survey, Caddo County, Okla., U.S.D.A. (S.C.S.) and Oklahoma Agricultural Experiment Station, 1973.

7) Soil Survey, Webster County, Neb. U.S.D.A. (S.C.S.) and University of Nebraska, Conservation and Survey Division, 1974.

8) Soil Survey, Grant County, Wisc. U.S.D.A. (S.C.S.); Wisconsin Geological and Natural History Survey; Wisconsin Agricultural Experiment Station, 1961.

9) Soil Survey, McLannan County, Texas U.S.D.A. (S.C.S.) and Texas Agricultural Experiment Station, 1942.

10) Aerial-Photo Interpretation in Classifying and Mapping Soils, Agriculture Handbook 294, Soil Conservation Service, U.S.D.A., 1966.

11) World Soils, E.M. Bridges (University Press: Cambridge, 1970).

12) S.C.S. Soil Group Classes, S.C.S. Hydrology Handbook.

Models & Modeling

1) Digital Simulation in Hydrology: Stanford Watershed Model IV, N.H. Crawford & R.K. Linsley, Dept. of Civil Engineering, Stanford University, July 1966.

2) Numerical Simulation of Watershed Hydrology (Texas Watershed Model), OWRR Technical Report HYD 14-7001.

3) Network Analysis of Runoff Computation (Chicago Hydrograph Model), C.J. Keifer, J.P. Harrison, T.O. Hixson, 1970.

4) "A Uniform Technique for Determining Flood Flow Frequencies Water Resources Council," 1967.

5) "Development of a Mathematical Model for the Simulation of Flat-Land Watershed Hydraulics," D.W. Deboer & H.P. Johnson, Iowa State University, November 1, 1969.

6) "Evaluation of a Deterministic Model for Predicting Water Yields from Small Agricultural Watersheds in Virginia," V.O. Shanholtz, J.B. Burford, & J.H. Lillard, Dept. of Agric. Engineering Research Division, Virginia Polytechnic Institute and State University, August, 1972.

7) "Investigation of a Linear Model to Describe Hydrologic Phenomenon of Drainage Basins," F.A. Schmer, Technical Report 19, Water Resources Institute, Texas A&M University, December, 1969.

8) National Weather Service River Forecast System Forecast Procedures, (HYDRO-14), Staff, Hydrologic Research Laboratory, December, 1972.

9) Computer Program for Project Formulation - Hydrology, Technical Release No. 20, U.S.D.A., Soil Conservation Service, May 1965.

10) A Generalized Streamflow Simulation System, U.S.D.C. (National Weather Service) and California Dept. of Water Resources, March, 1973.

11) A Distributed Linear Representation of Surface Runoff, W.O. Maddaus and P.S. Eagleson, MIT, Dept. of Civil Engineering, June 1969.

12) Water Balance Program, U.S. Forest Service, July, 1968.

13) "Continuous Hydrograph Synthesis With An API-Type Hydrologic Model," W.T. Sittner, C.F. Schauss, J.C. Monro, Water Resources Research, Oct. 1969 P 1007-1021.

14) Analog Computer Simulation of the Runoff Characteristics of an Urban Watershed, V.V. Dhruva Narayana, J.P. Riley, E.K. Israelson; Utah State University, Jan. 1969.

15) Mathematical Simulation of Hydrologic Events on Ungaged Watersheds, L.F. Huggins & E.J. Monke, Purdue Univ. Water Resources Research Center, March 1970.

16) Calibration of U.S. Geological Survey Rainfall/Runoff Model for Peak Flow Synthesis - Natural Basins, U.S.G.S., October 1973.

17) USDAHL-74 Revised Model of Watershed Hydrology, H.N. Holtan, G.J. Stiltner, W.H. Henson, N.C. Copey. U.S.D.S., July, 1974.

18) COSSARR Model - Streamflow Synthesis and Reservoir Regulation, U.S. Army Engineer Division, North Pacific, Portland, Oregon, January, 1972.

19) Runoff Evaluation and Streamflow Simulation by Computer, U.S. Army Engineer Division, North Pacific, Portland, Oregon, May, 1971.

20) Generalization of Streamflow Characteristics from Drainage Basin Characteristics, D.M. Thomas & M.A. Benson, U.S.G.S., 1969

21) "Soil Surface Characteristics and Rainfall-Runoff-Moisture Relationships on Coastal Plain Soils," Ronald E. Hermanson, Water Resources Research Institute, Auburn University, 1970.

22) "Stochastic Analysis of Hydrologic Systems," Ven Te Chow, Dept. of Civil Engineering, University of Illinois at Urbana-Champaign, Research Report No. 26, December, 1969.

23) "The Use of Analog and Digital Computers in Hydrology," Proceedings of the Tucson Symposium, International Hydrological Decade, UNESCO, 1969.

Floods & Flooding

1) Magnitude and Frequency of Floods in the U.S., U.S.G.S., 1964.

Part 2-A - South Atlantic Slope Basins, James River to Savannah River;

Part 2-B - South Atlantic Slope and Eastern Gulf of Mexico Basins, Ogeechee River to Pearl River;

Part 3-A - Ohio River Basin Except Cumberland and Tennessee River Basins;

Part 3-B - Cumberland and Tennessee River Basins;

Part 5 - Hudson Bay and Upper Mississippi River Basins;

Part 6-A - Missouri River Basin above Sioux City, Iowa;

Part 6-B - Missouri River Basin below Sioux City, Iowa;

Part 7 - Lower Mississippi River Basin;

Part 8 - Western Gulf of Mexico Basins;

Part 9 - Colorado River Basin;

Part 10 - The Great Basin;

Part 11 - Pacific Slope Basins in California - (Vol. 1 - Coastal Basins South of the Klamath River Basin & Central Valley Drainage from the West);

Part 11 - Pacific Slop Basins in California - (Vol. 2 - Klamath and Smith River Basins and Central Valley Drainage from the East);

Part 13 - Snake River Basin

2) "Estimation of 100 Year Flood Magnitudes at Ungaged Sites," C.H. Hardison, U.S.G.S., Water Resources Div., 1973.

3) Meteorology of Hypothetical Flood Sequences in the Mississippi River Basin, Hydrometeorological Report No. 35, Dept. of Commerce, Weather Bureau, December 1959.

4) Meteorological Criteria For Extreme Floods For Four Basins in the Tennessee and Cumberland River Watersheds, Hydrometeorological Report No. 47, Dept. of Commerce, National Oceanic and Atmospheric Administration, July 1971.

5) Arizona Floods of September 5 and 6, 1970, Natural Disaster Survey Report 70-2, Dept. of Commerce, National Oceanic and Atmospheric Administration, July 1971.

6) Black Hills Flood of June 9, 1972, Natural Disaster Survey Report 72-1, Dept. of Commerce, National Oceanic and Atmospheric Administration, August 1972.

7) Baltimore County Hydraulic Design Manual, Baltimore Co., Md., 1968.

8) Anne Arundel County Hydraulic Design Manual, Anne Arundel Co., Maryland.

9) The Missouri River Basin Comprehensive Framework Study, Missouri Basin Inter-Agency Committee, Vol. 1-7, December 1971.

10) "River Runoff Theory and Analysis," D.L. Sokolovskii, Environmental Science Services Administration, Dept. of Commerce, 1971.

11) "Suggested Criteria for Hydrologic Design of Storm-Drainage Facilities in the San Francisco Bay Region California," Dept. of the Interior, Geological Survey, Water Resources Division, November 24, 1971.

12) National Atlas of the United States of America, Dept. of the Interior, Geological Survey, 1970.

13) "A Concept for Infiltration Estimates in Watershed Engineering," H. Holtan, Agricultural Research Service, U.S.D.A., 1961.

14) "Derivation of an Equation of Infiltration," H.J. Morel-Seytoux and J. Khanji, Water Resources Research, August 1974.

15) "Systematic Treatment of Infiltration With Applications," H.J. Morel-Seytoux, Environmental Resources Center, Colorado State University Report No. 50, June 1973.

16) Annotated Bibliography on Hydrology and Sedimentation 1966-1968, U.S. and Canada, Joint Bulletin No. 10, Water Resources Council for Soil Conservation Service U.S.D.A.

17) Handbook of Applied Hydrology, Ven Te Chow McGraw-Hill Book Co., 1964.

18) Open Channel Hydrology, Ven Te Chow, McGraw-Hill Book Co., 1959.

7) The National River and Flood Forecast and Warning Service - (A Plan for Improving), Dept. of Commerce, Weather Bureau, December, 1969.

8) "Flood-Hydrographs Analyses and Computations," Engineering & Design, Corps of Engineers, U.S. Army, 31 Aug. 59.

9) "Generalized Skew Coefficients of Annual Floods in the U.S. and Their Application," C.H. Hardison, U.S.G.S., 1974.

10) "Implicit Dynamic Routing of Floods and Surges in the Lower Mississippi," D.L. Fread, for presentation at A.G.U. Spring Meeting, 1974.

11) "Estimation of Maximum Floods," World Meteorological Organization, Reprinted in 1972.

12) "Forecasting of Heavy Rains and Floods," World Meteorological Organization, 1970.

13) "Floods and Their Computation," Proceedings of the Leningrad Symposium, Volume 1, August, 1967 - UNESCO-WMO.

Hydrology & Hydrologic Processes

1) Water Atlas of the United States, Water Information Center, 1973.

2) The Water Encyclopedia, D.K. Todd, Water Information Center, 1970.

3) The Nation's Water Resources, U.S. Water Resources Council, 1968.

4) Water Publications of State Agencies, Water Information Center, 1972.

5) Representative and Experimental Research Basins in the United States, International Hydrological Decade, 1969.

6) Water Resource Development in Maryland, U.S. Army Corps of Engineers, North Atlantic Division, 1973.

19) Introduction to Hydrology, Viessmann, Harbauh & Knapp, Intext Educational Publishers, 1972.

20) "Time of Concentration for Overland Flow," W.S. Kerby, Civil Engineering, March 1959, p. 60

Watershed Sample

1) "Representative and Experimental Basins," C. Toebes and V. Ouryvaev, eds., International Hydrological Decade, UNESCO, 1970.

2) "Hydrologic Data for Experimental Agricultural Watersheds in the U.S., 1956 - 1967, Misc. Publications No. 1262, 1226, 1216, 1194, 1164, 1070, 904, & 945, Agricultural Research Service, U.S.D.A.

3) Monthly Precipitation and Runoff for Small Agricultural Watersheds in the U.S., U.S., U.S.D.A. Agricultural Research Service, June 1957.

4) Selected Runoff Events for Small Agricultural Watersheds in the United States, U.S.D.A., Agricultural Research Service, January 1960.

5) Annual Maximum Flows from Small Agricultural Watersheds in the United States, U.S.D.A., Agricultural Research Service, June 1958

Miscellaneous

1) Storm Water Management - A Comprehensive Study of the Muddy Branch and Seneca Creek Watershed, Cornell, Howland, Hayes, and Merryfield, Clair A. Hill & Associates, April, 1975

2) User Requirements and User Acceptance of Current and Next Generation Satellite Mission and Sensor Complement, Oriented Toward the Monitoring of Water Resources; ECOsystems International, Inc.; Castruccio, Loats, Fowler and Robinson, NAS5-20567, December, 1977

REFERENCES

1. The Application of Remote Sensing to the Development and Formulation of Hydrologic Planning Models, P.A. Castruccio, H.L. Loats, T.R. Fowler, S.L. Frech, contract NAS8-30539, January, 1975.

2. USDAHL-74, Revised Model of Watershed Hydrology, H.N. Holtan, G.J. Stiltner, W.H. Henson, N.C. Lopez, U.S.D.A., July 1974.

3. "Time of Concentration for Overland Flow," W.S. Kerby, Civil Engineering, March 1959, p. 60.

4. National Engineering Handbook, Soil Conservation Service, Section 4.

5. A Variable Response Overland Flow Model, Doctoral Dissertation. D.E. Overton, Department of Civil Engineering, University of Maryland, 1972.